DELFT UNIVERSITY OF TECHNOLOGY

Faculty of Mechanical, Maritime and Materials Engineering

Investigation of the Inhibition Effect of Basic Oxygen Furnace Slag on the Corrosion of Galvanized Steel

By

Joost van Dam

in partial fulfilment of the requirements for the degree of

Master of Science

in Materials Science and Engineering

to be defended publicly on Thursday August 27th, 2015 at 14:00 .

This page intentionally left blank

Master Thesis

Basic Oxygen Furnace Slag as Corrosion Inhibitor

Author: Joost P.B. van Dam
Student number: 4205448
Internship period: November 2014 - July 2015

Tata Steel IJmuiden
Research & Development
Coating Development

PO Box 10000
1970 CA IJmuiden
The Netherlands

Supervisor: Drs. A. Velzel
Co-supervisor: Dr. ir. B. Boelen

Delft University of Technology
Faculty of Mechanical, Maritime and Materials Engineering
Department of Materials Science and Engineering
Master Programme Materials Science and Engineering

Mekelweg 2
2628 CD Delft
The Netherlands

Supervisor:	Dr. ir. J.M.C. Mol,	TUDelft	,3ME
Thesis committee:	Prof. dr.ir. J. Sietsma,	TUDelft	,3ME
	Dr. Y. Gonzalez Garcia,	TUDelft	,3ME
	Dr. ir. D.A. Koleva,	TUDelft	,CiTG
	Drs. A. Velzel,	Tata Steel Europe	

PREFACE

The title of this thesis is: "The Investigation of the Inhibition Effect of Basic Oxygen Furnace Slag on the Corrosion of Galvanized Steel". This work is based on my research internship at Tata Steel in IJmuiden (NL) and completes the Master program Materials Science and Engineering at Delft University of Technology.

I would like to thank dr. Fouzia Hannour for giving me the opportunity to do my internship at the Coating development (COD) department of Tata Steel. I also want to thank everybody at Tata Steel for their kindness, support and assistance. I would like to thank Arun Mutgi for his lively discussions on our results and for being great company during these last couple of months in the laboratory.

Special thanks go to drs. Arjen Velzel for supervising my work, helping with measurements, interpretations and the writing of this thesis. I would also like to thank dr. ir. Arjan Mol for his supervision and feedback during his visits at Tata Steel.

Last but not least: I also want to thank Sophie Boven for her support and help on this thesis and my parents, for supporting me during my entire studies.

Leiden   J.P.B. van Dam
August 11th , 2015   (4205448)

ABSTRACT

Basic oxygen furnace (BOF) slag is a by-product of the steel conversion process in a basic oxygen furnace. A previous study at Tata Steel in Ijmuiden has discovered the inhibition effect of BOF-slag on the corrosion of cold rolled- and hot-dip galvanized steel. This inhibition effect and its mechanism was studied in this work and its was attempted to incorporate BOF-slag as a corrosion inhibitor pigment in an organic coating.

Its inhibition capacity was first assessed on bare galvannealed and hot-dip galvanized (Zn-Mg-Al) steel and its performance was benchmarked against commercially available corrosion inhibitors. The inhibition effect of BOF-slag on the corrosion of both substrates in a 0.1M NaCl aqueous solution was confirmed by linear sweep voltammetry and it proved to have the highest inhibition efficiency of all tested corrosion inhibitors.

The inhibition mechanism was further studied by electrochemical impedance spectroscopy (EIS),ICP-MS, SEM-EDS and XPS. The results showed the slag solution consisted of colloidal silicates, which upon anodic dissolution of zinc react with the zinc cations and precipitate on the surface. A protective gel-like network film is deposited on the surface, hereby suppressing both the anodic and cathodic current and reducing the corrosion current density by almost two decades.

A pigment was retrieved from the slag particles and was successfully incorporated into an organic waterborne coating and applied to both substrates. The corrosion resistance and barrier properties were evaluated by EIS and salt spray tests (SST). The results show the slag particles had a negative effect on the mechanical and barrier properties of the coating and caused severe damaging of the coating as a result of minor deformation. The particles showed no tendency to restore some of the corrosion resistance of the coating after damaging.

Chemical analysis showed the pigment was retrieved from Ladle furnace slag instead of BOF-slag. This explained inability of the pigment to restore the barrier properties of the coating or to inhibit the corrosion of the underlying substrate.

Key words: Corrosion; corrosion inhibitors; BOF-slag; hot-dip galvanized; EIS; SST; X-ray photoelectron spectroscopy

TABLE OF CONTENTS

1 INTRODUCTION

Corrosion of metals is one of the most prominent causes of the deterioration of materials. Not only does this have effect on the aesthetics of the material but above all it has severe consequences for the mechanical properties. This has large effects on structural safety and the economy [1].

Large efforts are made to prevent or mitigate corrosion to protect the valuable assets from depreciation. There are numerous ways to achieve this. Steel structures are often protected by the application of a zinc coating, called galvanizing. Another common way is to coat the metal substrate with an organic coating. The organic coating protects the metal by separating the metal from its corrosive environment. Despite their function as a separator, organic coatings tend to perform poorer over time. The formation of scratches and the penetration of aggressive ions can drastically alternate their properties and reduce their lifetime.

The addition of corrosion inhibitors appears to be an effective method to improve the performance of organic coatings. Currently chromate-, phosphate- and nitrate based compounds are commonly used due to their outstanding corrosion inhibition [2, 3]. But due to the toxicity of these compounds, their use is becoming undesired or even restricted. Researchers are therefore looking for cleaner alternatives.

The study of chemical and metallurgical processes that occur during corrosion is Corrosion Science. Corrosion Engineering is the design and application of methods to prevent corrosion [4]. So the aim of science is "knowing why", while technology deals with "knowing how". Engineers solve a lot of corrosion problems purely based on experience which is often is due to the complexity of the conditions. Great progress in dealing with corrosion can be obtained by the application of corrosion theory to practical problems. This point of view where science and engineering are combined is considered very useful as a basis for this study.

Basic oxygen furnace (BOF) steel slag is a residue from the basic oxygen converter in steel-making operations (production of 100 kg per ton of steel) with an estimated 12 million tons (Mt) and 8 Mt generated annually in Europe and the United States, respectively [5]. In most industrial countries, the use of BOF slag as a road ballast and land filler has had a very long history. But more and more research is done on new applications of BOF-slag [6].

A previous study by researchers of Tata Steel Europe has revealed the retarding effect of BOF-slag on the corrosion of galvanized steel. At the Tata Steel site in IJmuiden (NL), pig-iron is being converted into steel using a basic oxygen furnace (BOF). At the end of this process large quantities of slag are retrieved and find use as road ballast or land filler. These large quantities could have great potential of being transformed into a working corrosion inhibitor in organic coatings.

In this research, the inhibition of BOF-slag on the corrosion of galvanized steel was investigated and its application as an additive to an organic coating. The first part of this study consisted of "knowing why" this inhibition of corrosion occurs and subsequently try to "know how" we can use this knowledge to improve the corrosion protective properties of the organic coating.

The first part of this work is focussed on the effect BOF-slag on the corrosion of different types of galvanized steel in solution. First the inhibiting properties were evaluated versus commercially available inhibitors using voltammetry. Subsequently the mechanism by which the BOF-slag inhibits the corrosion was studied by combining a large set of techniques and correlating their results. Electrochemical impedance spectroscopy (EIS) and Voltammetry were used to study the

electrochemical behaviour of the inhibitor. Scanning electron microscopy (SEM) and x-ray photoelectron spectroscopy (XPS) were used for surface analysis to assess the formation of protective layers and corrosion products.

The second part of this work is focussed on the effect of BOF-slag in an organic coating. The BOF-slag is incorporated in the coating formulation and applied to substrates which are coated with different zinc-alloys. The performance of the coating is evaluated using EIS and by its performance in a salt spray test (SST).

Chapter 2 deals with the basic theories of corrosion, corrosion inhibitors and the protection of metals against corrosion by the application of organic coatings. The techniques mentioned above and used in this thesis are explained in the last paragraphs of this chapter. In chapter 3, detailed information will be provided on the used materials, instrumentation and methodology during this study. The results and observations of the performed measurements are presented and discussed in chapter 4. Like this entire research, chapter 4 is divided into two parts. The first part presents the results from the study on the performance and mechanism of the inhibitor in solution. The second part presents the results concerning the performance of the organic coating. Chapter 5 concludes the results presented in the previous chapter and provides remarks and recommendations for future research.

The entire study was conducted during a 9 month internship at the Research & Development – in the coating development group, part of the surface engineering department - of Tata Steel Europe in IJmuiden (NL).
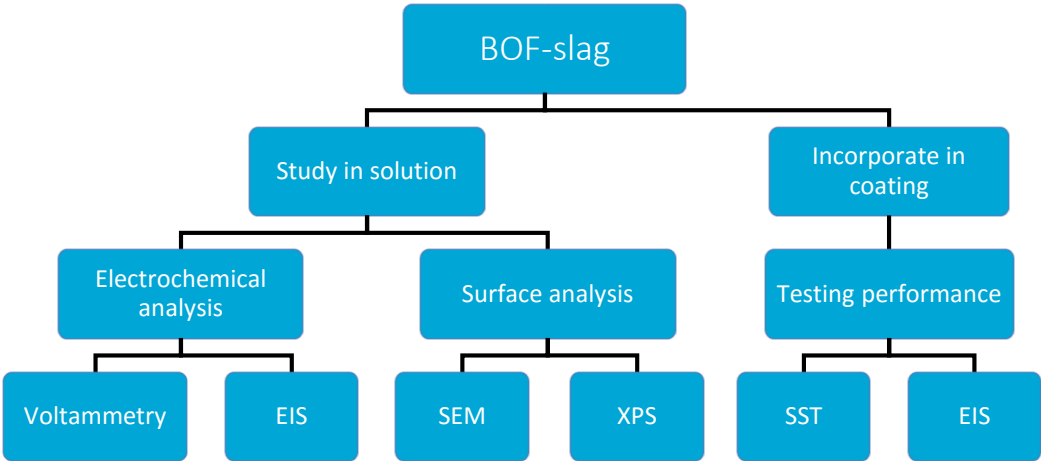
Figure 1: Schematic representation of the techniques used and the way they are linked during this research.

2 BACKGROUND

Corrosion is the gradual deterioration of a material as a result of chemical reactions between the material and the surrounding environment. The most common form of corrosion to most people is rust, the corrosion of iron [7]. Other familiar examples are the formation of a green/blue layer on copper but also the cracking of a rubber tire and the corrosion of glass, also known as glass disease. In the context of this thesis we will further refer to corrosion as the electrochemical degradation of metals and metal alloys.

Corrosion is a serious societal problem and can be found everywhere. Unprotected metals naturally corrode and the range of effects of this reach from merely inconvenient, like the corrosion of a car panel, to catastrophic, like the collapse of an oil rig.

In order to prevent corrosion, engineers aim to remove or reduce the effect of one or more of the conditions leading to corrosion. Various methods exist to achieve this and all of them are based on either:

- o Changing the material
- o Changing the environment
- o Or Changing the interaction between the metal and its environment

Changing the material is often the easiest and logical solution to prevent corrosion since not all metals are as susceptible to corrosion in a certain environment. Apart from the use of pure metals, alloying is a good method to enhance a metal's corrosion resistance. The foundation for this lies in the thermodynamics of corrosion, which will be elaborated in section 2.1 Corrosion of Metals.

Changing the environment is another method to achieve mitigation or completely prevent corrosion. This can for example be done by modifying the pH or remove aggressive chloride ions from the solution. Another way is via the addition of corrosion inhibitors. Inhibitors are substances or mixtures that in low concentration and in an aggressive environment inhibit, prevent or minimize the corrosion [8]. Corrosion inhibitors will be further discussed in section 2.3 Corrosion Inhibitors.

The last option is to remove the interface between the metal and its corrosive environment. By coating the metal a barrier is formed and corrosion is for some time prevented. These coatings can be organic, inorganic or metallic of nature and will be covered in section Protective coatings.

Engineers often implement a combination of these three methods to design multifunctional systems that exhibit the best protection against corrosion for the designated metal/situation.

All these precautions and measures come at a high cost. These costs together with the costs of control services, R&D, education and training fall under the heading 'direct costs of metal corrosion'. NACE international (formerly known as the National Association of Corrosion Engineers) conducted a research on the annual direct costs of *metallic* corrosion. They estimate these costs to be about ~3,1% of the Gross Domestic Product (GDP), of which 88,3% is attributed to organic coatings. On top of these direct costs, there are the 'indirect costs of corrosion'. Indirect costs include such factors as lost productivity because of outages, delays, failures and litigation; taxes and overhead costs; and indirect costs of operator activities. The authors roughly estimate the indirect costs to be equal to the direct costs, coming to a total of about ~6% of the nation's GDP. If we would apply these numbers to the current economic status in the Netherlands, the annual total costs of metallic corrosion in the Netherlands alone sum op to ~43 billion Euro [1, 9].

Apart from these severe costs, the authors also estimate all costs can be reduced by up to 30% if all scientific knowledge on corrosion was fully implemented. This clearly indicates the importance of corrosion science, but moreover the importance of the collaboration between corrosion scientists and corrosion engineers.

2.1   CORROSION OF METALS

Metals naturally occur in minerals, in the form of oxides. To extract the metal from these minerals requires the addition of large amounts of energy. This energy is than stored in the metal and this same amount of energy is emitted during the reactions that produce corrosion. During corrosion the metal is returned to its combined state in chemical compounds that are similar or even the same as the minerals from which the metals were extracted.

Nonmetallic materials have their chemical potential satisfied by the formation of bonds with other reactive atoms. This makes them unsusceptible to electrochemical reactions with their environment (corrosion) and they degrade by mechanical wear/erosion and physical breakdown. Unlike these materials, pure metals do not have their chemical reactivity satisfied. Nearly all of the reactions with their environment therefore involve transfer of electrons. So corrosion is an electrochemical process which means that it does not occur due to the direct reaction of a metal with its environment but rather due to the transfer of charge between neutral or ionic reactants and the conducting metal. During this transfer of charge, the reactive species change valence by either the gain of electrons and lowering of their valence (reduction) or loss of electrons and increase of valence (oxidation). These two reactions are called half-cell reactions and once coupled they form an electrochemical cell. Within this cell, reduction occurs on one electrode and oxidation on the other. They are therefore referred to as respectively the cathodic and anodic reaction.

Within the electrochemical cell the electrons travel via the anodic and cathodic electrode. In corrosion this is usually the bulk material of the metal. In order for a current to flow and the total reaction to occur, the electrical circuit needs be to be closed. In order to achieve this, the presence of an electrolyte is required. An electrolyte is an ion-conducting liquid that forms an interface with both electrodes. By the transport of charged ions, the electrolyte is capable of conducting an electrical current. The most common electrolyte is an aqueous solution but other liquids can also function as electrolyte.

The anodic half-cell reaction of the corrosion process is the oxidation of a metal. In this reaction the metal loses ne^- electrons and hereby increases his valence (0.1). Where n is dependent on the metal (e.g. for zinc n=2 and for aluminium n=3).

$$M(s) \rightarrow \mathrm{M}^{n+}(aq) + ne^-$$
(0.1)
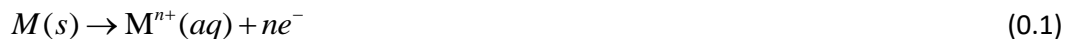
The cathodic half-cell reaction electrons are being consumed in the reduction of active ions/species. One of the most common cathodic reactions in aqueous solution is the reduction of hydrogen ions and leads to the formation of molecular hydrogen gas.

$$2H^+(aq) + 2e^- \rightarrow H_2$$
(0.2)

This is the predominant cathodic reaction in solutions with low pH [3]. Another reaction is the reduction of oxygen. During this reaction oxygen reacts in combination with hydrogen ions to form water (0.3). In neutral and basic conditions hydrogen reduction can still occur but the reduction of dissolved oxygen is predominant. During this reaction oxygen also reacts in combination with hydrogen ions but this time to form hydroxyl ions (0.4).

$$O_2 + H^+(aq) + 4e^- \rightarrow 2H_2O(l)$$
(0.3)

$$O_2 + H^+(aq) + 4e^- \rightarrow 4OH^-(aq)$$
(0.4)

Although the two half-cell reactions occur at different electrodes, they can occur on the same surface. The surface of a metal is never completely homogeneous, due to irregularities in chemical composition, the presence of grains of different phases, grain boundaries, edges and dislocations. All of these heterogeneities can create sites with different potentials. The presence of these potential differences creates anodes and cathodes on the surface and is a driving force for the movement of electrons [10]. The metal and the electrolyte then form the 'charge' connection between the anodic and cathodic sites.

At the anodic site the metal loses ne^- electrons (where n depends on the metal) en gets oxidized to M^{n+}. The created metal ion then dissolves and passes into the solution, as is depicted in Figure 2 . The removed ne^- electrons are then conducted through the bulk material of the electrodes (the metal) towards the cathodic sites. This movement is a response to the resulting potential difference. At the cathodic site, the present reactive species in the electrolyte, the oxidants, consume the electrons at the metal-electrolyte interface and gets reduced.
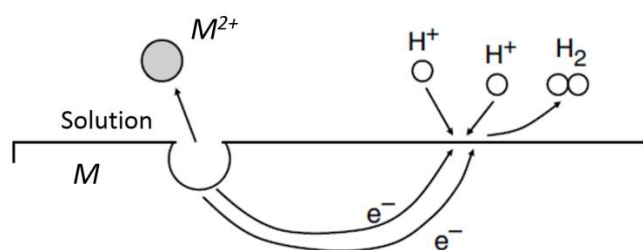
Figure 2: Anodic and cathodic half-cell reactions occurring at different sites on the metal surface. The two electrons from the anodic dissolution of the metal are consumed in the cathodic hydrogen-reduction reaction.

In the case of Figure 2 these active species are hydrogen ions getting reduced to a hydrogen atom. The formed hydrogen atoms then recombine to form a molecule of hydrogen gas. The metal ion can either stay in solution or can recombine with anions in solution to form a solid precipitate on the surface.

The two reactions are directly coupled and will therefore proceed simultaneously and with the same speed in order to prevent the accumulation of charge (either electronic or ionic).

The coupled electrochemical reactions occurring at the different sites on the metal surface than sum up to the net (corrosion) reaction:

$$M(s) + 2H^+(aq) \rightarrow M^{2+}(aq) + H_2(g) \tag{0.5}$$

Which in this case is the corrosion reaction for a metal in acidic aqueous media as illustrated in Figure 2. The cathodic reaction does not involve the loss of metal and therefore appears not to be a corrosion reaction. From (0.5) it can be seen that due the direct couple of the cathodic half-reaction the anodic reaction (metal oxidation) can be accelerated or retarded by stimulation or inhibition of the cathodic reaction. A concept that will be further discussed in section 2.3 Corrosion Inhibitors.

It was mentioned above that both half-cell reactions have their own potential and the difference of these potentials is the source for cathodic and anodic sites. This potential is called the standard potential of the half-cell reaction. These potentials are expressed in V (1 V = 1 JC^{-1}). If the standard potential is large, then the electrons can do a large amount of electrical work. If the system would be in equilibrium, the potential would be zero and therefore the cell would not be able to perform work. The standard potential is therefore often called the electromotive force (emf) of the cell.

2.1.1 Thermodynamics of corrosion

Thermodynamics gives an insight into the energy changes that go along with the electrochemical reactions on the surface. These energy changes provide the driving force behind the reaction and determine the direction of the electrochemical or charge transfer reaction during corrosion, as for any chemical reaction. The thermodynamics of a chemical reaction are determined by the Gibbs energy (G), which is dependent on temperature (T) and pressure (P). Thermodynamics provides us the information to determine in which conditions corrosion is possible or not.

A change in Gibbs energy (ΔG) is associated with an electrochemical reaction. If ΔG is negative, the overall energy is reduced and the reaction occurs spontaneously.

As mentioned above, both half-cell reactions have their own potential where the difference in these potentials is the creator of anodic/cathodic sites. This is the half-cell potential or redox potential of the half-cell reactions and is denoted by either e_a (anodic) or e_c (cathodic). Once coupled in an electrochemical cell this results in the creation of a potential difference, the cell potential (E) or the electromotive force (emf) of the cell. All these potentials are being expressed in Volts (1V = 1JC^{-1}) and the cell potential can be constructed from the half-cell potentials by:

$$E = e_a + e_c \qquad (0.6)$$

The cell potential and the change in Gibbs energy (in kJ/mol) are related by:

$$\Delta G = -nFE \qquad (0.7)$$

Where F is the Faraday constant (96500 Coulombs per equivalent), n is the number of equivalent electrons and E is the cell potential. Due to the negative sign in (0.7) we see that a positive potential is associated with a negative change in Gibbs energy en the right-going reaction is spontaneous.

In order to demonstrate the significance of Gibbs energy, let's take a look at the corrosion reaction of zinc in acidic aqueous solution(0.8).

$$Zn(s) + 2H^+(aq) \rightarrow Zn^{2+}(aq) + H_2(g) \qquad (0.8)$$

This reaction can be divided into two half-cell reactions at which the exchange of electron is involved; the anodic dissolution of zinc (0.9) coupled to the reduction of ionic hydrogen (0.2).

$$Zn(s) \rightarrow Zn^{2+}(aq) + ne^- \qquad (0.9)$$

$$2H^+(aq) + 2e^- \rightarrow H_2 \qquad (0.2)$$

Both half-cell reactions have a defined half-cell potential in the standard state[1]. These potentials are denoted by e_a^0 and e_c^0. The actual half-cell potential is affected by the concentration of the reactants and products. An organized summation of the standard half-cell potentials is called the standard emf series. In this list all standard half-cell potentials are mentioned for reduction reactions going from left to right, thereby giving the reduction potential. Figure 3 shows a reduced version of the standard emf series. The list goes from negative values of ~-3 V up to positive values of ~1,5 V.

The positive top of this list is the noble end of the series, which got his name from the traditionally noble metals constructing this section of the list (like gold and platinum). The other end of the list is

---

[1] The standard state is arbitrarily defined and expressed in species activity. In the case of corrosion the activity of dissolved species may be approximated by concentration. For gasses 1 atm. is taken as the standard state and for solids, the solid is taken as unit activity [7].

called the active part of the list due to the presence of active metals (like lithium and potassium). So the more negative the reduction potential, the more active, and the more positive, the more noble is the character of the species.

In order to determine the standard potential one cannot just measure one reaction for no electrical circuit is present. The half-cell needs to be coupled to another with a known half-cell potential. The reduction of hydrogen has a standard potential of 0 V as can be seen in Figure 3. Although the actual potential is not 0 V for this is chosen for convenience. The cell which is being used to determine the potential of the half-cell reactions is called the standard hydrogen electrode (SHE). The SHE consists of a platinum electrode submerged in 1 unity of active acid and 1 atm H_2 (standard state). The platinum is inert in this setup and the reduction of hydrogen ions and the reverse reactions take place at the surface with a potential of *0* V.

Reaction	E^0(V vs. SHE)
$Au^{3+} + 3e^- \rightarrow Au$	+1.498
$Pt^{2+} + 2e^- \rightarrow Pt$	+1.18
$Ag^+ + e^- \rightarrow Au$	+0.800
$Cu^+ + e \rightarrow Cu$	+0.521
$Cu^{2+} + 2e^- \rightarrow Cu$	+0.342
$2H^+ + 2e^- \rightarrow H_2$	0.000
$Sn^{2+} + 2e^- \rightarrow Sn$	−0.138
$Ni^{2+} + 2e^- \rightarrow Ni$	−0.257
$Fe^{2+} + 2e^- \rightarrow Fe$	−0.447
$Cr^{3+} + 3e^- \rightarrow Cr$	−0.744
$Zn^{2+} + 2e^- \rightarrow Zn$	−0.762
$Ti^{2+} + 2e^- \rightarrow Ti$	−1.630
$Al^{3+} + 3e^- \rightarrow Al$	−1.662
$Mg^{2+} + 2e^- \rightarrow Mg$	−2.372
$Na^+ + e^- \rightarrow Na$	−2.71
$Ca^{2+} + 2e^- \rightarrow Ca$	−2.868
$K^+ + e^- \rightarrow K$	−2.931
$Li^+ + e^- \rightarrow Li$	−3.040

Figure 3: Reduced form of the standard emf series [5]

All reactions coupled to this electrode are therefore completely responsible for the observed residual potential. In the case of the oxidation of zinc (0.9), this observed potential would be +0.762 V. This is the reversed potential of the reduction of zinc, given in Figure 3. Using the standard emf series, one can also approximate the potential of two coupled half-cell reactions in the standard state.

Earlier it was stated that the change in Gibbs energy can be determined on the basis of the cell potential (0.7). From this equation it is clear than we can also determine the potential of a cell with a certain composition ones the change in Gibbs energy is known. It is also known that the Gibbs energy is dependent on the composition of the reaction mixture:

$$\Delta G = \Delta G^0 + RT \ln Q \qquad (0.10)$$

Where *Q* is the reactions quotient (activity$_{products}$/activity $_{reactants}$), *R* is the gas constant (8.314 JK^{-1}mol^{-1}) and *T* is the temperature. If we combine equations (0.7) and (0.10) we get an equation better known as the *Nernst*-equation (0.11).

$$E = E^0 - \frac{RT}{nF} \ln Q$$

<div align="right">(0.11)</div>

This equation enables us to calculate the potential in terms of the composition and is both applicable to the cell potential (E) as to the half-cell potential (e) and a large application is the calculation of ion concentrations and the pH. We can see from equation (0.11) that with a reduction of Q, E becomes more positive. So with an increase in concentrations of the reactants (Zn and lowered pH) the potential increases.

We have seen that if we know the conditions of the total reaction or of the half-reactions we can calculate the change in Gibbs energy and the associated potential. In the standard emf series all reactions are illustrated as reduction reactions. So once we couple two half-cell reactions, one of the reactions has to run in the reverse direction (left) in order to form a electrochemical cell or a galvanic couple. When the reaction runs in the reverse direction, the sign of the potential must change. From (0.6) we see that if E>0 (in order for ΔG<0) the half-cell reaction with the most negative potential (active) is to be the oxidation reaction and the reaction with the most noble potential will be the reduction. This principle can have detrimental effects if one chooses the wrong combination of different metals and one of the metals is anodically sacrificed. Looking at it from a different angle, one can also use this concept to protect a metal from oxidation by sacrificing another. This is cathodic protection as is to be further discussed in section 2.2.1 Metallic coatings.

From the Nernst-equation (0.11) we get that by changing the environment/conditions we can alter the cell potential. So we can alter the conditions in such matter that E becomes negative and the reaction is no longer spontaneous. Using this principle, we can construct a map-like chart of E vs. pH, where every section denotes the stable phases of the metal (see Figure 4). Such a E,pH diagram is often called a pourbaix-diagram after prof. M. Pourbaix [11].
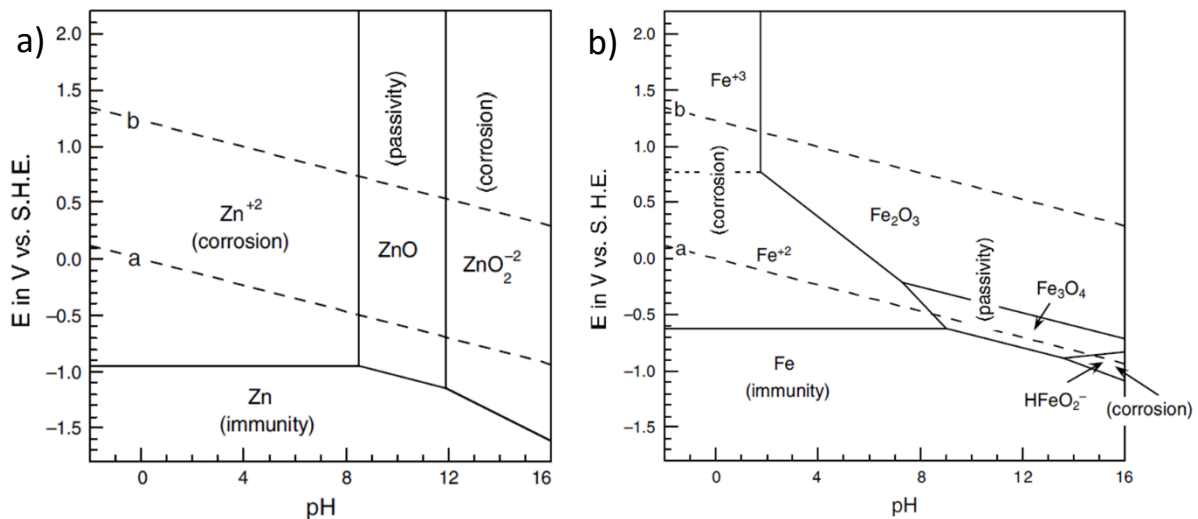
Figure 4: Pourbaix (E,pH) diagram for Zinc (a) and Iron (b) at 25°C [3]

The borders of the different 'phase-areas' have been derived from the *Nernst*-equation. The diagram tells which reactions and phases are favoured at a certain potential and pH. The pourbaix-diagram often consists of three different type of phases: corrosion, passivity and immunity (as can be seen in Figure 4). If we look at the pourbaix-diagram of zinc Figure 4a we see that zinc corrodes/dissolves at pH>12 (as ZnO_2^{2-}) and at pH<8.3 (as Zn^{2+}). In between these two regions zinc passivates by the formation of a protective oxide layer on the surface (ZnO). At very low potentials, zinc is immune to corrosion and reduced zinc atoms are most stable.

The pourbaix –diagram of iron is a bit more complicated. Iron can be oxidised to divalent or trivalent iron cations at low pH and at high pH to $HFeO_2^-$. When iron passivates it either forms red iron oxide/red rust (Fe_2O_3) or black iron oxide/black rust (Fe_3O_4).

For corrosion scientists and engineers, these diagrams are of great aid to see whether the corrosion of a metal is thermodynamically favoured or not. One can alter the pH or the potential of the cell in order to make corrosion thermodynamically unfavourable.

2.1.2 Kinetics of corrosion

Despite their information whether corrosion is possible (based on thermodynamics), pourbaix-diagrams do not give any information on the rate of corrosion. Of course this is something both scientists and engineers are interested in. In order to determine or predict the rate of corrosion one is to consult the kinetics of the electrochemical reactions.

Once a metal gets in contact with an aqueous solution (the electrolyte in the case of wet corrosion) a boundary layer is formed between the solid and liquid phase, called the electrical double layer (edl). This mainly consists of a thin sheet of positive charge underneath the metal surface and a sheet of negative charge in the solution (or vice versa). The Helmholtz model is a simplified model to describe this phenomena at which an arrangement of dipoles and ions arises and is illustrated in Figure 5. Due to the coordination of the hydrogen atoms to the oxygen at a 104.5° angle, H_2O is an asymmetrical dipolar molecule. The negative side of the asymmetrical molecules is drawn towards the conductive (positive) surface in Figure 5. In the solution, charged ions are surrounded by polar water molecules, forming a hydration sphere. By the formation of the oriented sheet on the surface and the hydration sphere, the charged anions are at a defined distance from the surface. The imaginary plane running through the centre of these ions is the Outer Helmholtz Plane (OHP). The result of this coordination is the formation of a structured interface and the separation of charge which forms the previously mentioned edl. The edl has capacitor-like behaviour because it retards fast and easy charge transfer and thereby limits the electrochemical reactions on the surface. There is a potential difference over this capacitor which (in this model) changes linear within the edl, with the electrode on one side and the OHP on the other. This potential across the interface is the origin of the electrode potential. As was discussed earlier, changes in this potential can cause changes in the driving force, G, and influence the thermodynamics of the anodic or cathodic reactions and thus influence the kinetics of the total reaction.
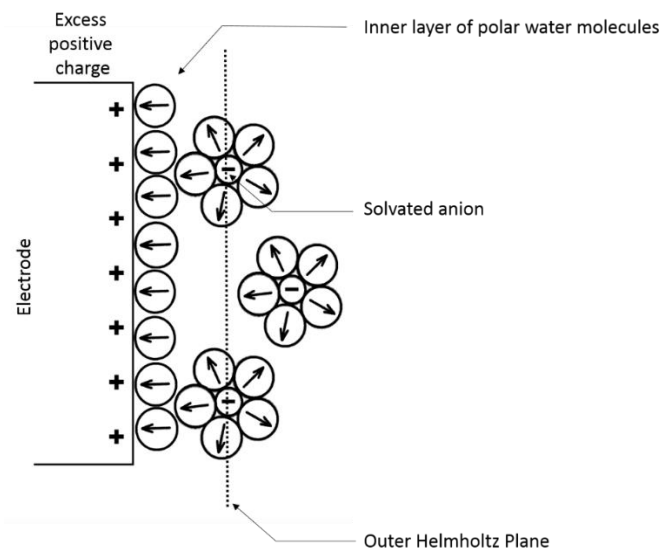
Figure 5: Formation of an electrical double layer according to the Helmholtz-model. The arrow marks the direction of the negative pole.

For the continuation of the corrosion process, dissolved metal cations must pass through the edl in order to be absorbed by the solution and reacting species in solution must pass through the edl to get to the electrode surface. Since corrosion includes the charge of transfer and mass over the metal/liquid interface, the rate of corrosion is determined by the transfer rate. The properties of the edl have great influence on the kinetics of the corrosion process.

The unit for charge is Coulomb (*C*), which is a product of the current and his passing time. Current I is measured in Ampere (*A*) (where $1\ A = 1\ Cs^{-1}$ and 1 Coulomb of charge is equal to *6.2*10^{18}* electrons). The unit for mass is gram which can be obtained from the equivalent of metal lost and the equivalent weight of the metal.

Faraday's Law provides the link between the transfer of charge and mass by describing the mass of metal that has corroded as:

$$m = \frac{Ita}{nF}$$
(0.12)

where *I* is the current in amp, *t* is time in seconds, *a* is the atomic weight of the metal, *F* is the Faraday constant (F=96500C/equivalent) and *n* is the number of equivalent electrons transferred per mole metal, e.g. *n=2* for zinc and *n=3* for aluminium.

If we divide (0.12) by time (*t*) and surface area (*A*), we get the mass per time per surface area which is known as the corrosion rate, *r* (0.13).

$$r = \frac{ia}{nF}$$
(0.13)

Here i is the current density, the amount of current per surface area so I/A. This relation provides a direct proportionality between the corrosion rate (mg/dm^2/day) and the current density (µA/cm^2). The constant in this relation is a/nF. Unlike the current, one can now directly correlate the current density to the corrosion rate. Current densities can be measured from very small values (10^{-9} A/cm^2) up to several amps per square centimetre. The combination of these two properties makes measuring the current density via electrochemical measurements a very interesting tool to study corrosion behaviour.

The net current density at an electrode is the difference between the current densities derived from the anodic and cathodic reactions. And the net potential as a result of coupled half-cell reactions is the standard potential. At the standard potential the reaction is in an equilibrium state, at which the total rate of the anodic reactions (r_a) equals the total rate of the cathodic reactions (r_c):

$$r_a = r_c = \frac{i_0 a}{nF}$$
(0.14)

In (0.14), i_0 is the net current density or the exchange current density. Where in thermodynamics *ΔG* is the fundamental parameter, in kinetics i_0 is.

The exchange current density can be measured at the standard potential of the electrochemical cell. Due to the fact that at this potential no extra potential is applied to the electrochemical cell, this potential is often referred as the open-circuit potential (OCP) or the corrosion potential (E_{corr}). If the potential of the cell were to be adjusted to *E'* by an external source, than the reaction would deviate from its standard potential (*E*) by *E+η=E'*. Here *η* is the polarization. When cathodically polarized, *η <0* and the resulting potential at the electrode is more negative. This is caused by an accumulation of electrons and at this potential, the cathodic reaction and current are predominant, hence the name. When *η >0* the resulting potential is more positive than the equilibrium standard potential. The surface is depleted of electrons and the anodic reaction and current are predominant. There two features that can contribute to this polarization.

Activation polarization ($\eta_{activation}$) is described by the kinetics of charge transfer and is the main contribution to polarization when a small polarization is applied. There is a direct relation between the activation polarization and the current density, and therefore also with the corrosion rate. This relation that describes the charge transfer kinetics is given by:

$$i = i_0 \cdot \left[\exp\frac{\alpha_a nF\eta}{RT} - \exp\frac{\alpha_c nF\eta}{RT} \right] \tag{0.15}$$

and called the Butler-Volmer formulation. In this η is the polarization or overpotential, i is the measured current density, i_0 is the exchange current density (or corrosion current density in the case of corrosion) R is the universal gas constant, F is Faraday's constant, T the absolute temperature, n the number of electrons transferred in the anodic and cathodic reactions and α_a and α_c represent the anodic and cathodic charge transfer coefficients respectively. One of the assumptions of the Butler-Volmer equation is the negligible transfer of active species from the metal/surface interface. At low current densities, this assumption is valid and a uniform distribution of active and reactive species over the solution can be assumed.

For sufficiently high values of the applied potential, equation (0.15) can be simplified to the Tafel equation:

$$\eta = \beta \log\frac{i}{i_0} \tag{0.16}$$

where β is the Tafel constant. For anodic polarization, β_a is to be positive and in the case of cathodic polarization, β_c is negative. The absolute values of the Tafel constants usually range from 0.03 to 0.2 V and are usually not equal for the anodic and cathodic reactions [7].

For small values of η, so close to the standard (or corrosion) potential the Butler-Volmer formulation (0.15) can be simplified to give

$$\eta/i = \frac{\beta_a\beta_c}{2.3i_0(\beta_a+\beta_c)} \tag{0.17}$$

Here η/i is a measure of the resistance to polarization or transfer of charge, which is often expressed as:

$$\eta/i = R_p = \frac{B}{i_0} = \left(\frac{\Delta E}{\Delta i}\right)_{\Delta E \to 0} \tag{0.18}$$

And is known as the Stern-Geary equation, where R_p is the polarization resistance and B is the proportionality constant which can be determined empirically or calculated using the Tafel constants.

$$B = \frac{\beta_a\beta_c}{2.3(\beta_a+\beta_c)} \tag{0.19}$$

The corrosion rate can also be correlated to the polarization resistance, knowing the Tafel parameters. From equation (0.17) it can be seen that the polarization resistance is inversely proportional to the corrosion current density. This is why the R_p is often used instead of the exchange current density to express and compare the corrosion resistance.

The plot of the logarithm of the current density versus the polarization is called a Tafel plot. In which in the ideal case, the slope of the curve is given by β_a and β_c (according to equation 0.16) and the interception of the cathodic and anodic polarization curve gives the exchange current density.

In the preceding section, the transfer of active species towards and away from the metal/liquid interface was neglected. This assumption is true when low values of overpotential/current density are assumed and the limiting step in the corrosion reaction is the transfer of charge. For higher values of the overpotential this assumption becomes invalid in real situations, especially in the case of low concentrations of oxidizer. At high current densities the consumption of reactive species from the solution is very fast. The diffusion of active species towards the surface and reacted species away of the surface is limited, causing a concentration gradient and thereby limits the rate of the reaction. A larger increase in potential is required in order to get the same increase in current density. The logarithmic no longer shows linear/Tafel behaviour. This phenomena is called concentration polarization.

The concentration polarization ($\eta_{concentration}$) is a contribution to the polarization caused by the limitations of mass transfer (diffusion of active species). When the response in current density reaches a limiting value, i_L, the polarization is no longer controlled by activation but by concentration polarization.
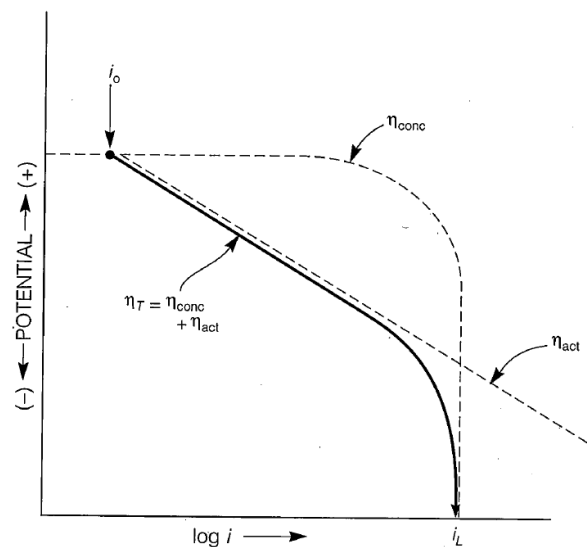
Figure 6: Combined polarization curve for activation and concentration polarization on a cathode [7].

Figure 6 shows the contribution of the activation and the concentration polarization in the total cathodic polarization. This ideal representation shows the initial polarization follows the Butler-Volmer formulation and displays Tafel behaviour. When the response in current density due to polarization approaches i_L, concentration polarization becomes dominant and the curve no longer obeys Butler-Volmer.

2.2 PROTECTIVE COATINGS

Thermodynamics and kinetics provide us information on how to prevent corrosion and how to calculate and retard corrosion rates by means of material choice and adaptation of the environment. Protective (or corrosion resistive) coatings allow for added protection of metal surfaces by acting as a barrier to inhibit the contact between the metal and the corrosive environment. One type of coatings often applied are metallic coatings.

2.2.1 Metallic coatings

A distinction can be made between two kinds of metallic coatings which are being used to protect objects from corrosion; sacrificial metallic coatings and noble metallic coatings.

The first of these is based on the principle of cathodic protection. During cathodic protection, two dissimilar metals are coupled in both a physical and electronic way. The metal with the most negative standard potential will be functioning as the anode whilst the more noble metal, with a less negative or positive potential will function as the cathode, hence the name cathodic protection.

By making the right selection of materials, one can make use of this feature to protect metals against corrosion. Down in the active part of the standard emf series you will find magnesium, aluminium and zinc which are all three common metals used to protect steel objects. This can be done in two ways; by connecting a piece of metal to the sacrificial metal or by covering it in a metallic coating. By just connecting it, the more active metal (Zn, Al, Mg) will sacrifice itself by corroding instead of the protected object. The most common way to protect steel though is by applying a thin coat of zinc (galvanizing). This coating has a double method of working. Zinc has good passivation properties in neutral to basic conditions, forming a dense and closed protective oxide layer to separate the substrate from the corrosive environment by removing the solid/liquid interface and preventing reactive species to reach the surface. If the coating gets damaged and the substrate is yet exposed it has another working mode due to the galvanic couple. The zinc coating will function as a big anode, sacrificing itself whilst the small section of exposed steel functions as the cathode.

The second type of metallic coating is the use of noble metallic coatings. Nickel and tin are commonly used for coating steel (in the battery- and food industry respectively). They both have a more noble potential than the underlying steel (as shown in the standard emf series in Figure 3). So unlike in the case of zinc coatings, the steel is the anode and the tin/nickel coating is the cathode in case of damage to the coating. Their protective property is therefore not based on the galvanic couple between the two metals but on the more corrosion resistive properties of the coating. This can have very negative side effects. When the coating is damaged and the steel is revealed, the steel cathodically protects the coating and corrodes. Due to the relatively big surface of the cathode and small surface of the anode in the case of a small scratch, high current densities can be obtained causing very local and deep corrosion.

2.2.1.1 Hot dip galvanized steel

The process of hot dip galvanizing includes the passing of a sheet of metal through a bath of molten zinc in order to create a homogenous zinc layer formed on the surface. Typically 0.1-0.2 wt% of Al is added to the bath to prevent the formation of a thick, continuous layer of Zn-Fe intermetallic on the zinc/steel interface that could lead to poor coating adhesion during forming later on. Lead (typically 0.04-0.2 wt%) is usually also added to the bath to improve the baths' fluidity and to improve the adhesion and uniformity of the zinc coating [12].

When the hot dip galvanized sheets leave the zinc bath, the surface immediately oxidizes. In combination with water and carbon dioxide a layer of zinc carbonates is formed with very strong adhesion which seals the zinc surface.

2.2.1.2 Galvannealed steel

The galvannealed (GA) coating is obtained by post-annealing a plate of hot dip galvanized (HDG) steel at around 500-550 °C. During this annealing four intermetallic phases of Fe-Zn form in the coating. They are referred to as the; zeta (ζ) phase ($FeZn_{13}$), delta (δ) phase ($FeZn_7$), gamma-1 (Γ_1) phase (Fe_5Zn_{21}) and gamma (Γ) phase (Fe_3Zn_{10}) going from the surface to the substrate [13, 14]. The morphology, composition and structure of the coating can have great influence on the corrosion resistance but also on the formability, weldability and paintability.

The surface is characterized by two different morphologies; a compact and flat structure and an elongated rod-like morphology. Looking at a cross-section of a galvannealed steel sample, shows a cracked coating which is caused by the generated stresses during the annealing process. This cracking

of the coating is clearly illustrated in Figure 7, with the steel substrate on top and the galvannealed coating below. The outermost layer of the GA structure is known to be the zeta phase and the two regions that be distinct from each other are referred to as the compressed and the crystallized zeta phase. The compressed part is formed during the temper rolling process which is done to improve the surface quality [15].
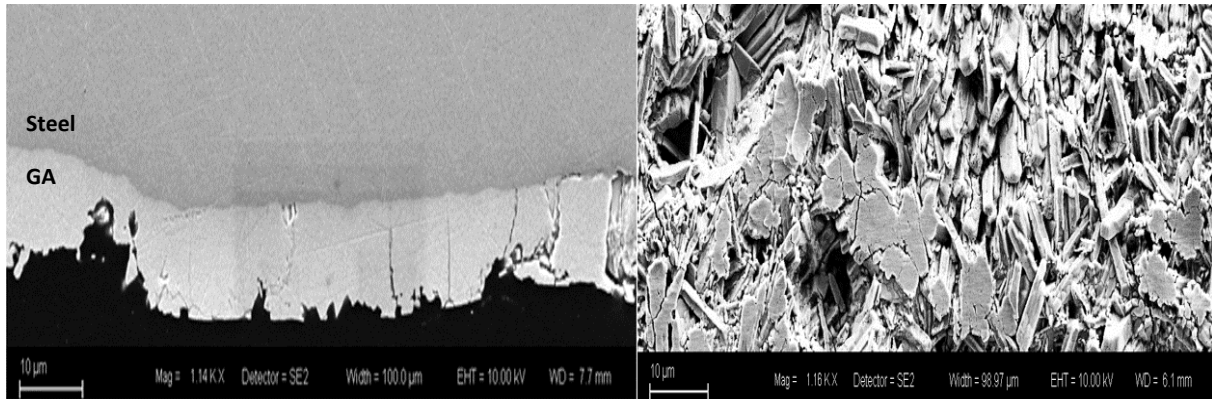
Figure 7: SEM image (left) of a cross section and (right) a top view of the surface of a GA coated steel sample.

Like GI, the GA coating protects the steel substrate in two ways. By forming an impermeable barrier and by cathodic protection. When corroding, initially the compressed zeta phase will corrode first. For this phase has increased internal energy due to the compression. The dissolution of this phase causes increased cracking of the surface. Subsequently the crystallized zeta phase and delta phase are to be dissolved. Once the initial dissolution of the delta phase has exposed some of the gamma phase, the gamma phase will preferentially corrode due to the galvanic couple between the delta and gamma phase [16, 17].

Upon the formation of oxides on the corroding surface red rust forms generally fast on GA due to the presence of Fe in the coating. For many manufacturers this an undesired property for it is detrimental for the aesthetics as soon as the material starts to corrode. Despite this feature, GA is still a commonly used metallic coating due to the improved corrosion resistance and weldability compared to GI. The improved corrosion resistance or lower corrosion rate is due to the lower potential difference between GA and the steel substrate resulting in a lower rate of corrosion reactions [18].

2.2.1.3   Zn-Mg-Al coated steel

Many research studies have been performed on the improvement of the corrosion resistance of galvanized steel sheets and on the reduction of the coating weight by alloying [19, 20]. Initially the aluminium content was increased. These coatings showed good corrosion resistance because they provided sacrificial protection by zinc and a strong physical barrier formed by the aluminium [21].

Magnesium was also found to be able to improve the corrosion resistance of zinc coatings. Unfortunately the addition of just magnesium can cause dross formation (solid impurities floating on the molten metal) due to the high oxygen affinity of magnesium[20, 22]. It was found that the addition of aluminium suppressed the oxidation of magnesium and therefore resulted in improved coating quality [23]. By the combination of these two alloying elements the Zn-Mg-Al coated was created. Tata Steel also produces a Zn-Mg-Al coated steel under the name MagiZinc® (MZ), which consists of a Zn-1.6wt.%-Mg-1.6wt.%-Al alloy.

When the Zn-Mg-Al coating is applied by hot dip galvanizing (as is being done in the hot dip galvanizing line of Tata Steel in IJmuiden) different intermetallic phases arise in the coating. Large Zn-rich phases are formed and are denoted by 'a' in Figure 8. These phases are surrounded by two different Mg-rich phases ($MgZn_2$ and Mg_2Zn_{11}), denoted as 'b' in Figure 8, and in these phases small dark grains of Al-rich phases can be observed. In between these phases some binary and ternary phases can also form. The ternary eutectics tend to form in the region where small dark spots of Al-rich phases are observed (in
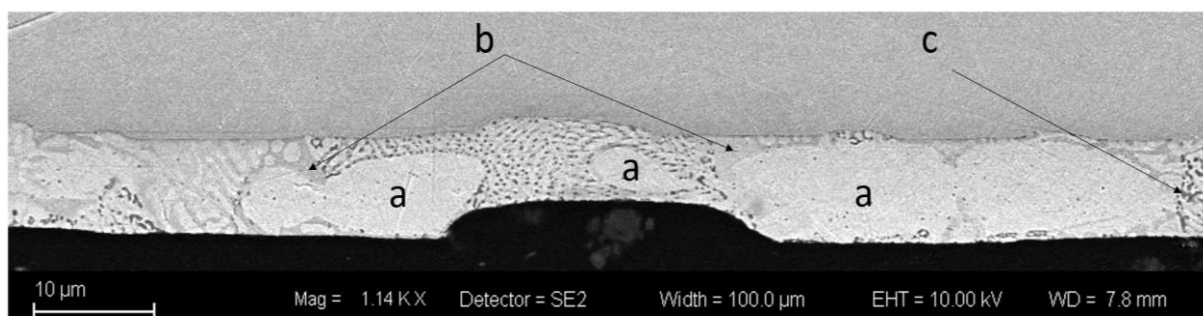
Figure 8: SEM image of a cross-cut made from a MZ coated steel sample.

the centre and right side of Figure 8) where the binary eutectic can be found between the Zn-rich and Mg-rich phase [23, 24].

The un-corroded surface of Zn-Mg-Al coatings consists predominantly of a thin protective oxidic layer rich in magnesium oxide (MgO) and aluminium oxide (Al_2O_3) with small amounts of hydrozincite ($Zn_5(OH)_6(CO_3)_2$) covering the bulk material. MZ shows superior corrosion resistance compared to GI coatings [25]. Upon corrosion, magnesium oxide corrodes and then forms again on the surface as $Mg(OH)_2$ and metallic zinc and aluminium convert to hydrozincite and aluminium oxide. The formations of these oxides is stabilized by magnesium ions forming low protective complexes with anions in solution. The combination of these oxides leads to the formation of Zn-Al/Zn-Mg layered double hydroxides (LDH), a dense and protective oxide layer for the underlying bulk material. At high enough concentrations, chloride ions are able to attack the oxidic layer. Magnesium and aluminium preferentially corrode over zinc and after longer exposure, this causes the surface to deplete from magnesium and aluminium and the surface to mainly constitute of hydrozincite, zinc hydroxide ($Zn(OH)_2$) and stable simonkolleite ($Zn_5(OH)_8Cl_2$).

The superior corrosion resistance of MZ in chloride containing environment is due to their ability to form simonkolleite ($Zn_5(OH)_8Cl_2 \cdot H2O$) on the surface after cyclic corrosion tests, where GI was not able to [25].

2.2.2 Organic coatings

Organic coatings are applied in addition to or instead of metal coatings to metal structures to improve its corrosion resistance or add additional functionalities to the material. Organic coatings can be applied to improve aesthetics, lubrication, self-cleaning properties or electrical insulation. But above all, organic coatings are applied to protect metals from their environment. The first way in which an organic coating does this is by serving as a physical barrier to separate the metal substrate from the environment. Hereby disabling contact between the metal and reactive/aggressive species like water, oxygen and chlorides. For the underlying metal will not corrode if no electrochemical cell is present at the surface. Second, the organic coating may function as a matrix for pigments/corrosion inhibitors.

An organic coating consists of two primary components: a vehicle and a pigment. The vehicle contains the ability to form a film once it is changed from a liquid to solid. Next to the film-forming properties it functions as the carrier for the pigments. Pigments, which do not have to be present are the colouring agents and corrosion inhibitors since organic coatings are often not perfect barriers upon application (porous) or can get damaged upon use. The addition of corrosion pigments can help to improve the barrier properties of the coating by either enhancing the resistance of the coating to permeation of active species or by reducing/preventing corrosion of the underlying metal substrate upon permeation of the active species.

Organic coatings usually consist of a series of coats/films, where each coat has its own functionality. A schematic diagram of an automotive multiple layer coating system is shown in Figure 9. Here it is illustrated that the average automotive coating system consist of a 6 layered-system (metallic coating included).

The pre-treatment layer or conversion layer is applied to improve corrosion resistance, lubricity and the adhesion of subsequent coats. On top of the pre-treatment comes the E-coat (Electrophoretic-coat). The E-coat provides high corrosion resistance and can reach all the corners of the sub-frame components giving a uniform density of coating. The is primer provides good adhesion between the e-coat and the subsequent coats. The primer is the coating in which corrosion inhibiting pigments are incorporated in order to further improve the corrosion resistance of the coating system. The incorporation of 'active' pigments is currently a hot topic. In the case of physical damage to the coating system the concept is to get the pigments to leach out of the primer. The pigments can than protect the metal by either improving the corrosion resistance of the metal or by forming a new physical barrier/polymer coating [26, 27].
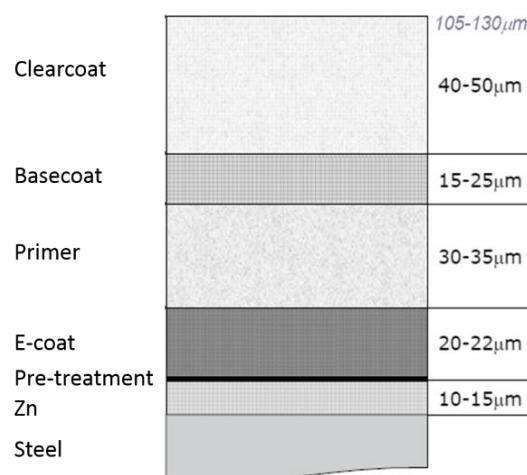
Figure 9: Schematic diagram of a galvanized sample coated with a multi-layered automotive coating system.

The base coat provides the colour of the coating system and has very low corrosion protective properties. Due to this property a thick clearcoat is applied. This is a hard transparent coating proving protection from permeating species, scratches and diminishing of the colour by UV-radiation thereby extending the lifetime of the underlying coatings [3].

2.3 CORROSION INHIBITORS

In the preceding chapter corrosion inhibitors were mentioned as pigments, added to an organic coating to improve the corrosion resistance of the coating and the metal. But corrosion inhibitors are used in a wide variety of applications, reaching from inhibitors in potable water to inhibitors in cooling fluids in engines to usage in the oil recovery process [28, 29].

2.3.1 Classification of inhibitors

A corrosion inhibitor is defined as a chemical substance that, when added in a low concentration to the corrosive environment can increase the resistance to corrosion [30]. Inhibitors can be organic or inorganic species which act by blocking or competing with the mechanism that lead to corrosion.

They can do this by:
- Hindering the corrosive species from getting to the metal surface
  - by depositing a protective layer on the surface
  - by reacting with the corrosive species

- Reacting on the anodic and cathodic sites and lowering the kinetics
  - By forming a complex with the metal

The classification of inhibitors is often not based on their working mechanism but on their ability to either slow down the anodic or cathodic reaction rate or both. Polarization measurement enables us to determine which reaction they affect.

Anodic inhibitors are able to slow down the anodic half reaction of the corrosion reaction by either depositing on the anodic sites of the metal or by reaction with the dissolved metal ions (near the anodic sites) and forming a protective oxide film/passivation layer. The concentration of anodic inhibitors is a critical factor playing part. A too low concentration can cause insufficient coverage of the metal surface. This causes a significant local increase of the current density of the remaining unprotected anodic sites, which leads to local attack of the metal.
Anodic inhibitors can be recognized in a Tafel plot by the reduction of the current density in the anodic polarization curve often paired with a shift of the corrosion potential towards more noble values.

Cathodic inhibitors do not have a critical concentration. Even a small amount of coverage of the surface causes a reduction of the cathodic reaction rate and slowing down the corrosion rate. Cathodic inhibitors work by reducing both the available area for cathodic reaction by covering the surface or by depleting reactive species from the solution (e.g. dissolved oxygen, H^+ and Cl^-).
Cathodic inhibitors can be recognized in a Tafel plot by the reduction of the current density in the cathodic polarization curve. In the case of the so called 'scavengers' who deplete the surface from reactive species, one can observe a change in the polarization curve. Typically hydrogen evolution and oxygen reduction are distinguishable and a switch between the half-cell reactions can be observed.

Mixed inhibitors have the ability to reduce the reaction rate of both half-cell reactions. This can be done in three ways: physical adsorption, chemisorption and film formation. They thereby cover the entire surface and have no particular preference for anodic or cathodic sites. Organic corrosion inhibitors often work based on this principle and hereby inhibit both the anodic and cathodic reaction. Some combinations of anodic and cathodic inhibitors can have a synergistic effect causing both a reduction of the anodic and cathodic current density. The mixture of the two inhibitors can then also be considered a mixed inhibitor.

Many corrosion inhibiting compounds are toxic, like for example chromium-VI of which the use is been limited and soon restricted. Currently lots of research is therefore been done in the discovery/development of 'green' inhibitors that have the same outstanding corrosion inhibiting performance as chromium VI [31]. The difficulty in developing a suitable corrosion inhibitor does not only lie in the ability of the chemical to inhibit corrosion (despite its name).
In the case of adding corrosion inhibitors to organic coatings, more challenges are to be encountered. The inhibitor should be compatible with the matrix, since adhesion of the inhibitor to the matrix' molecules and particle size can have detrimental effects on both mechanical and barrier properties of the coating. If the inhibitor has superior inhibiting properties but badly compatible, capsules can be used to incorporate inhibitors into the matrix [27].
Ideally the inhibitor should have some form of mobility in the coating. If it is able to dissolve in the electrolyte it could leach to damaged parts of the coating or move with the electrolyte to the metal/liquid interface. And final, the inhibitor should be able to perform over a longer period of time.

2.4 BASIC OXYGEN FURNACE-SLAG

A recent study at Tata Steel R&D has resulted in the discovery of the potential of slag to enhance the corrosion resistance of steel products [32]. This can be achieved by either treating the surface of the steel with an aqueous solution, containing slag, or by using slag as a corrosion inhibitor in a coated system.

The process of making steel starts with the production of pig iron, which happens in the blast furnace (BF). During this process iron ore and cokes are smelted and pig iron is being obtained at the end of the process. In order to produce steel, the pig iron needs to be converted by reducing the carbon content. One of the processes (and the one being utilized by Tata Steel IJmuiden) to convert pig iron to steel is the use of a Basic Oxygen furnace (BOF). In the basic oxygen furnace, oxygen and neutral gas are blown into the furnace with liquid steel in order to oxidize carbon and lower the carbon content. During this conversion process lime [CaO] and dolomite [$CaMg(CO_3)_2$] are added to the mixture. Dolomite is added to protect the refractory material of the ladle while lime is added to remove the silicon and phosphorous from the pig iron. In order to control the temperature and prevent the mixture from overheating, steel scrap is added. The lime, dolomite and the molten impurities then form a non-metallic slag on top of the surface of the liquid steel. The chemical composition of the slag is determined during conversion, for this gives information about the progress of the conversion process [33–35]. The steel and slag are then separated by tapping the liquid steel from the bottom of the ladle and the slag then is poured off in the molten state at approximately 1.600°C, solidifying to form a crystalline material.

The composition of basic oxygen furnace slag varies with every batch of steel due to different desired chemical compositions of the different grades of steel that are being produced. Mineralogically the slag is very constant in composition but the proportions of the different phases tend to vary. The mineral compositions of basic oxygen furnace steel slag include olivine, merwinite, dicalcium silicate (C2S), tricalcium silicate (C3S), tetracalcium aluminoferrite (C4AF), dicalcium ferrite (C2F), CaO–FeO–MnO–MgO solid solution (RO phase) and free- CaO, of which C2S, C3S and RO phase are the main phases [34, 36][36]. The mineralogy can be simplified to 5 different minerals. These minerals, their structure and weight distribution in slag is given in Table 1.

Table 1: Chemical composition of BOF-slag determined by SEM-PARC (micro-analysis)[2]

Compound	Structure	wt%
Lime	CaO	5
Wuestite	FeO	30
Srebrodolskite	$Ca_2Fe_2O_5$	20
Larnite	Ca_2SiO_4	31
Hatrurite	Ca_3SiO_5	15

Basic oxygen furnace slag is a significant residue of the steel production with about 100-200 kg being produced for every ton of steel [5]. It is estimated that every year 12 million tons (Mt) are generated in Europe of which approximately 650 kiloton (kt) is produced annually at the IJmuiden-site of Tata Steel [37].

Much research is being done on the reutilization of basic oxygen furnace slag because for long time it has simply been stored[38][39][40]. Most of this work is done in the area of civil engineering. Because of the higher CaO content than in an electric arc furnace (EAF) and BF-slag, BOF-slag is less preferred

---

[2] *summarized composition of BOF-slag, for full details see Appendix A.

as material for use in the manufacturing of concrete. This is primarily due to the increased risk of cracking caused by the hydration reaction of CaO.

Next to basic oxygen furnace slag there are more slags coming from the steel-making process. All of these slags are named for the process at which they are produced: Blast furnace (BF) iron slag, Electric arc furnace (EAF) steel slag and Ladle furnace (LF) slag. Ladle furnace slag is a different type of slag than basic oxygen furnace slag, but also comes from the steel plant on the IJmuiden-site. After tapping from the basic oxygen furnace, the ladle furnace is used to refine the alloying of the steel. In this refining process the liquid steel is arc heated and argon is blown through. During this process the deoxidization, desulphurization and adjustment of chemical composition are completed [41].

2.5   ELECTROCHEMICAL ANALYSIS METHODS

Before evaluating the impact of inhibitors in real systems, i.e. coated metals, the potential of inhibitors must be assessed in terms of corrosion inhibition "capability" on the material of interest (steel with GA and MZ coating in the case of this study). Therefore, tests that put the bare surface of the material in contact with corrosive solutions containing the potential inhibitors should be performed. This gives an indication of inhibition efficiency, excluding the issue of inhibitor/polymer matrix compatibility. Two types of methods can be used which are complementary: immersion tests and electrochemical methods. During electrochemical tests we control or measure the potential difference, magnitude of polarization and current during reactions. The study of potentials as a driving force is founded in thermodynamics and the study of current measurements is founded in kinetics of corrosion, as was shown earlier.

2.5.1   Voltammetry

Voltammetry is the collective name for all electrochemical techniques during which current is measured as a function of applied potential. Voltammetry can be used to study the kinetics of an electrode but can also be used to identify species in solution or to determine their concentration. It is possible to directly measure the corrosion potential of the system for it is the potential at the OCP. But it is not possible to directly measure the exchange current density at the OCP. To measure the exchange current density one needs to bring the system out of the equilibrium state by means of anodic and cathodic polarization. By plotting the recorded current as a function of the applied current or polarization, one can construct a polarization curve. The obtained plot is then the Tafel plot, as was covered in section 2.1 Corrosion of Metals.

The experimental setup for recording a Tafel plot is illustrated in Figure 10. The working electrode is the electrode in which one is interested (your metallic sample). Between this working electrode and the inert counter electrode (usually platinum or graphite) a current is send by an external source (potentiostat).
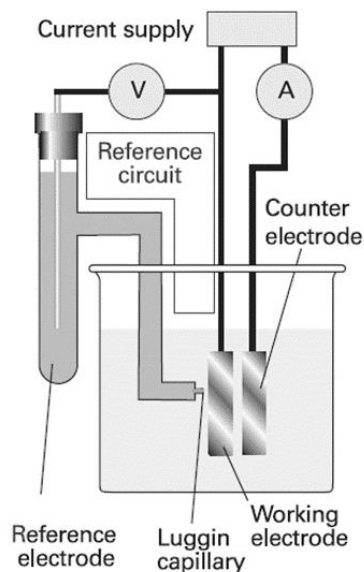
Figure 10: Experimental setup for electrochemical measurements using a standard calomel electrode (SCE) [6].

In order to measure the potential and the change in potential as a response to the applied current, the presence of a third/reference electrode is required. Earlier the standard hydrogen electrode (SHE) was explained. The resulting potential from this reference electrode is set to 0 V, so all measured potential originates from the system under observation. Another frequently used reference electrode is the saturated calomel electrode (SCE). The saturated calomel electrode consists of pure mercury covering a platinum wire which passes through a sealed glass tube. The mercury is covered with mercurous chloride and immersed in saturated potassium chloride. The reference reaction is;

$$Hg_2Cl_2 + 2e^- \rightarrow 2Hg^+ \; 2Cl^-$$

(0.20)

The resulting potential of this electrode is -0.268 V vs. SHE. Electrodes whose potential barely varies when a current flows through the system are called non-polarizable electrodes. SHE and SCE are a good example of this type of electrode. This property makes it suitable as a reference electrode.

The reference electrode is in contact with the working electrode via the electrolyte to complete the reference circuit. The reference is to be close to the surface of the working electrode via the Luggin probe and capillary. This is in order to prevent potential differences due to ohmic resistance. By changing the current through the working circuit (no current goes through the reference circuit) the potential of the working electrode changes which can be recorded by a voltmeter versus the reference electrode. The overpotential can then be acquired by taking the difference between the open circuit potential and the recorded potential. The current density is acquired by dividing the applied current by the surface area of the working electrode. The reverse can also be utilized to record the polarization curve. By changing or 'sweeping' the potential between the working electrode and the reference electrode linearly in time, the current at the working electrode changes. This response in current density can be recorded to plot the polarization curve. This method in which the potential is swept linearly in time is called Linear Sweep Voltammetry (LSV).

2.5.2   Electrochemical Impedance Spectroscopy

Electrochemical impedance spectroscopy (EIS) can be considered a well-established technique in corrosion research which has been applied successfully in studies of many corrosion systems [42–44]. The reason for this is because EIS is a powerful tool to study the kinetics of electrode reaction processes in a non-destructive manner. EIS can be used to study the metal solution interface, oxide layers but

also to assess the corrosion behaviour of organic coatings on metals. EIS is therefore very suitable to assess not only the corrosion rate but also to study and determine the corrosion/inhibition mechanisms [3].

Unlike voltammetry, EIS consists of imposing a small alternating current (AC) signal, ranging from 5-20mV versus OCP, to the electrochemical system and analyse the response of the system.

The concept of electrical resistance is well known and describes the ability of an electric system to resist the flow of current. This concept is described by Ohm's Law ($R = V/I$) but holds for only one circuit element, the ideal resistor. An ideal resistor is a resistive element that follows Ohm's Law, independent of current, voltage and frequency. This means that in response to an alternating current (AC) the voltage and current signals are in phase.

There are many other circuit elements who exhibit more complex behaviour and for these element we use Impedance, Z. Where impedance is the ability to resist alternating current.

Figure 11 shows a sine wave voltage applied to an electrochemical system. The current through the system in response to this potential is also shown. Like the voltage, it is a sine wave but it has shifted in time due to the slow response of the system. This shift in phase can be expressed as a phase angle. The ratio of the size of the voltage sine wave (in volts) to of the current sine wave (in amps) gives the impedance of the system. The magnitude of the impedance is given in ohms, just like resistance, and is written as |Z| [45].

In order to evaluate the impedance of a system you need three parameters; the magnitude of impedance |Z| (Ohm), the phase angle Φ (degree) and the frequency f (Hz). These three parameters are then plotted on a Bode plot and are often used to analyse EIS data.
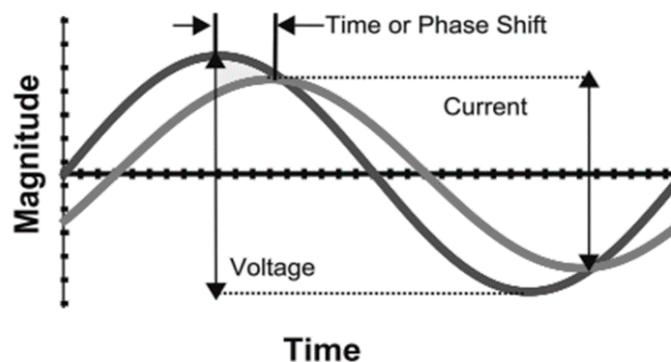
Figure 11: Current and voltage as a function of time. Note the time/phase shift between them [45]

The magnitude and phase angle information from the bode plot can be displayed in a polar figure as a vector where the length of the vector is represented by the magnitude and the angle of the vector by the phase angle. The end of the different vector can be plotted in a Cartesian coordinate system where the x-axis is labelled as the Real part and the y-axis as the Imaginary part of the impedance:

$$Z = X + jY \; where \; j = \sqrt{-1} \tag{0.21}$$

This plot where the Cartesian coordinates of the impedance at multiple frequencies is plotted, is referred to as the Nyquist plot and is together with the Bode plot used to analyse EIS data.

The electrochemical systems that are imposed by the AC potential (e.g. corroding surface or coated metal) can be described as electrical circuits consisting of different electrical equivalent circuit (EC)

elements. A list of some common equivalent circuit models with their complex notation is given in Table 2. The resistor was mentioned earlier and obeys Ohm's Law, hence $Z = R$. The phase angle of a resistor is zero since its response in current is completely in phase with the applied voltage. Also the amplitude of the current wave only depends on the value of R. An example of a pure resistor is the resistive behaviour of the electrolyte [45].

Table 2: Table 2: List of common equivalent circuit models.

Element	Symbol		Impedance
Resistor	R		$Z = R$
Capacitor	C		$Z = \dfrac{1}{\omega C}$
Inductor	L		$Z = j\omega L$
Constant Phase Element	C		$Z = \dfrac{1}{(j\omega)^n Y_0}$
Warburg (semi-infinite diffusion)	W		$Z = \dfrac{1}{\sqrt{(j\omega)}Y_0}$
Warburg (finite diffusion length)	W$_s$		$Z = R_d \left[\dfrac{\tanh(j\omega B)^n}{(j\omega B)^n}\right]$ with $B = \dfrac{\delta_N}{\sqrt{D}}$
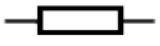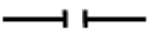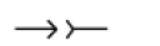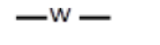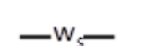
The capacitor is another simple circuit element and can be thought as a non-conducting material (dielectric) sandwiched by two conducting plates. The phase angle of a pure capacitor is -90°. At high frequencies the voltage alternates rapidly and the current reaches high values which leads to smaller impedance. If the frequency goes to low values the current is zero due to the dielectric element and the impedance approaches infinitely large values. The Bode magnitude plot of a capacitor is a straight line with a slope of -1 and the phase angle is a straight line at -90°. The electric double layer is an example of a capacitor but also an organic coating on a metal substrate can have capacitor-like behaviour.

In order to process the data obtained by EIS one needs to construct an electrical circuit that is equivalent to the measured electrochemical circuit. A simple example of this is the Randles Cell, illustrated in Figure 12. The Randles-cell constitutes of a capacitor combined with two resistors. This model is often used to represent an intact coating or a corroding surface [46–48].
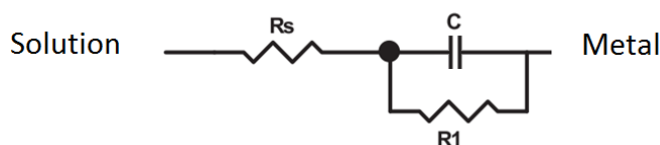
Figure 12: The Randles-cell equivalent electrical circuit. Described by the solvent-resistance in series with a capacitor and resistance.

If this model was to be applied to a corroding metal surface, Rs would represent the resistance of the electrolyte solution between the surface of the coating and the reference electrode. The capacitor, C, represents the double layer capacitance (Cdl) created by the electric double layer (edl) on the metal/solution interface. The double layer capacitance usually has values between 10-100 µF/cm2 (where F is farads). The resistor parallel to the capacitance represents the polarization or charge transfer resistance of the metal (Rp). If we simulate a Randles cell, we obtain a Bode- and Niquist plot like the ones in Figure 13. It was mentioned that a resistor is independent of frequency and gives a straight line in the magnitude plot and a 0° phase angle. This is represented in the Bode plot in the high and low frequency region. Where the high frequency region (right side of Bode plot) gives the impedance of the solvent (R_s) and the straight line in the low frequency region represent the sum of the polarization resistance and the solvent resistance (R_s+R_p). The capacitor has infinite impedance in the low frequency region and acts as if it is not there, hence the line only represents R_s+R_p. In the high frequency range, the impedance of the capacitor goes to very low values, causing all current to pass through the capacitor and no current through the parallel resistor. The impedance then is only R_s.
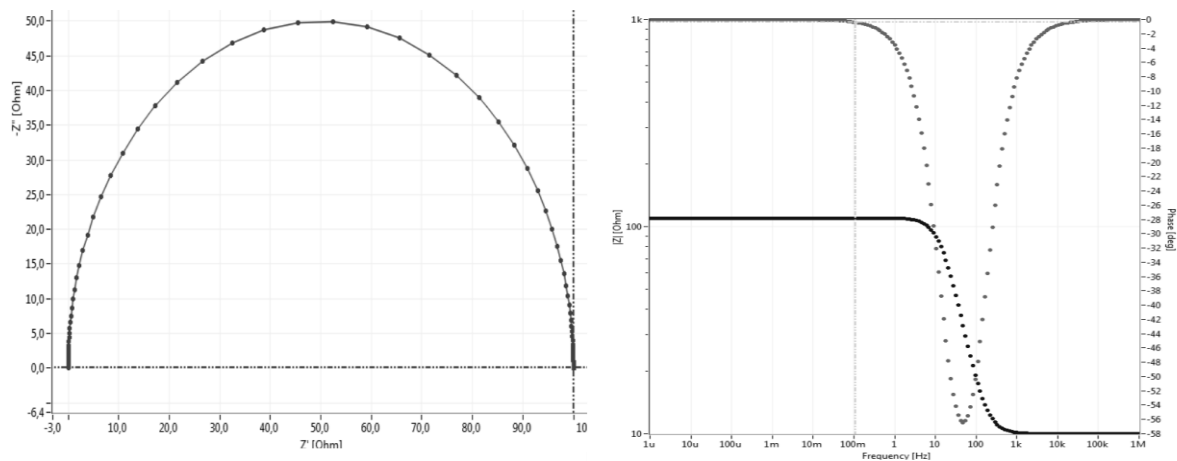
Figure 13: (left) Nyquist plot and (right) Bode plot for the Randles cell.

In the mid frequency range the capacitor can be identified. It has a significant contribution to the impedance and causes current also passing through R. This results in the value of |Z| lying in between R_s and R_s+R_p. In the middle of this region, the phase angle starts to approach -90°, the angle for a capacitor. In the Niquist plot the same trends can be observed, only here the values of R_s and R_p+R_s can be read from the intersection of the semi-circle with the x-axis. The Niquist plot runs from right (low frequencies) to the left (high frequencies).

The randles cell is a simple example of how an equivalent circuit can be fitted to an electrochemical system. Usually more complex equivalent circuits are required as will be seen in later chapters.

2.6 SURFACE ANALYSIS

Surface analytical instrumentation can help us by providing data which helps us to understand corrosion (inhibition) mechanisms. Techniques like SEM and XPS can provide much information on the corrosion (inhibition) mechanisms on an atomic level and have therefore proven useful in many studies [42, 49–51].

2.6.1 Scanning electron microscopy

Scanning electron microscopy (SEM), together with energy dispersive spectroscopy (EDS), is frequently used in various investigations of materials [52]. With these two techniques one can study the surface morphology and determine the composition of the surface locally on a microscale.

With SEM an image of the surface is formed by the use of moving electron beams. These beams of high-energy electrons generate a variety of signals at the surface. The accelerated electrons in the beam carry sufficient kinetic energy and interact with the atoms of the specimen. These interactions will generate electrons due to elastic and inelastic collisions. The electrons that are emitted again from the surface are then detected as secondary electrons (SE), backscattered electrons (BSE or AsB) and diffracted backscattered electrons (EBSD). Apart from emitted electrons, photons are emitted upon the interactions between the incident electron beam and the bounded electrons of the material. These characteristic X-rays can then be used for elemental analysis.

2.6.2 X-ray photoelectron spectroscopy

X-ray photoelectron spectroscopy (XPS) is a surface analysis spectroscopic technique that is able to measure the element composition, chemical state and the electronic state of the elements that exist within a material.

In XPS, the surface of the studied materials is excited with mono-energetic x-rays (often Al kα x-rays) who via the photon absorption process emit photoelectrons from the surface [53]. During the photon absorption process, the entire energy hν of the photon is transferred to the atom's electron. The kinetic energy of the emitted electrons that escape without energy loss is then measured with an energy analyser, see Figure 14. The kinetic energy is directly related to the binding energy of an electron in the target atom.
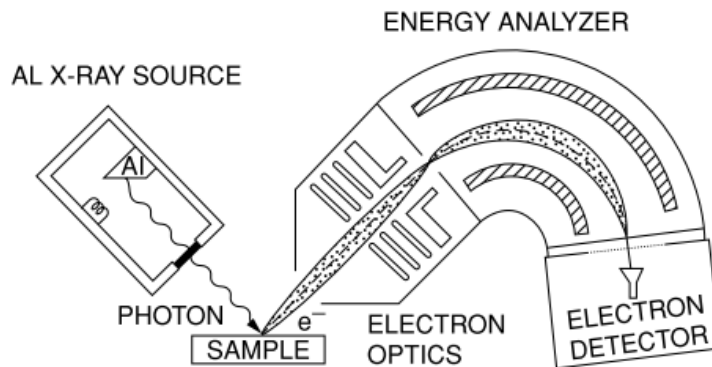
Figure 14: Schematic setup used in X-ray electron spectroscopy (XPS). The x-ray photons are generated in the aluminium anode and then impinged on the sample. The absorption of the photons cause emission of photoelectrons whose kinetic energy is then measured in the energy analyser [53].

The data is represented as a graph of intensity versus electron energy. Each element has a characteristic electronic structure and thus a characteristic XPS spectrum. From the binding energy and the intensity of the peak, the elements and their chemical state can be determined. By the number of counts per peak a quantification of the elemental composition can be made.

2.7 COATING PERFORMANCE TESTING

2.7.1 Salt spray test

The salt spray test (SST) is a widely used technique. Especially in the construction material industry it is often used to investigate the corrosion resistance of diverse metals and coatings. The salt spray test is an accelerated degradation test which enables the investigation of long term corrosion resistive performance of coatings. The main advantage of this technique is the relatively short duration of the test (common test duration is 21 weeks).

A common procedure is described in the ASTM B117 standards. During this procedure panels are being placed in a constant, high relative humidity (RH) environment (~97%). The corrosive media is usually a 5 wt% NaCl solution of around 35 °C [54].

Samples that are to be tested using the salt spray test are often scribed. If the samples are not damaged intentionally but bended or kept flat, the failure of the coating reflects the presence of pores and cracks in the coating [55].

2.7.2 Electrochemical Impedance spectroscopy

As was mentioned in section 2.5.2, electrochemical impedance spectroscopy (EIS) can be used to study the kinetics and mechanism of open system corrosion (bare metal in solution) but also to study the kinetics and performance of organic coatings. In order to be able to assess the performance of organic coatings a stress must be included in order to induce the failure of the coating. The failure coating of the coating is then observed by monitoring the periodic EIS-measurements.

A metal substrate coated with a perfect (undamaged) coating could be represented by the Randles-cell, which was explained earlier. But in the case of coated metal 'R' and 'C' do not represent the polarization resistance and the double layer capacitance. Let's assume the coating has tiny pores (due to the applied stress) in which the electrolyte slowly leaches. These pores have a certain resistance and this resistance to electric current by the pores is represented by 'R', usually depicted as the 'pore resistance'.

The capacitor 'C' represents the coating which is characterized by the thickness and dielectric constant of the coating material. Due to the absorption of water the dielectric constant of the coating changes and the value of the capacitance will do so too. Monitoring the value of the capacitance is a common method to assess the water-uptake of organic coatings [56].
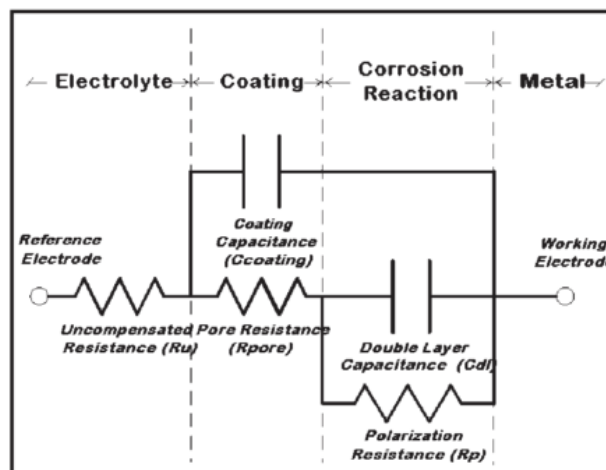
Figure 15: Equivalent circuit of an organic coating on a metal substrate that is corroding [57]*.*

When the pores start to get bigger and their resistance starts to drop the electrolyte can penetrate to the metal surface, which than starts to corrode. Two more circuit elements need to added in order to represent the current electrochemical system under surveillance. We then acquire the equivalent circuit illustrated in Figure 15.

The electrolyte that has penetrated the coating is causing corrosion of the metal. Just like in the open system an electric double layer is formed on the metal-liquid interface, represented by the double layer capacitor. And the second 'R' represents the polarization resistance of the corroding metal.
Just like in the case of an open system, there are many more complicated coated systems and complicated equivalent circuits that are needed to represent them. More details will be discussed in the section Results and discussion.

3 EXPERIMENTAL

3.1 INSTRUMENTS
This paragraph aims to give the specific details of the used instruments. All experiments were carried out at the R&D research centre of Tata Steel IJmuiden (NL) in collaboration with the Coating development group.

3.1.1 Potentiostats
Linear sweep voltammetry (LSV) was performed on a Solartron Analytical 1280C Potentiostat. The potentiostat was used to measure the open circuit potential (OCP) and to apply a potential to polarize the sample and acquire the corresponding current density. The software used to obtain these measurements was Corrware 2.9b2.
Electrochemical impedance spectroscopy (EIS) measurements were performed using a Zahner IM6 modular electrochemical workstation with a frequency range up to 8 MHz at ±3.0 A and a compliance voltage of ±14 V. The software used for the interpretation of the measurements was ZIVE ZMAN™ 2.3. Both EIS and LSV were performed using standard calomel electrodes (SCE) as reference electrode (RE).

3.1.2 Scanning electron microscope
Scanning electron microscope images were acquired using a Zeiss Ultra Plus. The secondary electron mode and the backscattering electron mode were the operation mode for gathering the images. The primary electron beam was accelerated to 10 keV, unless otherwise indicated. The EDS detector was a Everhart-Thornley detector with a resolution of 129.65 eV. The EDS instrumentation by EDAX is integrated into the SEM installation. The software linked to this system was Zeiss Smart SEM for processing the image and EDAX Genesis for EDX analysis.

3.1.3 X-ray electron spectroscope
XPS measurements were performed using a Kratos AXIS Ultra DLD x-ray photoelectron spectroscope. Acquired data was subsequently analysed using Kratos Vision Acquisition and Processing software.

3.1.4 Salt spray equipment
The salt spray tests (SST) were conducted in a Q-Fog SSP cyclic corrosion tester. The various coating systems have been evaluated through salt spray (fog) test according to ASTM B117 standards.

3.2 MATERIALS

3.2.1 Metal substrates

Most of the tests have been performed on three different types of hot dip galvanized (HDG) steel; Galvannealed (GA), Galvanized (GI) and Zn-Al-Mg (MZ or MagiZinc©) coated steel. All GI, GA and MZ samples were produced on commercial production lines and their physical/chemical details are given in Table 3.

Table 3: Physical and chemical details of used substrates

	Coating weight evaluated side (g/m2)	*Coating thickness (μm)*	*Al%*	*Mg%*	*Fe%*
GA	45	7	0.3	<0.01	10.2
GI	69	10	0.4	<0.01	0.36
MZ	44	7	1.6	1.6	0.13

The difference in between GA and GI is due to the post-galvanizing heat-treatment (annealing) of the metal. This creates different Zn/Fe rich phases and a different morphology in the GA coating than is to be found in GI.

3.2.2 Inhibitors and solution preparation

The inhibitors used in this work are commercially available inhibitors provided by different suppliers. These inhibitors have been used to make a comparison of the inhibitor efficiency with the main inhibitor. The used chemical are listed in Table 4.

Table 4: Inhibitors used and characteristics.

Name	*Compound*	*Source*
Halox® SW-111[3]	Strontium polysilicate	ICL\ Advanced Additives
Novinox® XCA02[4]	Silica based	SNCZ
Novinox®ACE-110[5]	Zinc phosphate + add.	SNCZ

The main inhibitor used in this work is grinded basic oxygen furnace (BOF) slag. The BOF slag was obtained from the oxysteel plant on the TATA Steel site in IJmuiden (NL). The chemical composition of the slag has been determined in previous work by S. Van der Laan et al [37] and their results are shown in Table 1.

The electrolyte solutions were prepared by dissolving the inhibitors (1 or 2gL^{-1}) in a 0,1 M solution of NaCl in distilled water. In the case of BOF-slag, the electrolyte solution was stirred for 72 hours and filtered using Whatman® filter paper, retrieving a clear solution.

---

[3] In the rest of this report, Halox® SW-111 will be referred to as Halox.
[4] In the rest of this report, Novinox® XCA02 will be referred to as XCA02.
[5] In the rest of this report, Novinox®ACE-110 will be referred to as ACE-110.

3.2.3 Organic coating

3.2.3.1 Formulation

The coating used for this study is a water-based polyamide-imide based formulation. This formulation, supplied by Solvay Specialty Polymers has been developed in collaboration with Tata Steel and was chosen for its barrier properties, chemical and thermal resistance and environmental friendliness. This polymer will be referred to as "PXM 13159" in the coming pages. The polymer content of the formulation was adjusted to 8 wt% by the addition of distilled water. A wetting agent, BYK380N, was added to the formulation with a concentration of 0.3 wt% to guarantee good coatability. Three different coatings were formulated. A reference coating with no pigment added and two coatings with corrosion inhibiting pigments added. A 1 wt% concentration of pigment was added as was determined to be the best performing concentration in this formulation by M. Wainer [58]. Based on the results from the potentiodynamic polarization measurements, BOF slag and NOVINOX® XCA02 were selected as corrosion inhibitor. Formulations will be detailed along with the results.

3.2.3.2 Coating application

The substrates (GA and MZ) were cut to size (120x150 mm) and deburred along the edges to improve the application of the coating.

Prior to coating, the substrates were cleaned in an alkaline cleaning bath according to the following procedure;

- o Immersion of the samples in an alkaline bath (2,0 wt% solution of Cleaner 219) at 58°C +/- 2°C under agitation (stirrer set to 500 rpm) for 1 to 2 minutes.
- o Samples are further cleaned using a soft brush to remove all dirt and oil and subsequently thoroughly rinsed with distilled water.
- o The substrate is checked for homogeneous wetting/film formation (water break). If this is not observed the previous steps are repeated.
- o Samples are dried with an air-pressure gun.

The application of the coating formulation was done with a wire bar with an automatic bar coater; directly after the substrate cleaning process. After application on the substrate, the coating was dried in an oven at 100°C for 2 min and cured at 265°C for 8 min. After curing, the sample is cooled using a flow of distilled water. This should result in a dry coating thickness of 5-8 μm.

3.3 METHODOLOGY

3.3.1 Potentiodynamic Polarization Measurements

The steel samples were cleaned according to the same procedure as when the samples are to be coated (See procedure in Coating application). The samples are then placed in a Princeton Applied Research Model K0235 Flat Cell (see Figure 16). The Flat Cell is constructed of a Pyrex™ glass cylinder body with polypropylene end caps and with three electrodes. The counter electrode: Nickel mesh, the reference electrode: standard calomel electrode (SCE) and the working electrode: steel substrate with a surface area of 1 cm^2. All potentiodynamic polarization measurements were performed in a 0.1M NaCl solution +/- 1gL^{-1} inhibitor.
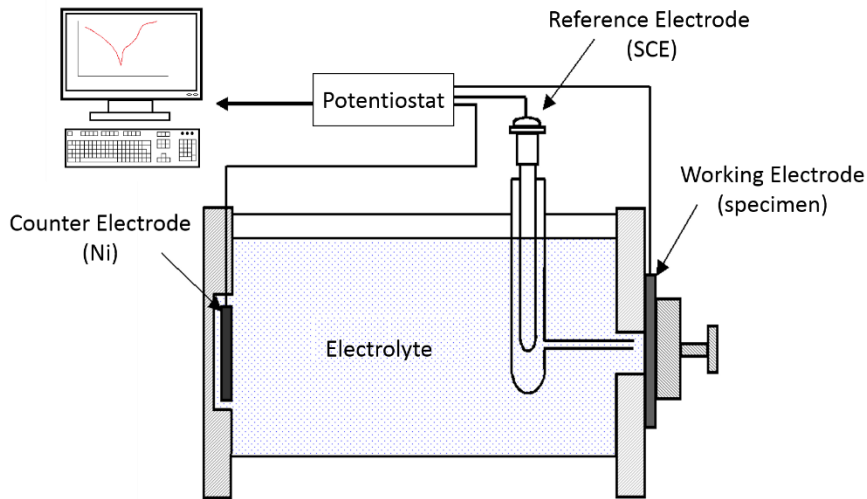
Figure 16: Schematic of the set up for potentiodynamic measurements

The program for anodic polarizations was set to:
- o   OCP measurement for 55 minutes
- o   Anodic polarization from -0.03V to 0.5V vs. OCP. Scanning rate was set to 1mV/s.

The program for cathodic polarizations was set to:
- o   OCP measurement for 55 minutes
- o   Cathodic polarization from 0.03V to -0.5V vs. OCP. Scanning rate was set to 1mV/s.

Only 1 measurement (anodic/cathodic) was performed per tested area. This is done because of the possible alteration of the surface chemistry and morphology after polarization.

3.3.2   Electrochemical Impedance Spectroscopy

Electrochemical impedance spectroscopy was performed on both bare substrates as on coated samples. For the prior the preparation of the sample is similar to the procedure for potentiodynamic polarization measurements. Samples of 50x70 mm of bare or coated specimens were clamped horizontally in a pvc electrochemical cell. The setup of this cell is illustrated in Figure 17.
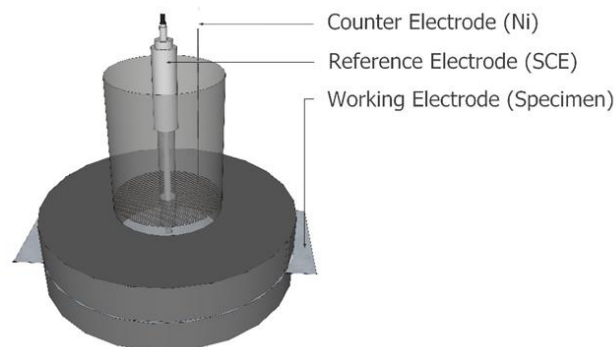
Figure 17: Schematic setup for electrochemical impedance spectroscopy measurements. The specimen was placed between the bottom disc and the top section.

The flat sample was placed between the bottom disc and the top section consisting of a circular flat element with a vertical tubular section with a surface of ~7 cm^2. The tubular section was filled with electrolyte to immerse the sample. A round and hollow nickel gauze was placed in the tubular with a standard calomel reference electrode in the centre.

The selected frequency range was from 100 kHz to 10 mHz. The open system, consisting of the bare substrate (GA/MZ) in contact with the electrolyte was tested using a 5 mV RMS sinusoidal perturbation vs. OCP as input signal.

Prior to testing of the coated specimens a hydraulic press was used to deform the coated samples pressing a dome with a dome height of 2 mm in the sample. Subsequently the samples were tested using a 10 mV RMS sinusoidal perturbation vs. OCP as input signal. The measurements were performed from 0 to 21 days of immersion.

3.3.3   Salt Spray Test

The various coating systems have been evaluated in a salt spray test (ASTM B117). Tested coatings either contain no or 1 wt.% of corrosion inhibitor pigment. Prior to testing the samples were deformed by a hydraulic press in a 90° angle lengthwise. The rear and uncoated edges of the samples were sealed and the samples were placed upright in a 60° angle, as is shown in Figure 18.
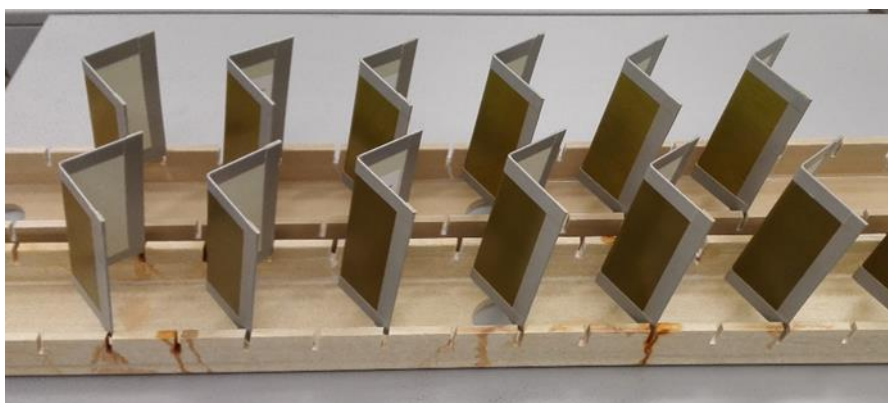
Figure 18: Experimental setup for the salt spray test. Bended samples were taped at uncoated areas and placed upright in a 60° angle.

4   RESULTS AND DISCUSSION

In the first section of this chapter the results of the first part of the study which has been performed on the 'open' system will be discussed. In the final section the results will be presented of the second part of the study, performed on the coated material.

4.1   THE EFFECT OF BOF-SLAG ON CORROSION IN SOLUTION

4.1.1   Potentiodynamic polarization measurements

Corrosion inhibition of two different types galvanized steel (GA and MZ) in solution was studied using Voltammetry. The inhibition of the corrosion of the zinc coating can be studied using the curves of the potentiodynamic polarization scans acquired using linear sweep voltammetry (LSV). The inhibiting effect of the added compounds can be read from the change of the curves of the potentiodynamic scans. Separate curves were acquired with anodic and cathodic polarization scans, who combined give the total polarization curve of the tested material. Multiple polarization scans were made to check the reproducibility of the data. The electrolytes consists of a 0.1 M NaCl aqueous solution with 1 gL^{-1} of commercial inhibitor or 2 gL^{-1} of BOF-slag (for full preparation of the solution see section: 3.1.2 Inhibitors and solution preparation). A potentiodynamic polarization scan of the two substrates without inhibitor was performed as a reference measurement.

Figure 19 shows the results of the Potentiodynamic polarization measurements of GA in the reference and four inhibitor-containing solutions. The anodic polarization scan is performed towards the more positive potential values versus OCP and represents the anodic dissolution of the coating material. The cathodic polarization is performed towards the more negative values of the potential versus OCP and this part of the curve represents the reduction of dissolved oxygen. The anodic and cathodic curves congregate in a sharp peak which represent the open-circuit potential and equals the corrosion potential of the tested material. In the case of the reference measurement, the OCP is -0.901 V (vs. SCE). From the anodic peak we can observe no passivation and we see that the anodic dissolution of zinc from the coating is initially activation controlled up to approximately -0.82 V (vs. SCE). At increasing positives potentials the curvature of the curve changes and the reaction becomes more and more diffusion controlled. This is indicted by the nearly flat shape of the curve as it approaches -0.40 V (vs. SCE). The cathodic curve is almost linear and the cathodic current density is rather low (~20 µA cm^{-2}) from the vicinity of OCP up to ~-1.10 V (vs. SCE). This value agreed with data reported in literature for oxygen reduction on the interface [59]. At approximately -1.22 V (vs. SCE) a small peak can be observed which corresponds to the reduction of a very thin oxide layer which has formed during the exposure to air and the exposure time to the solution prior to polarization.
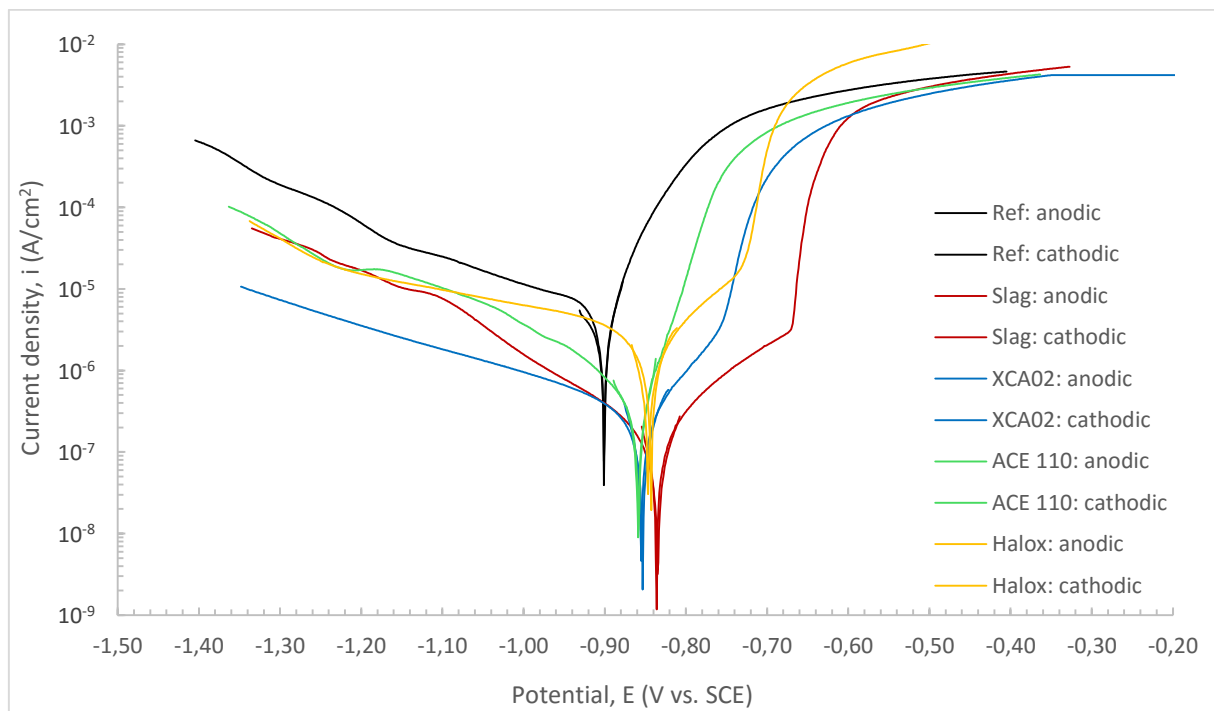
Figure 19: Tafel plot (i,E diagram) of the tested inhibitors on GA

After the reference measurement was performed, a range of commercially available corrosion inhibitors were tested to benchmark the performance of the BOF-slag against. Since the chemical composition of some of these inhibitors was not fully known, a concentration of 1 g L^{-1} was chosen. The results of the potentiodynamic polarization measurements performed on GA exposed to these different solutions are also given in Figure 19. It can be observed that all inhibitors have shifted the open-circuit or corrosion- potential to more positive (noble) values. The curves reveal that all inhibitors reduce the cathodic current density, with slag and XCA02 having the largest effect and Halox the smallest. No true significant changes in the shape of the cathodic curves are observed, suggesting the type of reaction on the interface is unchanged.

The anodic current density is significantly affected by all. ACE-110 lowers the anodic current density but the shape of the curve is somewhat identical to the shape of the reference measurement. The three other inhibitor-containing solutions have significantly lowered the anodic current density. For the BOF-slag solution, this decrease in current even is about two decades at 150 mV from OCP versus the reference solution. Besides lowering the current, they altered the shape of the anodic curve which indicates the anodic dissolution is suppressed by the formation of a passivation layer or by the deposition of protective species on the surface.

Halox can be described as an anodic inhibitor due to its significant effect on both the values of the anodic current and the shape of the anodic curve. Nevertheless, its effect on the cathodic branch is minimal, hardly influencing the cathodic reaction.

The other three inhibitors (including BOF-slag) are mixed inhibitors based on the observation that they all have a reducing effect on both the cathodic and anodic branch of the polarization curve. On the other hand, they all have a more profound effect on both the anodic current and the shape of the anodic branch. Combining this with the shift of the corrosion potential to more noble values, suggesting the larger effect on the anodic reaction, would depict them as anodic inhibitors.

From Figure 19 it can be concluded that of the commercial inhibitors, XCA02 best inhibits the corrosion of GA in a 0.1 M NaCl solution. It can also be concluded that BOF-slag, when benchmarked against these commercial inhibitors, performs better. This can be seen more clearly in Figure 20. Where the polarization curves of XCA02, BOF-slag and the reference solution were smoothened and plotted in the same graph. Although the corrosion current density cannot be read directly from such a plot we can see that the curve of BOF-slag has the lowest overall current density in the vicinity of the corrosion potential of the three curves.
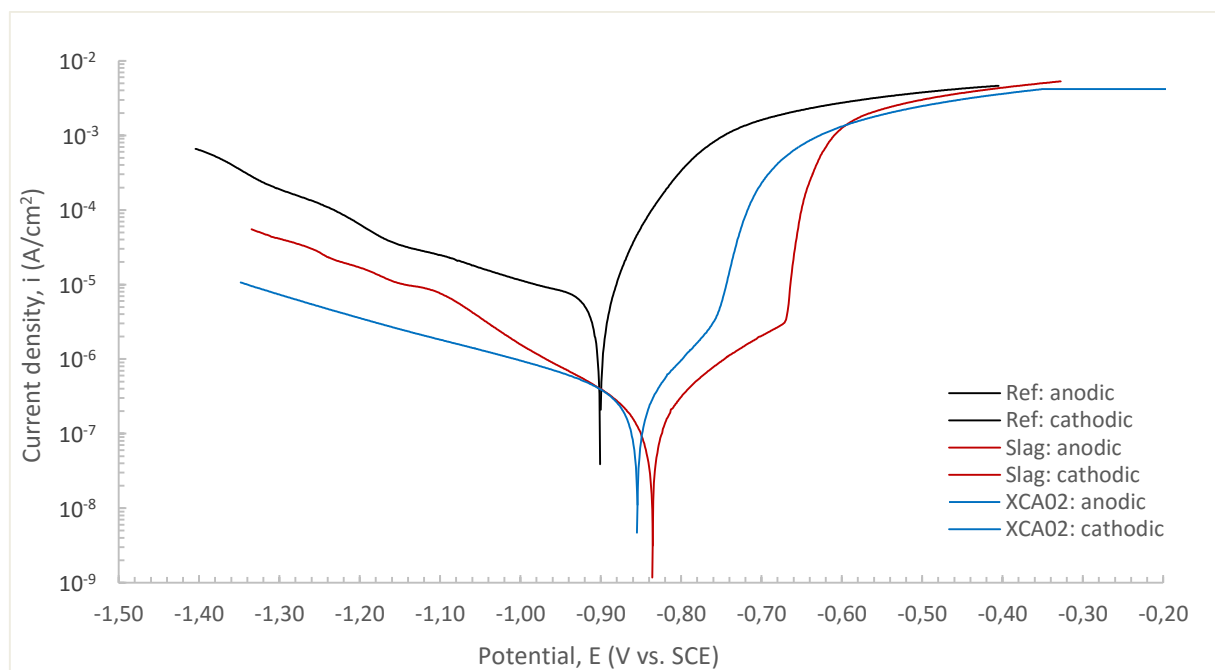
Figure 20: Tafel plot (i,E diagram) of XCA02 and BOF-slag vs. the reference solution on GA

The BOF-slag solution was prepared by adding 2 grams of BOF-slag to 1 L of DI water. The mixture was then stirred for a longer period of time, because it was discovered earlier that this enhances the inhibition performance of the slag [60]. The time the solution was stirred was studied again in order to find an optimum. Potentiodynamic polarization scans were done after 3, 24, 72 and 96 hours of stirring.

The effect of stirring time is shown in Figure 21, where for clarity only the curves after 3 h and 72 h are plotted. It can be seen that after 3 hours of stirring the solution reduces the anodic current but at ~0.12 V vs. OCP the current starts to increase and go towards uninhibited values. The solution that was stirred for 72 hours shows similar inhibition behaviour as the '3h-solution' but is able to suppress the current up to higher polarization values. At ~0.2 V vs. OCP the current is still two decades lower than the reference sample. When increasing the stirring time beyond 72 hours, no significant increase in the performance of the slag-solution is observed. This indicates that 72 hours is the most efficient stirring time.
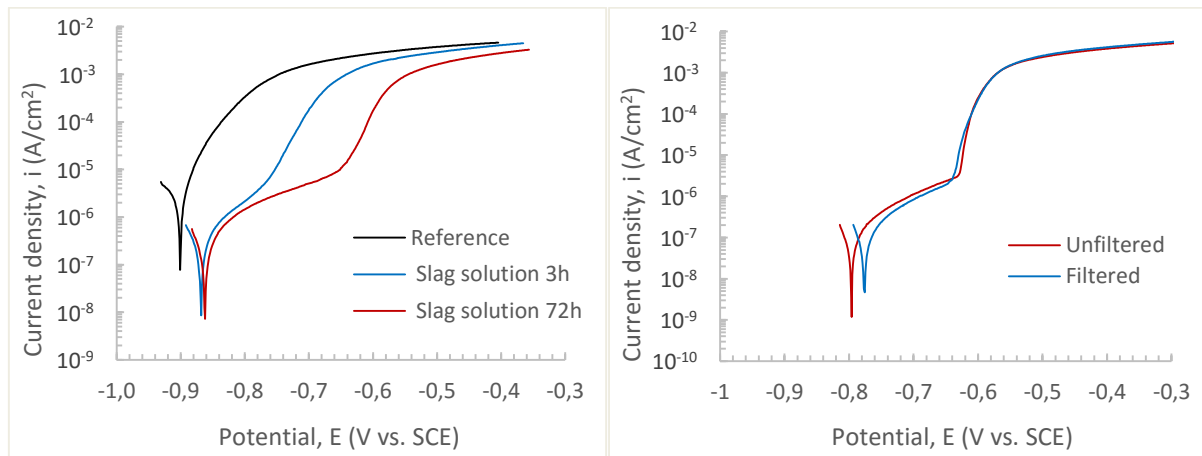
Figure 21: Tafel plot (i,E diagram) of (left) 2 slag solutions (2gL^{-1} BOF-slag) with different stirring times and (right) the effect of filtration on the performance of the slag solution.

The effect of stirring-time on the performance of the slag-solution suggest the slag reacts with the solution, either by direct dissolution or by hydrolysis of the crystalline phases in the slag. According to literature, the di- and tri-calcium silicate (C2S and C3S respectively) and lime are the main active components in BOF-slag. Upon hydration small amounts of calcium and silicate go straight in solution but the main products are Ca(OH)$_2$ and a Calcium Silicate Hydrate (CSH) gel with increasing Ca/Si ratio as alkalinity rises [34, 61]. The wuestite and srebrodolskite do not appear to react with the aqueous solution.

The leaching behaviour of the slag, where mainly silicates and calcium hydroxides go into solution, combined with the proven effect of stirring-time indicates the active components are the water-soluble product of the hydrolysis of the slag. The earlier used solution was a partial suspension of fine slag particles in the aqueous solution. An earlier study at Tata Steel suggested that the slag particles were able to enhance the formed oxide on the zinc surface. In order to investigate if all the active components of the slag are water-soluble, half of a slag-containing solution was filtered and the other half was left unfiltered. The results of the potentiodynamic scans with both solutions are shown in the right plot of Figure 21. It can be seen that after filtering of the solution similar results are obtained compared to the unfiltered slag solution, proving the active components of the slag are the water soluble hydration products.After confirming the active components are in solution, the chemical composition of the BOF-slag solution was determined using ICP-MS, see Table 5.

Table 5: Chemical composition of BOF-slag solution, prepared by stirring 2g of BOF-slag in 1 L DM-water, determined by ICP-MS

Element	Concentration
	mg/L
Al	0,4
Ba	<0.5
Ca	106
Cd	<1
Co	<1
Cr	<1
Cu	<1
Fe	2
K	1
Mg	1
Mn	0
Mo	<0.5
Ni	<0.5
P	0,1
Pb	<0.5
Sn	<0.5
SiO_x	106
Ti	<0.5
V	3
Zn	<0.5
Zr	<0.5

* ICP results of Si have been assigned to SiO_x

The solution contains traces of different metals, but mainly consists of calcium and silicates (silicon assigned to silicate). This matches to earlier statements in literature, describing the hydration of the calcium silicate phases in the BOF-slag.

The formation of $Ca(OH)_2$ and $HSiO^-$ upon hydrolysis of the slag particles, increase the pH value of the solution to ~11.5 . At this pH and corrosion potential (-0.835 V vs. SCE) zinc is passive according to the pourbaix diagram of zinc illustrated in section 2.1.2 Thermodynamics. The reduced corrosion current of GA and the change in shape of the curve could therefore just be assigned to the alkalinity of the BOF-slag solution. A control experiment was therefore executed in order to test this hypothesis. A reference solution was prepared with the pH adjusted to the same value as the BOF-slag solution (~11.5) by the addition of NaOH. Subsequently an anodic polarization scan was measured on GA in this alkaline reference solution. The results of this scan is plotted and compared with the standard (neutral pH) reference and the slag-solution scan in Figure 22. It can be seen that the increased alkalinity has an effect on the current density of the material, where the corrosion current density is about a decade lower than in the reference scan. The shape of the anodic curve is also slightly altered (0 - 0.1 V vs OCP), which can be attributed to the formation of a passive layer on the zinc surface but this effect is rather small.
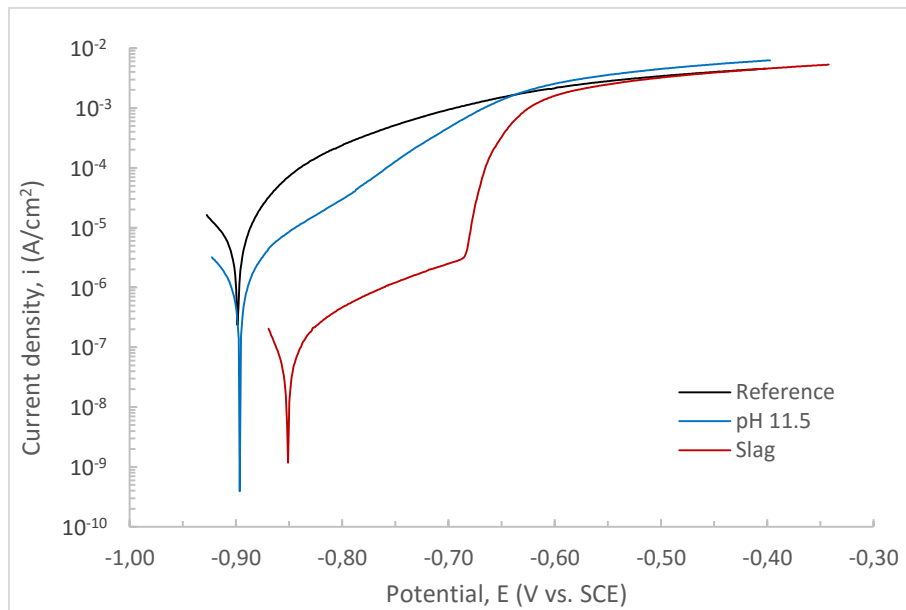
Figure 22: Tafel plot (i,E diagram), showing the effect of a BOF-slag solution and an alkaline solution (pH=11.5) on the anodic branch of GA vs. the reference solution.

The reduction of the current by the slag-solution is much more significant and the positive shift of the corrosion potential even more clearly indicates the additional inhibition of corrosion by slag. It appears that apart from the alkalinity of the slag solution, some other active species in the solution cause the inhibition of corrosion of the galvannealed coating.

The second material to be studied was Magizinc® (MZ), a hot-dip galvanized steel with a Zn-Mg (1.6)-Al (1.6) alloy coating. Magizinc has a more negative (active) potential than the galvannealed coating (-1.032 vs. -0.901 V vs. SCE) which is caused by the more active potentials of the two alloying elements magnesium and aluminium. Despite this more active potential, MZ has been shown to have enhanced corrosion resistance compared to GA, as was mentioned earlier. This is caused by the formation of a thick and protective oxide layer on the surface.

The potentiodynamic polarization scans in the reference solution and with the different inhibitors added, are plotted in Figure 23. Like GA, the anodic branch of the reference scan of MZ shows linear Tafel behaviour between ~ 8 -100 mV from OCP corresponding to the activation controlled dissolution of the metals. At higher anodic potentials the anodic dissolution of the metals become so active that the reaction becomes diffusion controlled, as can be seen by the plateau forming at ~-0.80 V (vs. SCE). The cathodic branch in the absence of inhibitors shows the O_2 reduction is diffusion controlled. Which can be concluded from the O_2-plateau at ~-50 - ~-100 mV vs OCP, again at current densities that agree with literature values. At higher cathodic polarization we see a number of peaks arising in the curve, corresponding to the reduction of the different oxides that have formed on the surface.
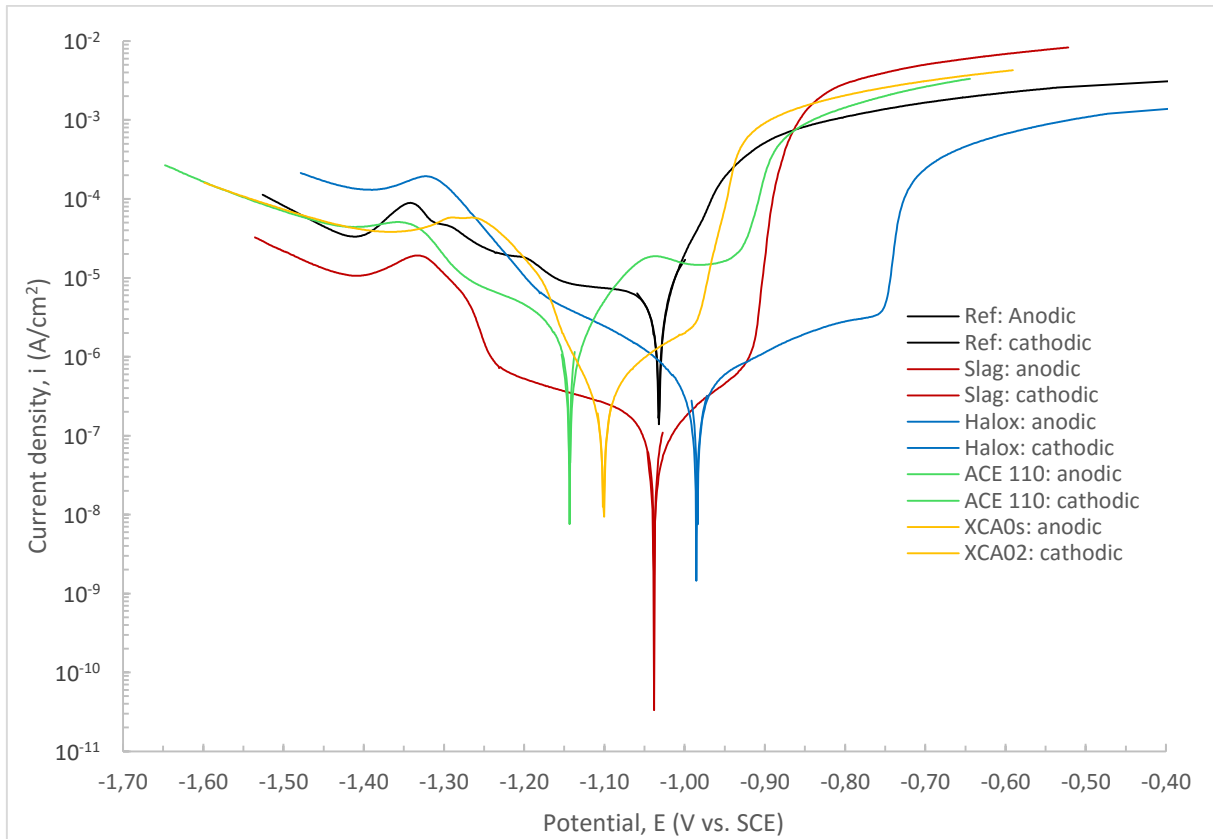
Figure 23: Tafel plot (i,E diagram) of different inhibitors on MZ vs. a reference solution.

Where the inhibitors had similar influences on the curves on GA, we see totally different behaviour of the inhibitors on MZ. If we look at ACE-110, we see an increase in the activity of the anodic branch with increased current densities. But at ~-1.05 V (vs. SCE) we see a decrease in the current. This indicates a blocking of the surface by corrosion product, thereby reducing the anodic dissolution. This is probably due to the recombination and precipitation of the inhibitor with the dissolved metal ions. We see a reduction of the cathodic current but no change of the shape indication no alteration of the mechanism but blocking of the cathodic sites with corrosion product. The corrosion potential has shifted into more negative values due to the activation of the material.

Halox significantly alters the anodic curve and stimulates passivation of the surface up to very high overpotential when the anodic dissolution significantly increases again around -0.75 V (vs. SCE). The corrosion potential is also shifted to more noble values. The angle of the cathodic branch has slightly increased indicating the reaction of no longer just diffusion controlled but partly controlled at the interface [62].

XCA02 has a similar effect as Halox but has shifted the corrosion potential to a more negative (active) potential. It has a more profound effect on the cathodic branch, again indicating the oxygen reduction is no longer just diffusion controlled.

The BOF-slag solution shows a significant decrease in the corrosion current of about one and a half decade. The slag solution reduces the cathodic current without altering the cathodic curve's shape, suggesting the same mechanism. The cathodic curve does not show small separate peaks like the reference but one large peak at ~-1.33 V (vs. SCE). Since the area under the peak corresponds to Q and is directly proportional to the thickness of the oxide, it can be concluded that a relatively thick oxide layer had formed compared to the other samples. The slag solution also lowers the anodic current with

almost 2.5 decades at +0.10 V vs. OCP, just like Halox. Compared to Halox, the slag solution has lower current densities but also a lower breakdown potential (-0.90 vs. -0.75 V vs SCE) stating that Halox is able to passivate the surface at a higher potential/driving force. The lowering of both the anodic and cathodic current can be attributed to the deposition, onto the metal surface, of reaction product between the solution and the zinc coating [59].

The slag solution slightly shifts the corrosion potential to more negative (active) values but this can be ignored and slag can be described as a mixed-type inhibitor due to its ability to considerably lower both the anodic and cathodic current.

XCA02 has a similar effect as BOF-slag on the anodic branch but appears to be altering the cathodic reaction. It strongly reduces the cathodic current, especially in the vicinity of the OCP, and the reaction is no longer diffusion controlled but shows linear/Tafel-like behaviour. Unlike its effect on GA, XCA02 appears to have little effect on the anodic current. Together with the shift to more negative values, one can describe XCA02 as a cathodic-type inhibitor on MZ.

As was mentioned for GA, the inhibition of the slag and the passivating behaviour of the substrate could be attributed to the alkalinity of the slag solution. Under these alkaline conditions and this corrosion potential zinc passivates, where aluminium starts to corrode. A control measurement was performed in order to test the effect of the pH on the corrosion behaviour of MZ. The results of this scan are plotted in Figure 24, together with the anodic curve of the reference and slag solution.
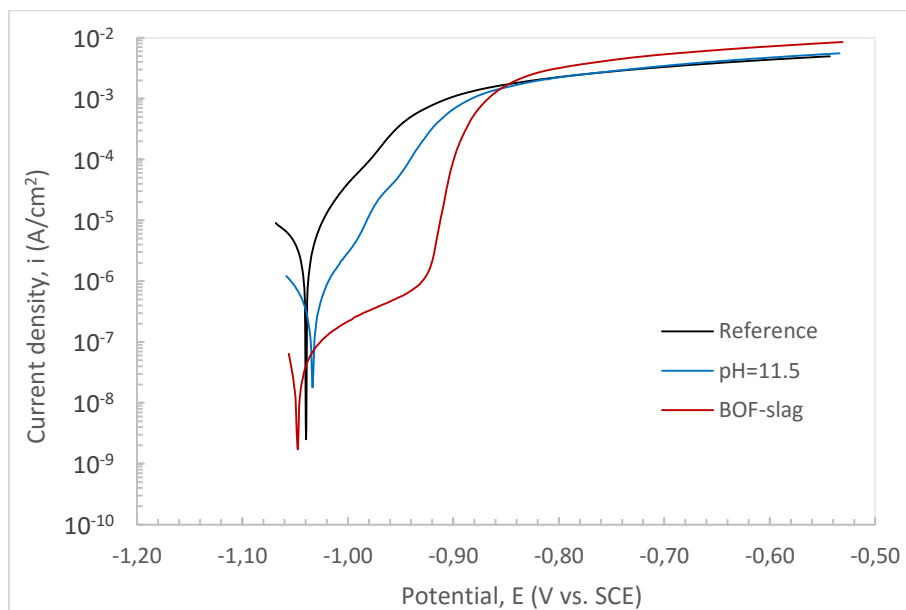
Figure 24: Tafel plot (i,E diagram), showing the effect of a BOF-slag solution and an alkaline solution (pH=11.5) on the anodic branch of MZ vs. the reference solution.

One can see that unlike in the slag solution, the potential shifted to a more positive (noble) value. A decrease in the anodic current can be observed but no passivating behaviour, like it shows in the curve of the slag solution. This is similar to the effect of pH we saw on GA. Again we can conclude that the inhibition of the slag solution on the corrosion of the MZ coating (reduction of the corrosion current) can be partially attributed to the high pH, but also to the other active components in solution.
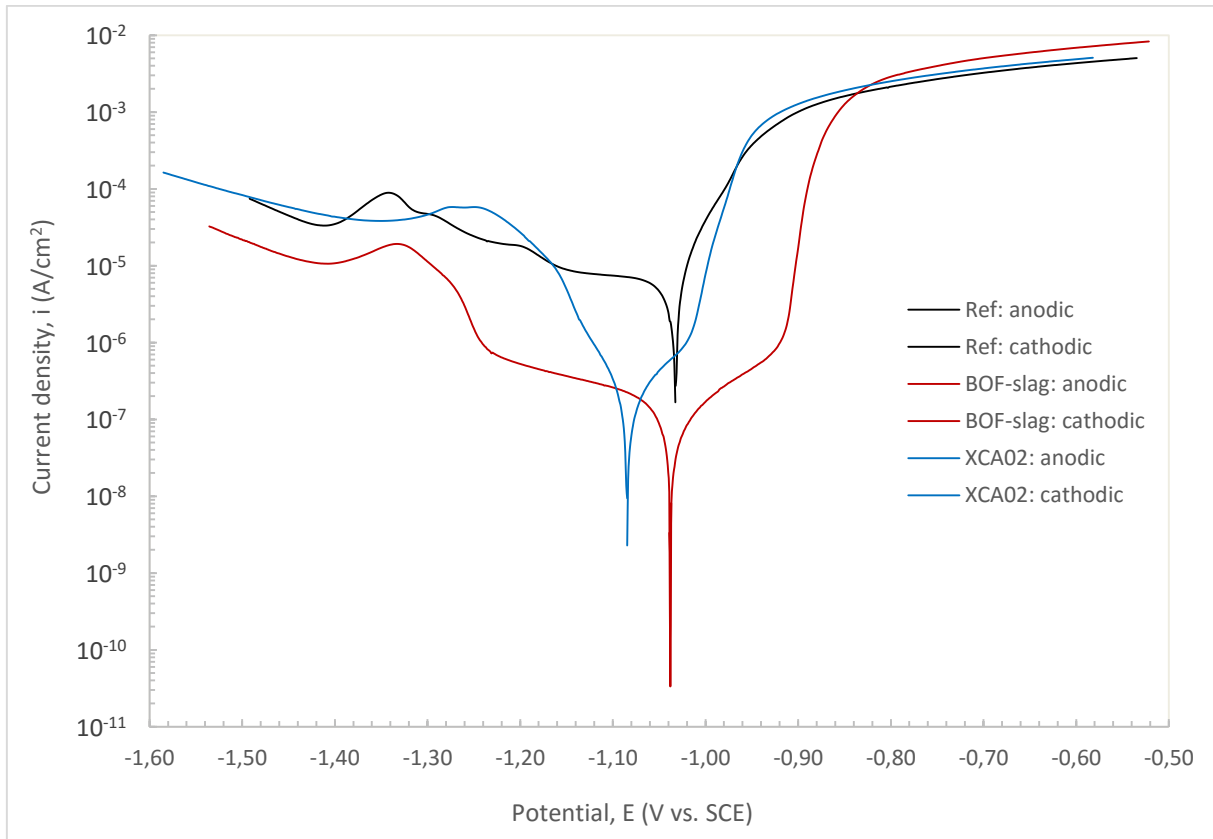
Figure 25: Tafel plot (i,E diagram) of the two best performing inhibiting systems vs. the reference measurement

Just as it is the case for GA, BOF-slag appears to have the best corrosion inhibition of the selected inhibitors, judging on the corrosion current density. Despite the passivating abilities and the high break-down potential, Halox seems to have a slightly higher corrosion current density than XCA02 due the influence of XCA02 on the cathodic current density. Figure 25 shows a plot of XCA02 and BOF-slag versus the reference solution. It clearly shows the mixed- and cathodic-type behaviour of the slag and XCA02 respectively with both reduced current densities of over a decade lower than the material has in the reference solution. It is typical that although XCA02 appears to have a different modus operandi on the two substrates, it produces the single lowest current densities for both materials.

4.1.2 Inhibition Efficiency

By observing the polarization curves of the two materials in contact with the different solutions a first assessment was made on the qualitative performance of the different inhibitors. In order to quantitatively rank the performance of the difference inhibitors, one needs to calculate the corrosion currents. For these are directly proportional to the corrosion rate of the material.

Two approaches were used in order to calculate the corrosion current from the potentiodynamic polarization scans; the Tafel extrapolation method and the determination of the polarization resistance.

This last method is based on the assumption that at small polarization/current densities the transfer of charge is the limiting step and the transfer of active species to the surface is neglected. When assuming small values of overpotential, i.e. for potentials close to the corrosion potential, the Butler-Volmer equation (0.15) could be simplified resulting in the Stern-Geary equation (0.18).

$$\eta / i = R_p = \frac{B}{i_0} = \left(\frac{\Delta E}{\Delta i}\right)_{\Delta E \to 0}$$

(0.18)

So if we polarize an electrode by forcing its potential away from its open circuit potential a resulting polarization current will flow. The polarization resistance is defined as the ratio between the applied overpotential (ΔE) and the resulting current density (Δi). If we rephrase the Stern-Geary equation to:

$$i_0 = \frac{\beta_a \beta_c}{2.3(\beta_a + \beta_c)} \frac{1}{R_p}$$

(0.22)

It becomes clear that the polarization resistance is directly proportional to the corrosion current density. Calculating the polarization resistance can therefore also be used to quantatively asses the corrosion resistance/performance of a material and has been widely accepted as a very useful method for monitoring corrosion rates [63]. A high polarization resistance implies high corrosion resistance and vice versa. In order to calculate the corrosion current density from the polarization resistance, the Tafel slopes must be determined from a Tafel plot to calculate the proportionality constant *B.* These Tafel constants may also be assumed for fast calculations. Since they are usually in the range of 0.1 V decade[-1], one is able to calculate the corrosion current density with a maximum error factor of 2.2, if 0.1 is chosen for both constants [64]. This again confirms the insensitivity of this method to the values of the Tafel constants.

The polarization resistance can be obtained from the linear potential - current density plot, by performing a linear regression on the data between 10 mV anodic and 10 mV cathodic relative to the corrosion potential. Typically, linear polarization resistance (LPR) scans are recorder by cyclically polarizing the surface +/- 15-25 mV. The low potential prevents altering of the surface chemistry and morphology (it is assumed non-destructive). Since the potentiodynamic polarization scans are initiated at +/- 30 mV, it is assumed that data from this scan is suitable for polarization resistance calculations[6]. The result of such a regression is shown in Figure 26, where the potentiodynamic polarization data (+/- 10 mV vs. OCP) of GA in the reference solution is taken. It can be seen that around the OCP (potential at which the current density is zero) the curve is linear. The slope of the linear section is determined which is the inverse of the polarization resistance.

---

[6] This assumptions was verified by recording LPR scans of GA and MZ, in the reference solution and one inhibitor containing solution. Values of R_p were calculated from the LPR and potentiodynamic polarization scan and compared. The values were in agreement with each other and the assumption taken as valid.
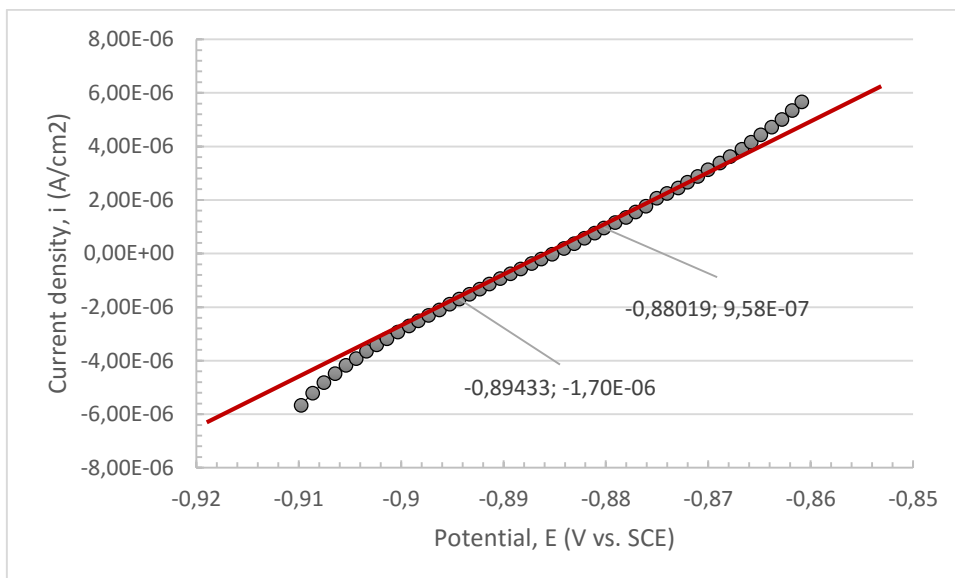
Figure 26: Polarization curve of GA in a 0,1M NaCl solution (ref). The curve is linear in the zone around OCP (i = 0) .

For the other solutions, identical calculations have been performed and the calculated values are shown in Figure 27. All inhibitors show increased polarization resistances indicating highly improved corrosion resistance of the material. The solutions containing BOF-slag and XCA02 show the highest polarization resistance/inhibition for both GA and MZ, which agrees with the observations from the Tafel plots. It is interesting to notice that these appear to be more effective on MZ than on GA, relative to the other inhibitors.
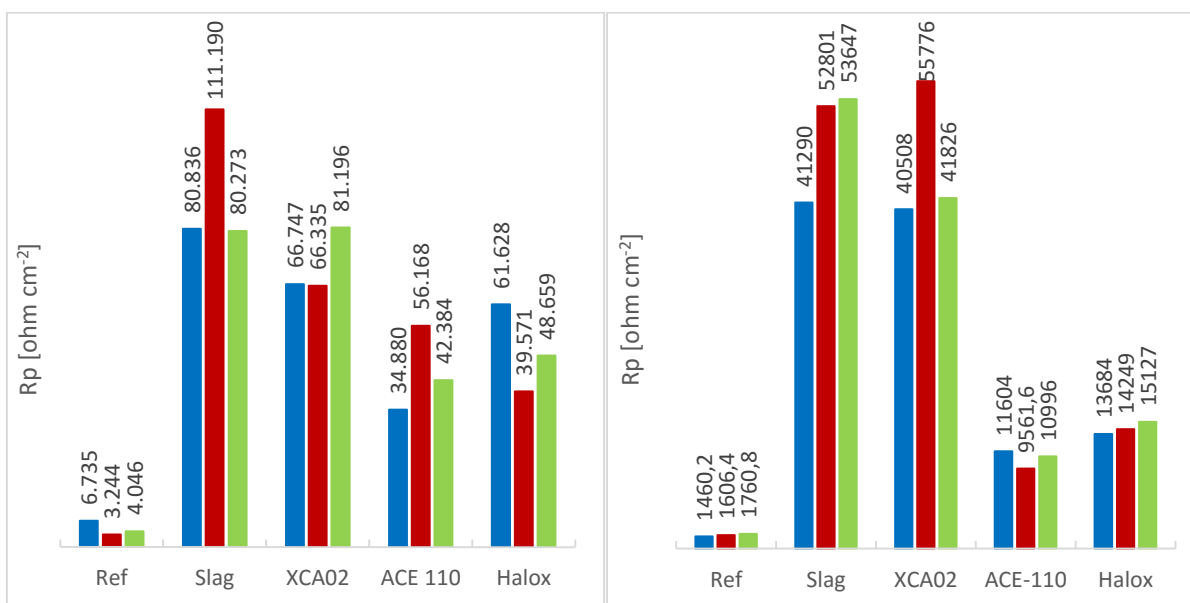
Figure 27: Polarization resistance calculated from polarization curves for (left) GA with different inhibitors and (right) MZ with different inhibitors.

All calculations were done in triplex in order to prove reproducibility of the results. All calculated values are averaged and these values were used for further calculations. The Tafel slopes were assumed to be 0.1 V decade^{-1}, which results in a proportionality constant of 0,0217. The assumed value for *B* was used to calculate the corrosion current density. The calculated polarization resistances and corrosion current densities are listed in Table 6. According to these calculations BOF-slag and XCA02 show the lowest current densities, hence the lowest corrosion rate of the material.

Table 6: Calculated polarization resistance values and calculated values of exchange current densities according to equation (0.18) using the average polarization resistance and assumed value for B.

Material	Inhibitor	R_{P1}	R_{P2}	R_{P3}	$\langle R_P \rangle$	$\langle i_0 \rangle$
		$(Ohm\ cm^{-2})$	$(Ohm\ cm^{-2})$	$(Ohm\ cm^{-2})$	$(Ohm\ cm^{-2})$	$(A\ cm^{-2})$
GA	Ref	6735	3244	4046	4675	5,56E-06
	Slag	80836	111190	80273	90766	2,86E-07
	XCA02	66747	66335	81196	71426	3,64E-07
	ACE-110	34880	56168	42384	44477	5,85E-07
	Halox	61628	39571	48659	49953	5,20E-07
MZ	Ref	1662	1606	1761	1676	1,55E-05
	Slag	41290	52801	53647	49246	5,28E-07
	XCA02	40508	55776	41826	46037	5,65E-07
	ACE-110	11604	9562	10996	10721	2,43E-06
	Halox	13684	14249	15127	14353	1,81E-06

The second method to calculate the corrosion current density is based on the extrapolation of the Tafel plots. The linear parts of the Tafel plots are fitted to obtain the Tafel slopes which are used for calculations. Figure 28 shows a Tafel plot with the anodic and cathodic polarization curves of GA in the 0.1 M NaCl reference solution. In this plot the overpotential or polarization is plotted against the current density (the OCP is set to 0 V). Both curves have linear sections starting round ~+/- 60 mV. This linear section obeys the Tafel equation:

$$\eta = \beta \log \frac{i}{i_{corr}} \tag{0.23}$$

which can rephrased as:

$$\log(i) = \frac{1}{b}\eta + \log(i_{corr}) \tag{0.24}$$

The slope of the linear sections in the plot corresponds to 1/b and the value of log(*i*) for η = 0 provides log(*i$_{corr}$*) . The fittings of the data in Figure 28 are given in the plot. The intersection of the fitted lines at the corrosion potential renders the corrosion current density.

The Tafel extrapolation method is only valid if the cathodic and/or anodic reactions are under activation control. In the case where one of the slopes is diffusion controlled or in the case of a passivation plateau, the method is not valid. In this case only one of the fittings is valid (either anodic or cathodic), one Tafel plot can be extrapolated and the corrosion current density if given by the intersection of the fitted line with the vertical line above zero overpotential (the corrosion potential).
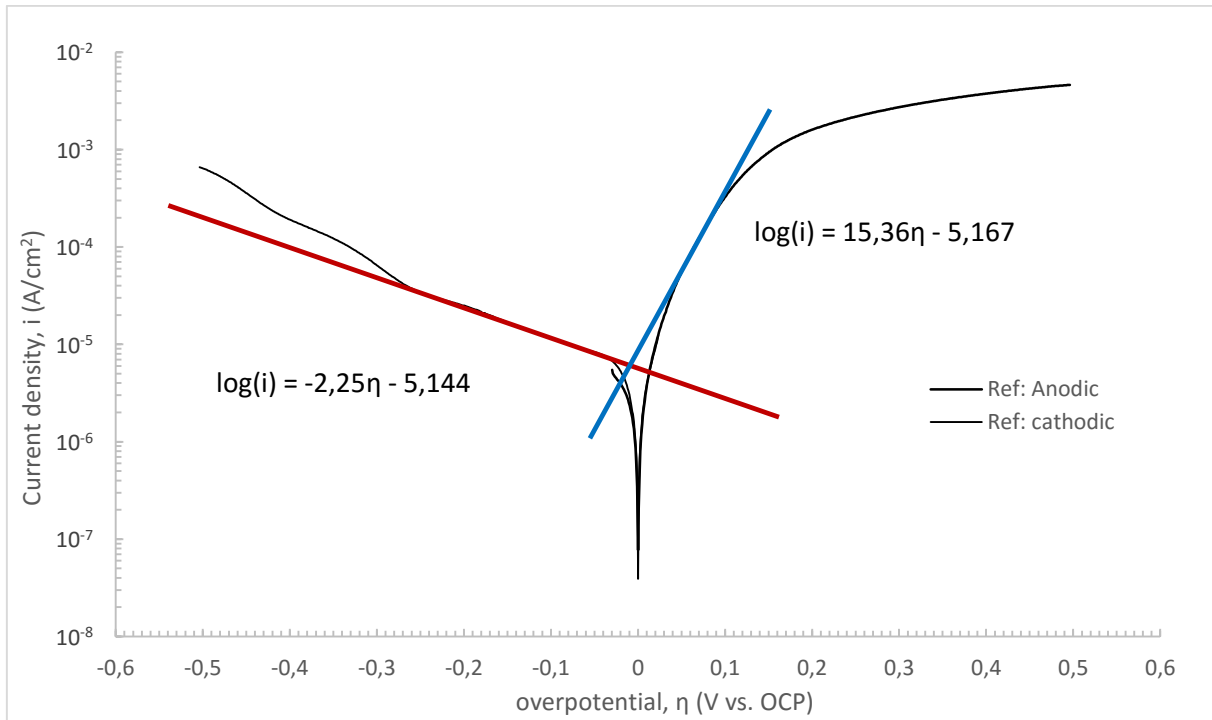
Figure 28: Polarization diagram of GA in 0.1 M NaCl solution (reference) with red and blue tangents of linear sections.

The fitting results of multiple scans per solution were averaged and are presented in Table 7. The Tafel constants were calculated by the inversion of the Tafel slopes and given in V decade^{-1}. The acquired average corrosion current densities and the average Tafel constants were insert into equation (0.22) in order to calculate the proportionality constant *B* and the polarization resistance. The high cathodic Tafel constants, b_c, for both GA and MZ indicate the corrosion rates are under cathodic control (oxygen diffusion control). This is confirmed by the shape of the polarization curves in Figure 19 and Figure 23.

The fitting results show BOF-slag and XCA02 were able to reduce the corrosion current density the most. This correlates with the observations of the Tafel plots and the results of the polarization resistance method.

Table 7: Polarization resistance and average Tafel parameters for MZ and GA using the Tafel extrapolation method

Material	Inhibitor	E_{corr}	i_{corr}	b_c	b_a	B	R_p
		(V vs. SCE)	*(A cm^{-2})*	*(V dec^{-1})*	*(V dec^{-1})*	*(V)*	*(Ω cm^2)*
GA	Reference	-0,901	7,13E-06	-0,493	0,065	0,033	4590
	Slag	-0,836	3,01E-07	-0,344	0,145	0,109	360196
	XCA02	-0,853	4,72E-07	-1,250	0,078	0,036	76184
	ACE 110	-0,858	1,92E-06	-0,321	0,051	0,026	13611
	Halox	-0,844	7,59E-07	-0,531	0,304	0,308	405443
MZ	Reference	-1,028	8,50E-06	-0,791	0,046	0,021	2492
	Slag	-1,038	2,53E-07	-0,291	0,101	0,067	266238
	XCA02	-1,101	3,03E-07	0,102	0,097	0,022	71106
	ACE 110	-1,143	2,72E-06	-0,243	0,113	0,091	33532
	Halox	-0,985	3,50E-07	-0,200	0,121	0,133	380905

The results of the two method are based on calculations performed on different sections of the polarization curves. Nevertheless the results for the corrosion current densities are quite similar. Based on the calculated corrosion current density it can be concluded from both methods that BOF-slag and XCA02 are the best performing corrosion inhibitors on both GA and MZ in 0.1 M NaCl aqueous solution. It is noticeable that there is a great deviation between the determined polarization from the polarization method and the value of the polarization resistance calculated with the Tafel slopes. This is one of the reasons Tafel extrapolation is sometimes criticized.

The efficiency of corrosion inhibitors (η,%) is often expressed in the change of corrosion current density, using the following equation

$$\eta = \frac{i_i - i_0}{i_0} \times 100\% \tag{0.25}$$

where i_i is the inhibited corrosion current density and i_0 is the reference (uninhibited) corrosion current density. The efficiencies of the two best performing inhibitors (slag and XCA02) have been calculated, based on the data acquired by the polarization resistance and the Tafel extrapolation method. These values, together with the calculated corrosion current densities of both methods, are listed in Table 8. It can be seen that there are minor deviations in the values of corrosion current densities between the two methods. But these deviations are well within the 2.2 error margin given by Pourbaix [64]. The two inhibitors were able to lower the current the corrosion current with about 95% where BOF-slag appears to be slightly more efficient than XCA02.

Table 8: Calculated inhibition efficiencies for BOF-slag and xcA02 on GA and MZ, using both data from the polarization resistance and Tafel extrapolation method.

Material	Inhibitor	$i_{corr}(Acm^{-2})$		$\eta(\%)$	
		R_p	Tafel	R_p	Tafel
GA	BOF-slag	2,86E-07	3,01E-07	-94,9%	-95,8%
	XCA02	3,64E-07	4,72E-07	-93,5%	-93,4%
MZ	BOF-slag	5,28E-07	2,53E-07	-96,6%	-97,0%
	XCA02	5,65E-07	3,03E-07	-96,4%	-96,4%

4.1.3 Open circuit potential variation

Immersion tests were carried out for 6 days in 0.1 M NaCl solution with and without slag. The test was performed on horizontal samples with clamped tubular reservoirs top (for full description see Experimental section).

In order to further study the inhibition mechanism of BOF-slag, the variation of the open circuit potential of GA and MZ as a function of the period of exposure (immersion) was measured against a saturated calomel electrode (SCE) in the absence and presence of BOF-slag during the immersion test. The acquired data are plotted in Figure 29. As mentioned earlier, MZ has a more negative (active) potential than GA due to the alloying elements in the coating. It is evident that the corrosion potential of all four electrodes firstly tends towards more negative values, giving rise to a short step. This behaviour of the potential represents the breakdown of the pre-immersion, air-formed oxide film present on the metal surface. The potentials of the reference samples, are shifted to slightly more noble values until steady state potential is established. The potential of MZ in the slag solution does

not show this increase and the steady state is reached at a more negative potential. The results of BOF-slag on GA clearly show that the potential was shifted in the noble direction which indicates that the anodic reaction in this solution was strongly affected by the presence of the inhibitor. The initial rise of the potential indicates film-build-up and ends up in full passivation of the material [65, 66].
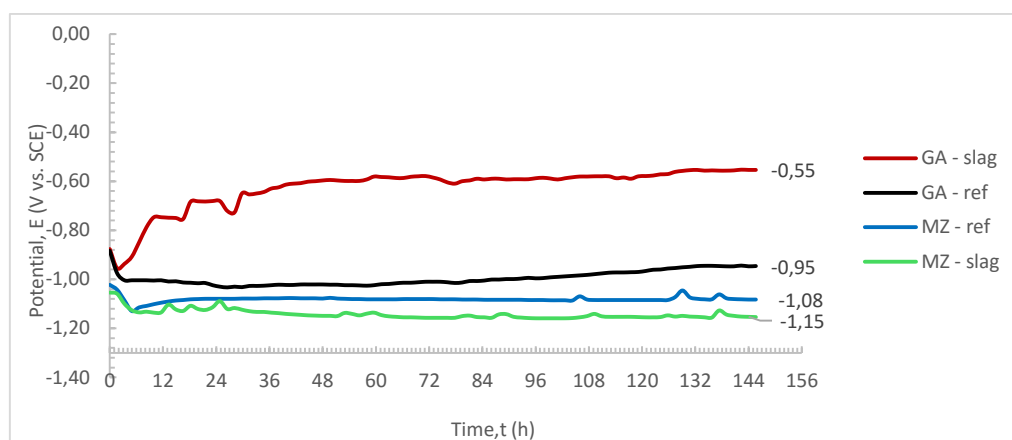
Figure 29: OCP evolution of immersed GA and MZ. Reference (in 0,1M NaCl solution) vs. slag (0,1MNaCl + 2gL^{-1} BOF-slag solution).

From these results it is noticeable that, as we saw earlier in the Tafel plots, the slag solution activates the MZ surface by shifting the potential to more negative values, where it raises the potential of GA to more noble values and the material tends to passivate.

4.1.4   Surface analysis

Subsequent to OCP-monitoring, the surfaces of the samples were analysed. Visual inspection of the surface provides first insight on the state of the coating but observation by SEM and analysis by EDS and XPS provided more information on the morphology and chemistry of the surfaces.

4.1.4.1   Visual analysis

Figure 30 shows images of the surfaces taken after seven days of exposure to the reference solution (Figure 30a and d), and to the slag solution (Figure 30b and c). The GA sample exposed to the reference solution (0.1 M NaCl aqueous solution) has a dull and very dark appearance from oxides formed on the surface with some small spots of white rust. The GA sample exposed to the slag solution shows almost no sign of corrosion and the surface remained clean and shiny (apart from a white glare on the sides of the circle). The absence of corrosion and the positivation of the potential are therefore related in the case of GA.

The observations for MZ in the reference solution shows the formation of corrosion products with some white rust and some darker areas and like GA has a dull appearance. Nevertheless, the surface of MZ is clearly less affected by the reference solution than the GA sample. The MZ sample exposed to the slag solution shows a large area of unaffected surface in the top right corner of the sample. It does have lost some of its shininess, as can be seen by comparing it to the unreacted surface outside the ring. A minor dull spot and some with rust was observed on the left side of the surface. The observation of the MZ surface does not relate well to the trend in the OCP variation. With the more negative potential, a more active and corroded surface was to be expected. On the contrary the material has to a great extent retained its lustrous appearance.
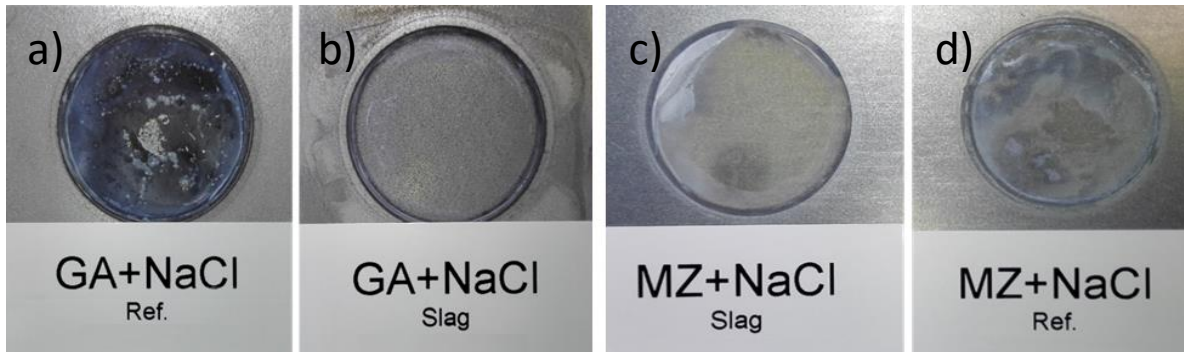
Figure 30: Surfaces of GA after exposure to the reference solution (a) and the slag solution (b) on the left and the surfaces of MZ after exposure to the slag solution (c) and the reference solution (d).

4.1.4.2   Scanning Electron Microscope

After examining the surface of the samples visually, the surfaces were analysed by means of scanning electron microscope (SEM) inspection and surface elemental analysis in order to obtain more insight into the processes on the surface. Figure 31 shows a backscattered electron image obtained by electron microscopy prior to immersion of the MZ sample and the associated EDS spectrum. In the backscattered image, brighter areas indicate the presence of heavier elements with higher atomic numbers. In this image brighter areas can be attributed to zinc-rich phases (Z_{zn} = 30, Z_{Al} = 13 and Z_{Mg} = 12) and the darker areas to the different aluminium and magnesium richer phases. The EDS spectrum of the area indicates zinc to be the major components with equal amounts of aluminium and magnesium, as was to be expected.
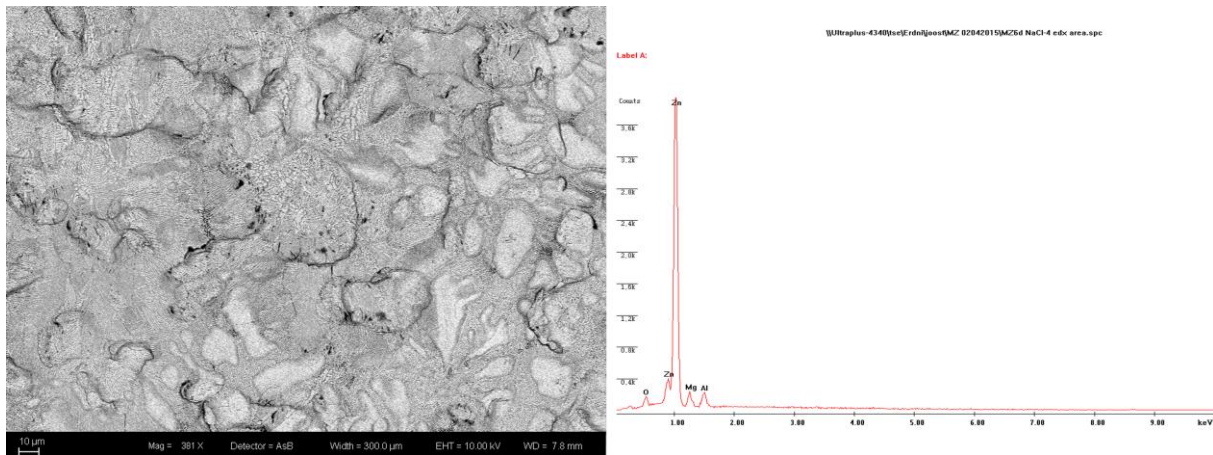
Figure 31: SEM backscatter image and corresponding EDS spectrum of untreated MZ surface.

Figure 32 displays a secondary electrons image of MZ after immersion in the reference solution. It shows a heterogeneous surface where corrosion products have formed, creating a porous structure with oxides growing out of the bulk. EDS analysis shows the 'large' oxides are preferentially growing on the magnesium and aluminium rich phases, thereby surrounding the large zinc-rich phases. This formation of oxides on specific grains explains the lowering of the magnesium- and high increase in the oxygen content in the EDS spectrum in Figure 32b. The larger zinc-rich grains that are surrounded by the porous oxides, have little pits formed into the surface. Indicating local attack of the protective oxide layer by chlorides.
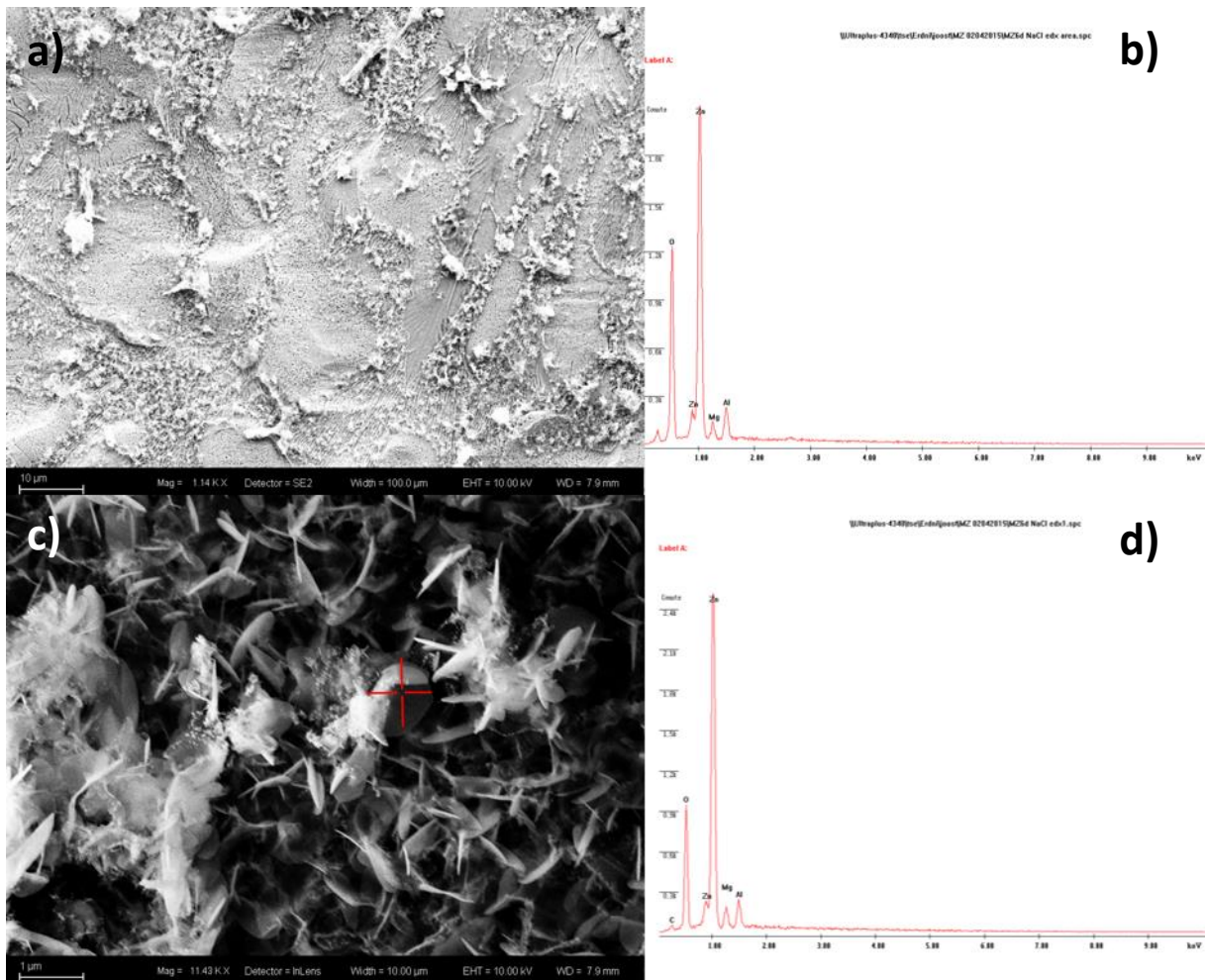
Figure 32: SEM secondary electron image (mag 381x) of MZ after immersion in reference electrolyte for 7d (a), EDS spectrum of total area (b), SEM InLens image of corrosion product (c) and EDS spectrum of spot (d).

At higher magnifications, the InLens-mode of the microscope is required in order to get a clear image of the surface due to the low conductivity of the corrosion products formed. The low conductivity of the surface causes it to light up in secondary electron mode. SEM observation in Figure 32c shows the presence of open leaf-structured oxides, which can be assigned to simonkolleite, with some oxides growing out of the surface as can be observed in the left corner of the SEM image [67]. The EDS spectrum in Figure 32b is identical to the spectrum in Figure 32d and both indicate a lowering of the magnesium content and the formation of oxides.

After exposing MZ to the slag solution, SEM observation shows a very different morphology than the reference sample. A secondary electron image (mag. 381x) of the surface of MZ after seven days of exposure is shown in Figure 33a. The metallic surface, which is indicated by the red circle, is barely visible due to a porous layer that has deposited over the entire surface. The EDS spectrum shows a significant decrease of the amount of aluminium and magnesium has completely disappeared form the spectrum. What of course is very noticeable is the large silicon peak that has come to present. At higher magnifications, the building blocks of this deposited layer become visible.
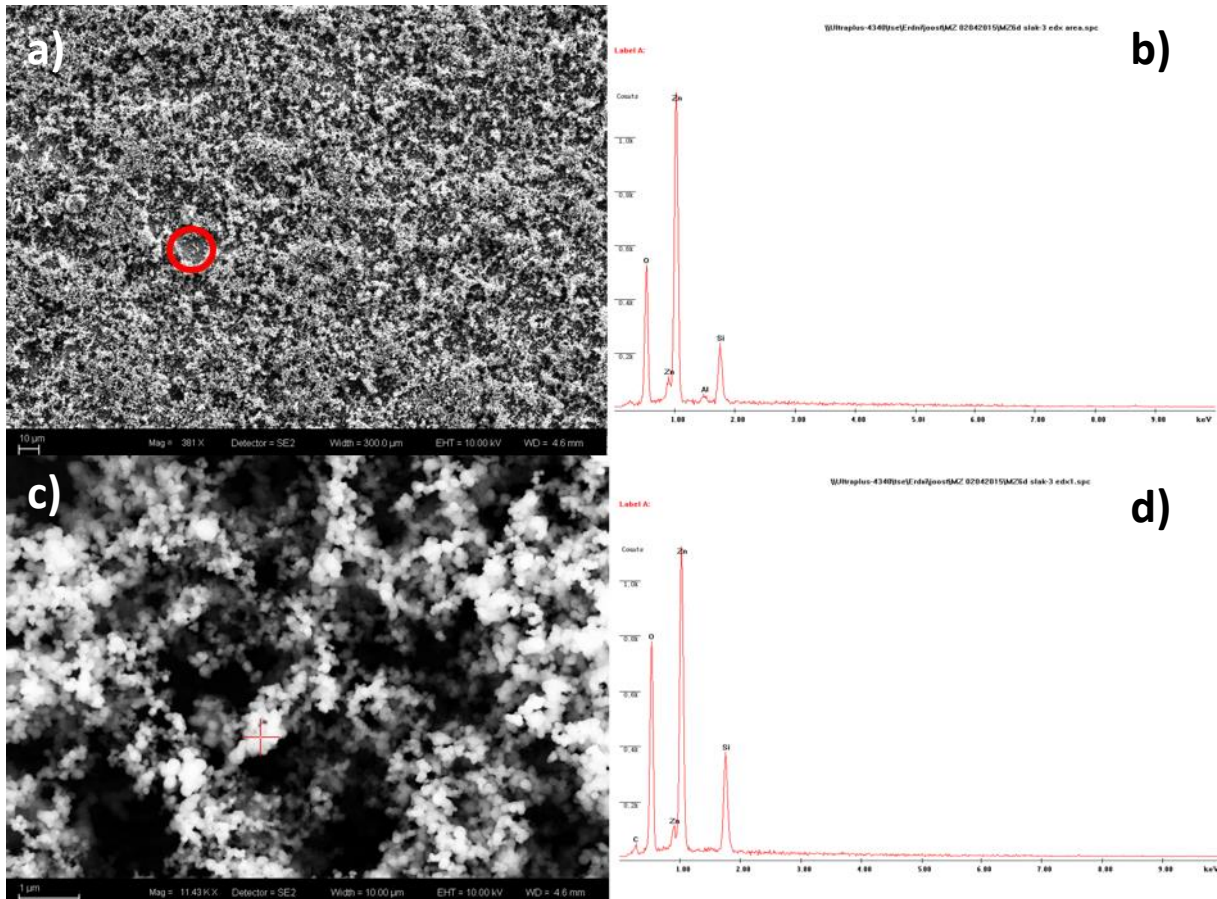
Figure 33: SEM secondary electron image (mag. 381x), where the red circle marks the metallic surface (a), the corresponding EDS spectrum of the entire area (b), SEM secondary electron image (mag. 11.43k x) (c) and the corresponding EDS spectrum of the deposited compound (d) of MZ after exposure to the slag solution for 7 days.

Figure 33c shows the formation of a gel-like film network over the surface that is comprised of small spherical particles which have clustered and precipitated on the metallic surface. EDS analysis of the precipitated compound shows the predominant components are Zn, O and Si which indicates that the layer consists of zinc and silicates. It is again noticeable that no magnesium and here also no aluminium is observed in the EDS spectrum. The spherical shape of the particles suggests the precipitated species originate from colloidal particles in suspension.

The surface of GA samples exposed to a slag solution for seven days were also analysed by means of SEM. The GA surface after exposure looks similar to the surface of MZ (Figure 34). At low magnifications the metallic surface is hardly visible and is appears to be completely covered by a layer of precipitated species. At higher magnification we see the deposited is layer is not as thick as the one we saw on MZ and has a much more heterogeneous dispersion.
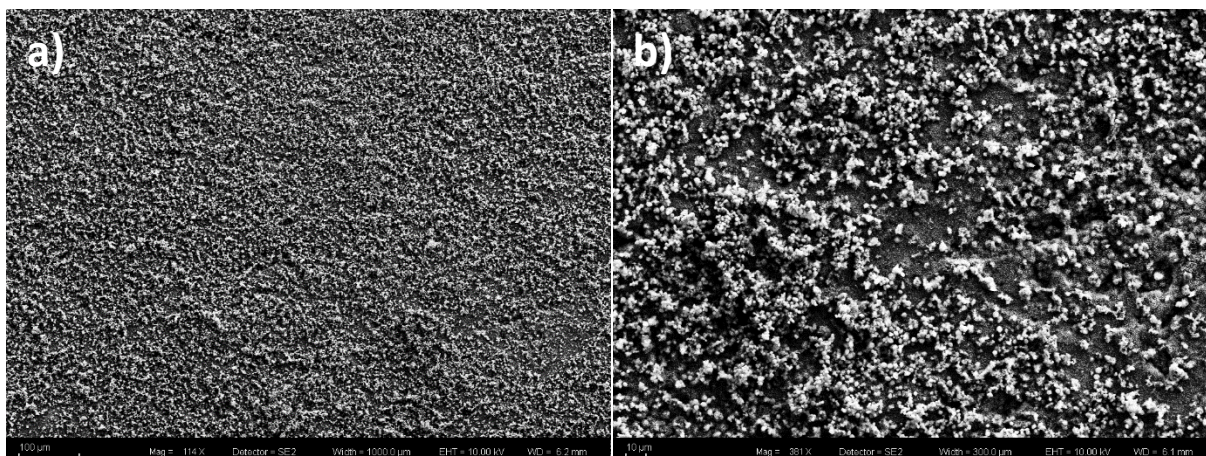
Figure 34: SEM secondary electron image of the surface of GA after 7 days of exposure to a slag solution with (a) magnification 114x (a) and 381x (b) showing a deposited layer on the metallic surface.

EDS analysis was done over the entire area of Figure 34a to determine the general chemical composition of the surface. The EDS spectrum of this scan (Figure 35) shows the main chemical components are O, Zn and Al with some traces of C. This indicates the presence of corrosion products of predominantly zinc are found, but also a significant amount of aluminium oxide. No silicon was detected on the surface which was to be expected based on the results obtained on MZ. The discovery of aluminium on the surface, especially in these quantities, is remarkable since it hasn't showed in any of the preceding EDS analyses.
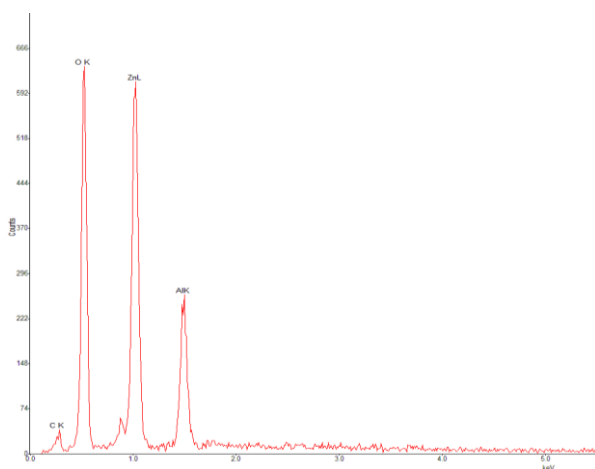
Figure 35: EDS spectrum of total area of Figure 34: SEM secondary electron image of the surface of GA after 7 days of exposure to a slag solution with (a) magnification 114x (a) and 381x (b) showing a deposited layer on the metallic surface.

According to the results of the ICP-MS analysis of the BOF-slag solution in section 4.1, the aluminium content of BOF-slag the solution is just ~0.4 mgL^{-1}. The aluminium is therefore unlikely to be coming from a BOF-slag solution. The solution to these conflicting results appears to be lying at the source of the slag.

The immersion tests with GA were performed later in this study than the immersion tests performed on MZ. This was due to a delay in the delivery of suitable material. By the time the new sheets of GA had arrived, the original batch of BOF-slag had been fully used and a new batch of slag was obtained from the oxysteel plant. Earlier studies had shown that the composition of the BOF-slag from the oxysteel plant at the IJmuiden site of Tata Steel was relatively constant, which is why no chemical analysis of the new slag was done. After the notable results obtained by SEM-EDS analysis on GA, XRF analysis was performed on the newly acquired slag. The analysis showed the new batch did not consist

of BOF-slag, but of Ladle Furnace (LF) slag. Unlike BOF-slag, LF-slag has a high percentage of aluminium oxides. LF-slag has very different leaching behaviour than BOF-slag in aqueous solution. During exposure to water LF-slag leaches alumina and this explains the large amounts of aluminium in the EDS spectrum. Like BOF-slag, LF-slag contains about 20 wt% SiO_x and 60 wt% CaO but much lower quantities leach and therefore no traces of silicon were found anywhere on the surface [41]. Unfortunately there was no possibility – due to time restrictions – to redo the 'failed' experiments on GA.

At the initial stage of this study, GI (hot-dip galvanized steel) was used as testing material together with GA and MZ. Based on the results obtained by voltammetry experiments it was chosen to proceed with MZ and GA. During this initial stage, immersion tests with GI in BOF-slag solution and subsequent surface analysis by SEM-EDS were performed.
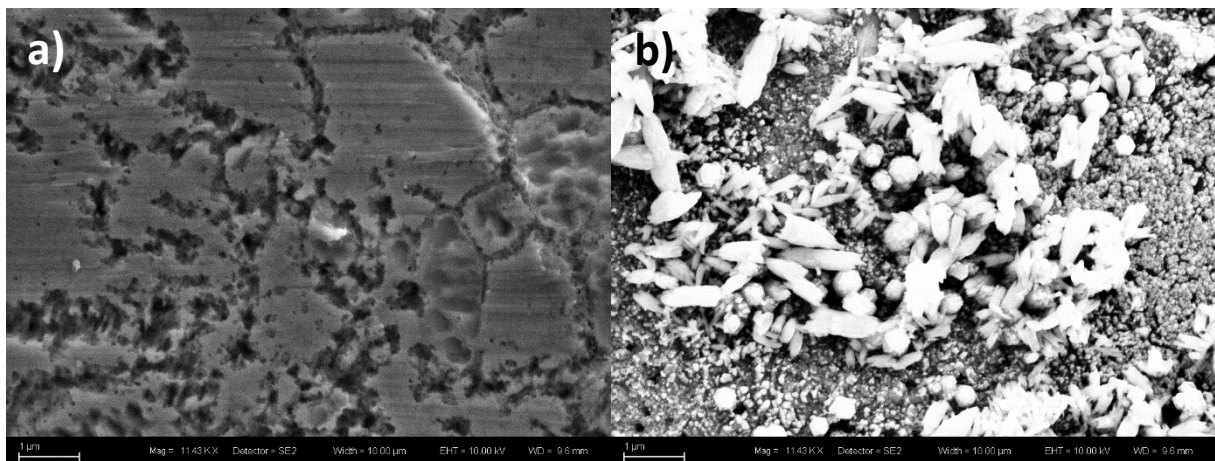
Figure 36: SEM secondary electron images of GI after immersion in the reference solution for 7 days.

Visual assessment of the surface of the GI sample immersed in the reference solution for seven days showed it was heavily corroded, due to the presence of a thick corrosion layer on the surface and signs of local attack. These observations were confirmed by the analysis of the surface by SEM observation (see Figure 36). Local pits on the surface were observed, as is shown in Figure 36a. EDS analysis of the area (not shown in this work) showed the surface consisted of pure zinc, indicating the surface was stripped from its oxide layer and is anodically dissolving. Looking at the area where a thick oxide appeared to have formed showed a very different surface (see Figure 36). Large porous oxides have grown out of the surface and the surface is locally attacked, as is indicated by little pits in the surface (observed in the lower left corner of Figure 36b). EDS analysis showed the main chemical components are Zn, O and Cl, indicating the presence of zinc oxide and simonkolleite.

The images obtained by SEM observation of GI after seven days immersion in the slag solution are shown in Figure 37. The image shows a protective layer has precipitated over the surface of GI (see Figure 37a. EDS analysis of the entire area indicates the general chemical composition of the surface mainly consists of Zn, O and Si. This spectrum is rather similar to the analysis of the surface of MZ after exposure to the slag solution. The spectrum indicates the presence of zinc (oxides) and silicates.
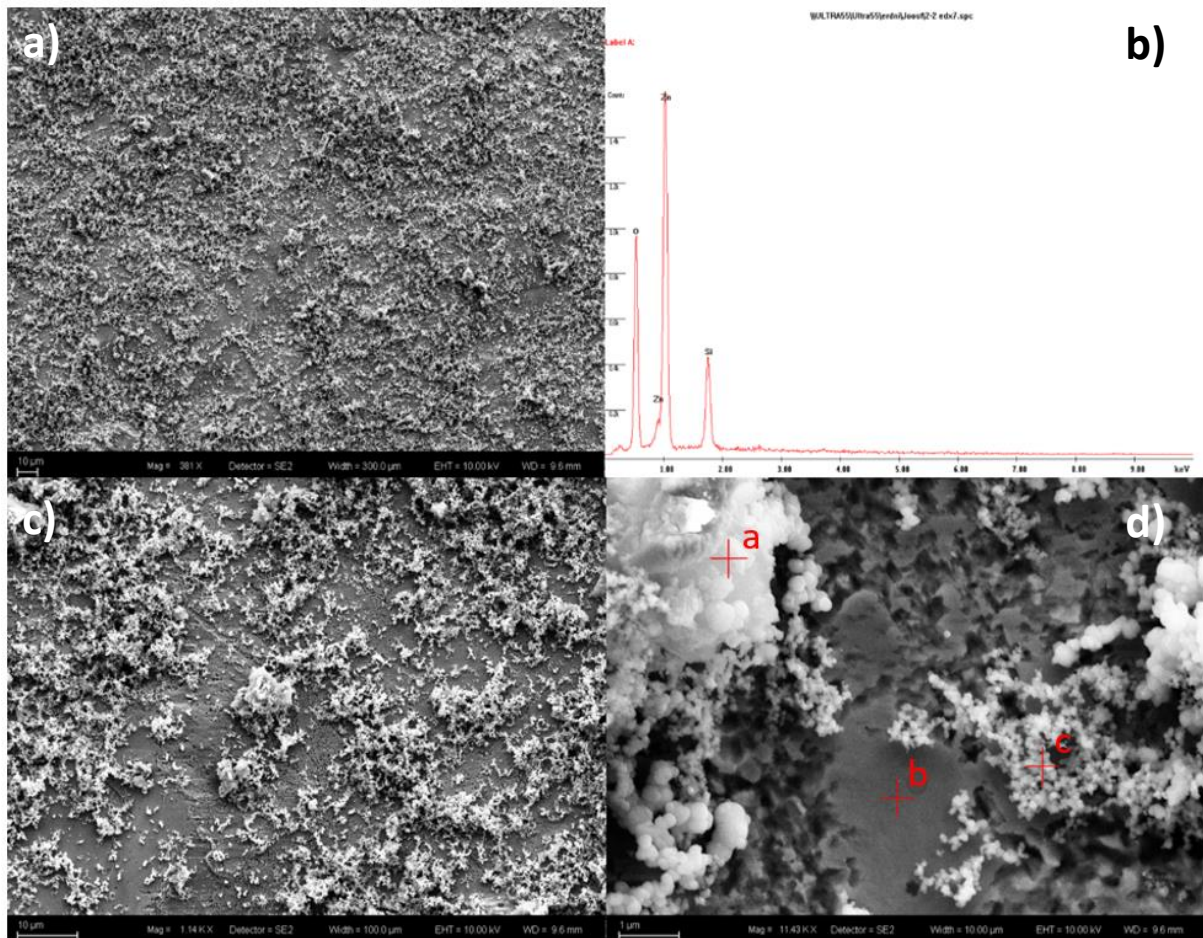
Figure 37: SEM secondary electron image at magnification 381x (a) and EDS spectrum of the surface of GI after immersion in slag solution for 7 days. Secondary electron images at higher magnifications 1140x (c) and 11.430x (d) show preferential deposition of precipitates.

At higher magnification it can be seen that the deposited layer is not as thick and dense as the layer we saw earlier on the surface of MZ. But the structure of the compound again shows a gel-like film network, consisting of different-sized spherical particles. The compounds appear to be precipitating at spots on the surface where the material has corroded and the corrosion-free spots are rather clean of precipitate. Three spots, marked in Figure 37d by 'a', 'b' and 'c', were analysed by EDS and the spectra are shown in Figure 38. EDS analysis shows the clean surface 'c' consists only of zinc with only a minor amount of oxygen, indicating the surface is almost entirely clean of any oxides and consists mainly of pure zinc. EDS analysis of the precipitated compound show the general chemical composition of the precipitate consists of O, Zn, Mg and Si. The difference in chemical composition at different spots and the different morphologies indicates multiple species have emerged on the surface. Spectra indicate the spherical particles, that are closest to the surface, are a mixture of zinc and silicates. At some spots magnesium, calcium and traces of different metal have been adsorbed to the zinc and silicate layer.
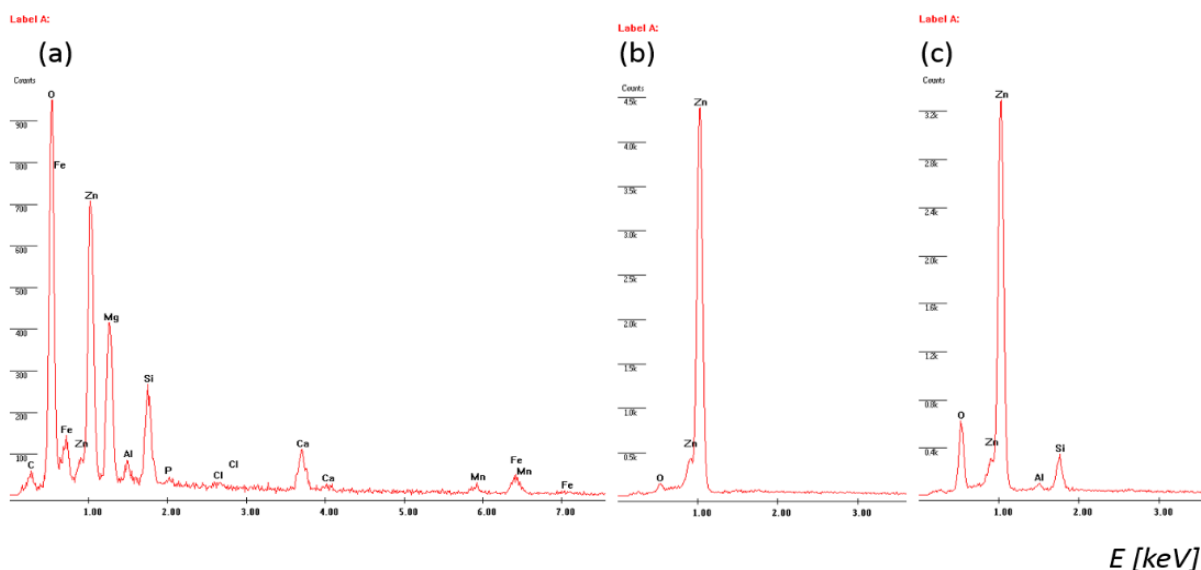
Figure 38: EDS spectra of three spots as indicated in Figure 18.

On both MZ and GI, EDS spectra indicate the presence of silicates on the zinc surface. Magnesium and aluminium were depleted from the surface of MZ after the exposure to the slag solution and on GI the precipitates appear to preferentially deposit on the anodic sites where the dissolution of zinc occurs. These suggests a mechanism where the colloidal silicates in solution react/recombine with the anodically dissolved zinc and precipitate on the surface. EDS analysis performed on the surfaces show the presence of zinc and silicates but give no further information on the bounded state and the condition of the surface underneath the deposited layer.

4.1.4.3 X-ray Photoelectron Spectroscopy

After exposure to the two solution, the amounts of corrosion products formed and thickness of the deposited layer were too low to be determined by mass loss/mass gain techniques. IR-spectroscopy (FTIR) was not relevant due to the high penetration of the technique and X-ray diffraction (XRD) only showed phases of zinc and some traces of simonkolleite. The latter indicates the deposited species are amorphous and therefore in the present work, depth-profile X-ray photoelectron spectroscopy (XPS) was used to determine the chemical natures of the products present from the surface to the bulk of MZ samples. Analysis of GA and GI samples is not done in the present work since the facilities – due to priority issues and time restrictions - were not available.

The results of XPS depth profiling on MZ exposed to the reference solution are presented in Figure 39 and on MZ exposed to the slag solution in Figure 40. The depth profile of MZ exposed to the reference solution shows the upper surface of the samples consists of a mixture of zinc-, aluminium-, and magnesium oxides. The amount of zinc oxide is high on the direct surface but deeper in the material the zinc oxide content drops fast and metallic zinc becomes predominant. The magnesium and aluminium content is high in the vicinity of the surface (~13% and ~12% respectively) compared to the bulk composition and both are almost completely present in the form of oxides.
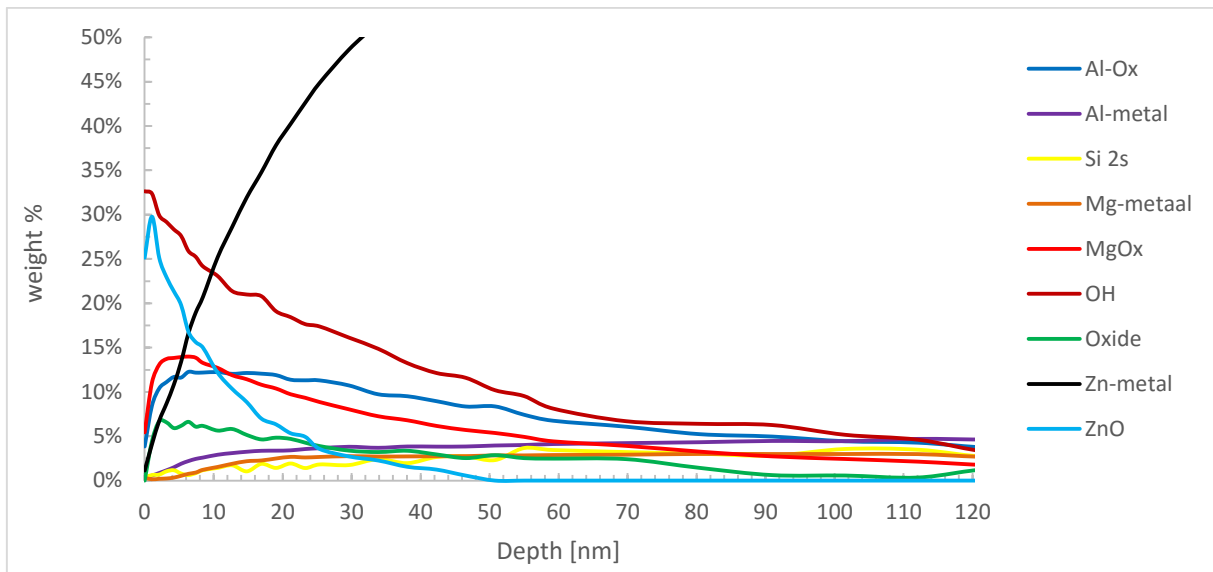
Figure 39: XPS depth profile of MZ exposed to the reference solution for seven days.

If we compare the depth profile of the sample exposed to the reference solution with the sample exposed to the slag solution we see a clear change in composition. As seen earlier in the EDS spectra, it is clear from the XPS depth profile that zinc-silicates have deposited on the surface of the specimen exposed to the slag solution. The correlation between the tangents of zinc and silicate indicates zinc and silicate are in a bounded state. XPS also confirms earlier findings by EDS, stating the surface is almost completely depleted of MgO_x and the amount of AlO_x is also much lower than in the reference sample. This is illustrated in Figure 41, where the MgO_x, AlO_x and ZnO_x content of the different samples are plotted against each other.
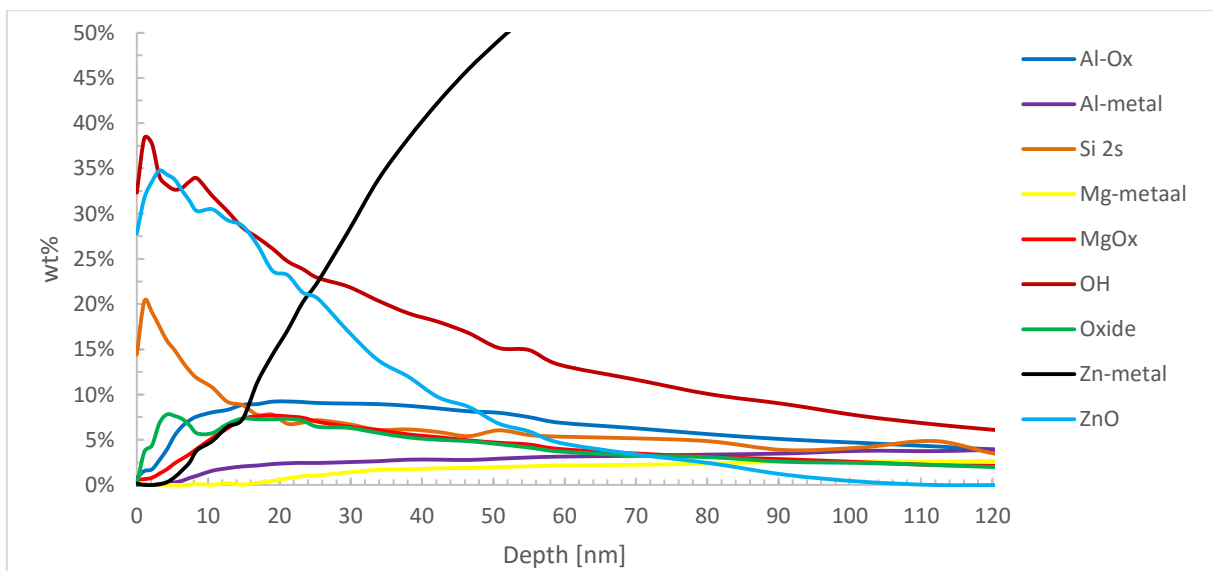
Figure 40: XPS depth profile of MZ exposed to the slag solution for seven days.

Looking at the depth profiles of MgO_x and AlO_x (see Figure 41) it becomes clear that both oxides are removed from the surface but are present in the same concentrations deeper in the material. Under alkaline conditions aluminium is active dissolves, which explains the depletions of aluminium from the surface. The layered double hydroxide (LDH) on the surface MZ can become unstable due to the dissolution of aluminium, which can cause the magnesium oxides to be stripped from the surface. Which explains the significant depletion of magnesium from the surface.

Another noticeable difference is the different depth profile of zinc for both samples. In the reference sample, the metallic zinc content raises quickly and the content of zinc oxides goes down as we go deeper in the material. In the sample exposed to slag, the surface is depleted of metallic zinc and there is a large increase in the amount of zinc oxide compared to the reference sample.
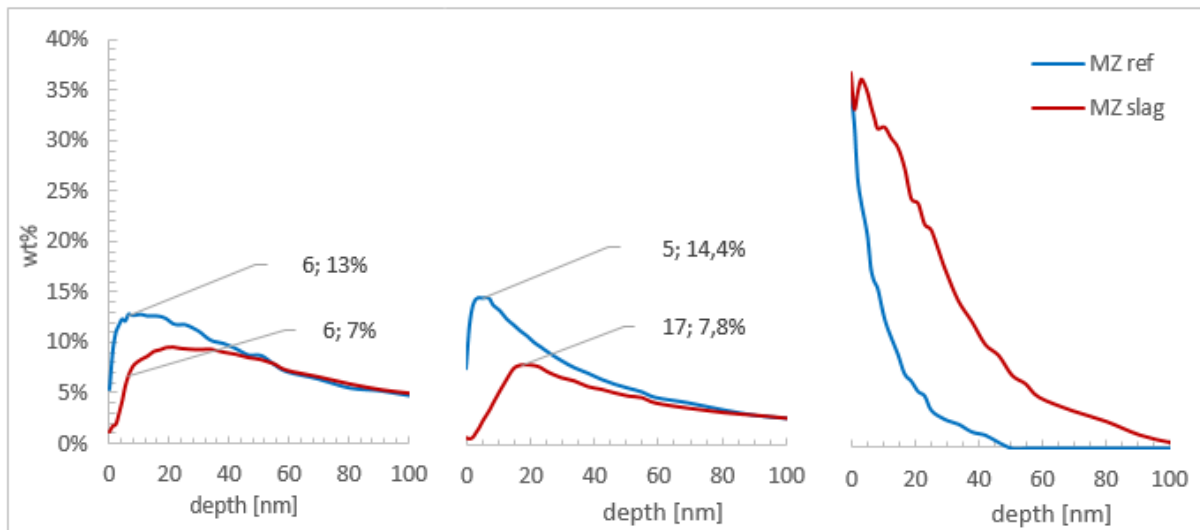
Figure 41: XPS depth profile of AlOx (left), MgOx (middle) and ZnOx (right).

This disappearing of metallic zinc from surface and an increase in OH and ZnO suggests the precipitation of $Zn(OH)_2$ and formation of ZnO on the surface subsequent to anodic dissolution of zinc. A second peak in the OH plot (~8.5 nm) correlates to the increase of AlOx and MgOx.

The plot of Si-2s and ZnO indicate that corrosion products of zinc (e.g. $Zn(OH)_2$) have formed on the surface prior to the deposition of zinc silicates.

4.1.5 Electrochemical Impedance Spectroscopy

Electrochemical impedance spectroscopy (EIS) was used as a tool to study the progress of the electrode reaction processes, which enabled the determination of the corrosion mechanism. The MZ and GA were clamped horizontal in clamp cells and immersed in the reference- and slag solution for 6 days. EIS scans were performed periodically to monitor the electrochemical processes on the surface.

4.1.5.1 GA reference measurement

The Nyquist and Bode plot of GA in the reference solution are shown in Figure 42. There is one capacitive arc in the Nyquist plots in the initial stage (4h ~ 12h), which correspond to the single peak in the phase-angle Bode plot. The initial increase of the capacitive loop in size, indicates the formation of a thickening layer and the corrosion protection improves. A second capacitive loop arises as immersion time is increased (from ~ 24h). The two loops in the Nyquist plot correspond to the two peaks in the phase-angle Bode plots and the two plateaus in the impedance Bode plot, indicating the presence of two time constants for the rest of the immersion time (24h ~ 120h). The high frequency capacitance (on the left of the Nyquist plot) corresponds to the electrode surface's passivation layer resistors and capacitors, low frequency capacitance corresponds to the charge-transfer behaviour between the zinc interface and the solution. As time passes, the value of the film resistance, R_1, was decreased from 3019 Ω cm^{-2} to 1011 Ω cm^{-2}, which implied that the rust layer absorbed on the electrode surface is damaged because of Cl$^-$ attack. The low frequency charge-transfer capacitance loop increases in size during 24h -48h indicating the thickening of the corrosion-layer. In the final stage

of the measurement (72h ~ 120h) the size decreases again which also implies the layer on the surface was damaged due to Cl⁻ attack.
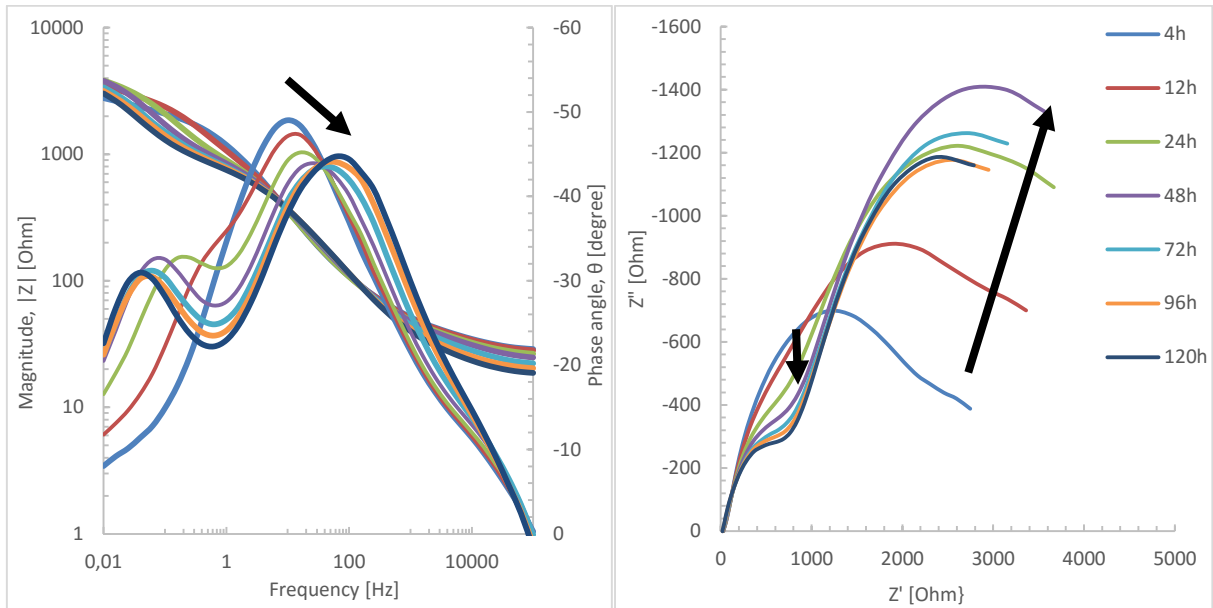
Figure 42: Bode (left) and Nyquist plot (right) of GA immersed in 0,1M NaCl reference solution.

Because of the two observed capacitive arcs, one for the charge transfer and the second one for the layer of corrosion products, the equivalent circuit shown in Figure 43b is used to fit the experimental data.
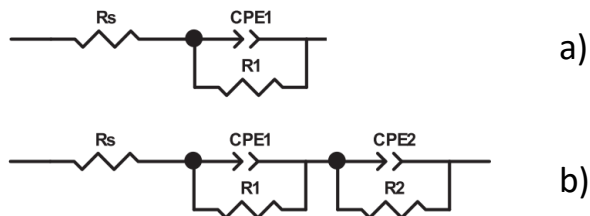
Figure 43: Equivalent circuits used to fit impedance data.

The obtained results of the data fitting are given in Table 9. The fitted data confirms the observations in the Nyquist and Bode plots, where the film resistance (represented by R_1) initially increases in the first hours indicating the thickening of the protective layer. After 12 hours the resistance of the layer reduces and the charge transfer resistance (R_2) of the material and the double layer capacitance (Q_2) increase due to corrosion products forming on the surface.

Table 9: Fitted parameters of the EIS data of GA in the reference solution after different immersion times.

Immersion time (h)	R_s	Q_1	n	R_1	Q_2	n	R_2
	$(\Omega\ cm^{-2})$	$(F\ cm^{-2}\ Hz^{1-n})$		$(\Omega\ cm^{-2})$	$(F\ cm^{-2}\ Hz^{1-n})$		$(\Omega\ cm^{-2})$
4	29	2,98E-04	0,56	3019	1,77E-05	0,74	2610
12	29	2,66E-04	0,57	3686	4,10E-04	0,56	2619
24	27	2,63E-04	0,57	2078	8,02E-04	0,80	2608
48	25	2,26E-04	0,58	1489	1,17E-03	0,66	3462
72	22	2,04E-04	0,59	1223	1,46E-03	0,62	3299
96	20	1,82E-04	0,61	1096	1,63E-03	0,74	3150
120	23	1,71E-04	0,62	1011	1,88E-03	0,63	3237

4.1.5.2   GA slag measurement

On GA in the slag solution, there is one capacitive arc in all the Nyquist plots (see Figure 44), corresponding to the single peaks in the phase-angle Bode plots. Both Nyquist and Bode plots show little change in the first stage of the observation (4h – 72h). A decrease in the size of the capacitance loop is observed, indicating a reduction of the charge transfer resistance and that the corrosion kinetics on the electrode surface are changed. After longer immersion time (96h – 120h) a large increase in the size of the capacitance loop is observed in the Nyquist plot. The phase angle Bode plot shows a new phase angle with a wider shape at higher frequencies ranges. This new phase angle means that the interfacial structure of the electrode has changed. The equivalent circuit in Figure 43a gave the best fit to the EIS data and the parameters obtained are given in Table 10.
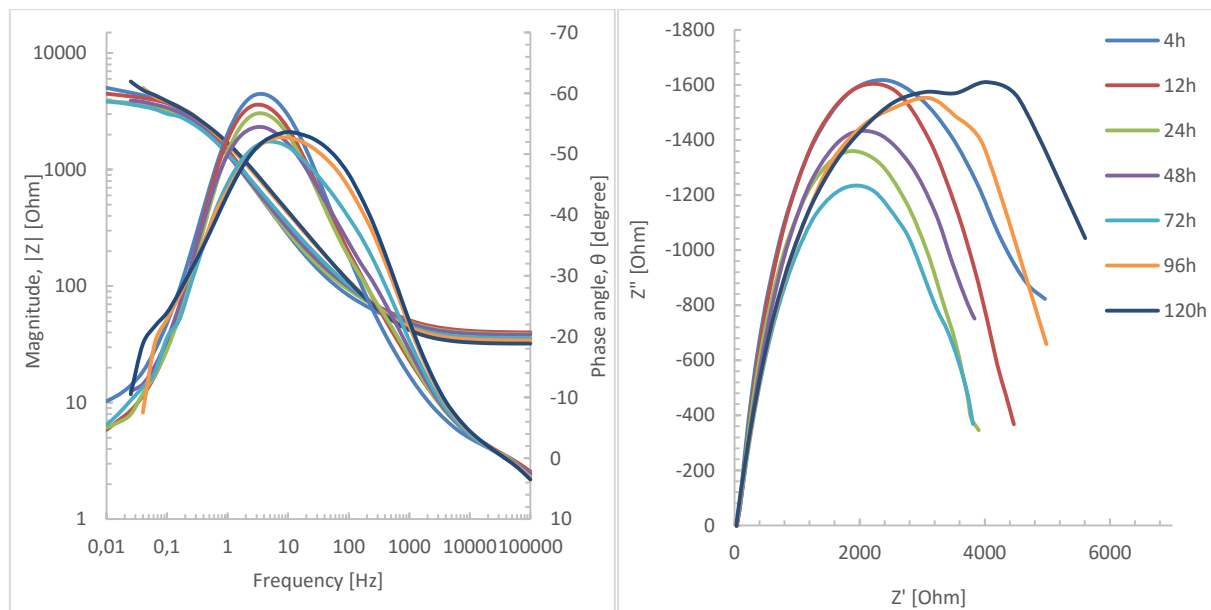
Figure 44: Bode (left) and Nyquist plot (right) of GA immersed in 0,1M NaCl reference solution.

The fitted data confirms the earlier statements based on the shape of the plots. The initial increase of the capacitance indicates film thickness reduction or the incorporation of species in the passive layer, lowering the dielectric constant of the passive layer. The shift in the phase angle in the final stage coincides with the reduction of the capacitance, indicating the thickening of the protective film. The decrease of the capacitance loop is represented by the reduction of the value of R_1, indicating the film resistance is decreasing. Despite this, the material appears to be behaving different from the material

exposed to the reference solution. The overall high resistance and low capacitance during the entire immersion time indicate the presence of a protective (passive) film on the surface [68]. Unlike the reference sample, no breakdown of the film and formation of corrosion products seems to be occurring, as is indicated by the absence of a second time constant. The values of Q_1 and R_1, correspond to the film capacitance and pore resistance respectively. These results confirm the observation of the visual assessment of the surface, where the surface was free from corrosion products. The results also correlate with the SEM observations, where the surface showed no breakdown of the passive film and the deposition of a protective film, consisting of aluminium oxides, on the surface.

Table 10: Fitted parameters of the EIS data of GA in the slag solution after different immersion times.

Immersion time	Rs	Q_1	n_1	R_1
(h)	$(\Omega*cm^{-2})$	$(\mu F*cm^{-2}*Hz^{1-n})$		$(\Omega*cm^{-2})$
4	41	1,72E-04	0,73	5.160
12	42	1,64E-04	0,71	4.804
24	40	1,82E-04	0,70	4.202
48	39	1,88E-04	0,68	4.645
72	35	1,79E-04	0,67	4.102
96	33	1,49E-04	0,67	5.366
120	31	1,46E-04	0,67	5.633

Unfortunately this analysis provides no further information in the study of the corrosion inhibition mechanism by BOF-slag. As was stated earlier, the slag used for the experiments conducted on GA, consisted of LF-slag and the mechanism showed no resemblance to the inhibition mechanism of BOF-slag. Despite this, LF-slag is able to passivate the surface and protect the surface from corrosion.

4.1.5.3   MZ reference measurement

The results of EIS measurements on MZ in the reference solution are presented in Figure 45, and show there are two capacitive loops in the Nyquist plots, again corresponding to the two peaks in the phase-angle Bode plots. This indicates the existence of two time constants during the experiment similar to the results of GA in the reference solution.

The high frequency capacitance (on the left of the Nyquist plots) corresponds to the electrode surface oxide layer resistors and capacitors, low frequency capacitance corresponds to the charge-transfer behaviour between the metallic interface and the solution. At the initial stage (4h – 24h), the value of the film resistance, R_1 was decreased from 828 Ω cm^{-2} to 587 Ω cm^{-2} ,which implied that the oxide layer absorbed on the electrode surface damaged because of the attack by chlorides. The low frequency charge-transfer capacitance loop decreases in size during this first period indicating the reduced corrosion resistance of the material. In the final stage of the measurement (48h ~ 120h) the size of both capacitance loops in the Nyquist plots increases again which implies the layer on the surface is thickening again and the presence of corrosion products (or the LDH) increases the charge transfer resistance of the coating. This observation in the evolution of the plots agrees with literature, stating that Zn-Mg-Al coatings are able to form dense protective oxide layers in saline conditions by the formation of simonkolleite. This explains why on MZ the oxide layer thickens where the layer is clearly damaged on GA.
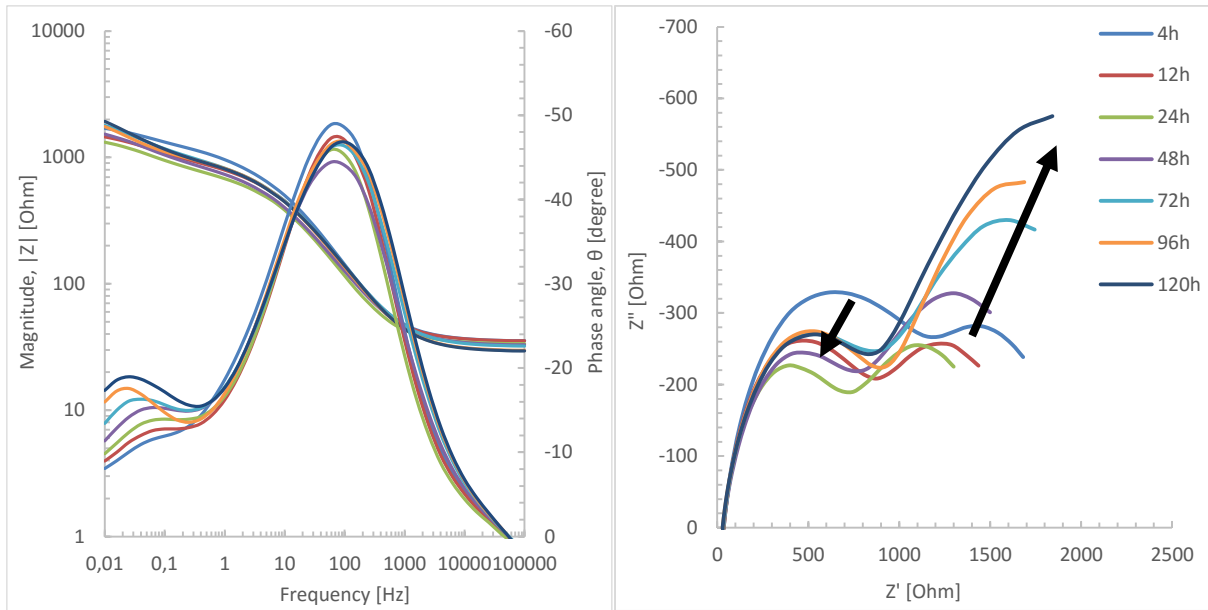
Figure 45: Bode (left) and Nyquist plot (right) of MZ immersed in a 0,1M NaCl reference solution.

The obtained data by EIS have been fitted using the equivalent circuit in Figure 43b. The first time constant $(Q_1|R_1)$ represent the oxide film on the surface and the second time constant $(Q_2|R_2)$ represents the double layer capacitance and charge transfer of the metal. The obtained results of the data fitting are given in Table 11. The fitted data confirms the observations in the Nyquist and Bode plots, where the film resistance (represented by R_1) initially decreases in the first hours indicating the break-down of the protective layer. After 12 hours the resistance of the layer reduces and the charge transfer resistance (R_2) of the material and the double layer capacitance (Q_2) increase due to corrosion products/passivation layer forming on the surface.

Table 11: Fitted parameters of the EIS data of MZ in the reference solution after different immersion times.

Immersion time	R_s	Q_1	n_1	R_1	Q_2	n_2	R_2
(h)	$(\Omega\ cm^{-2})$	$(F\ cm^{-2}\ Hz^{1-n})$		$(\Omega\ cm^{-2})$	$(F\ cm^{-2}\ Hz^{1-n})$		$(\Omega\ cm^{-2})$
4	35	1,57E-03	0,76	828	6,86E-05	0,60	1.134
12	32	2,35E-03	0,72	705	8,69E-05	0,53	1.088
24	33	2,51E-03	0,75	587	8,65E-05	0,59	1.023
48	32	2,45E-03	0,71	666	9,94E-05	0,59	1.235
72	31	2,20E-03	0,73	737	8,16E-05	0,58	1.661
96	29	2,07E-03	0,72	789	8,46E-05	0,59	1.899
120	28	2,35E-03	0,72	737	8,21E-05	0,59	2.212

4.1.5.4   MZ slag measurement

An EIS spectra were recorder on MZ during immersion in a verified BOF-slag solution after one hour, seventeen hours and six days. The corresponding Nyquist and Bode plot are given in Figure 46. At the initial stage of immersion (after one hour) the Nyquist plot shows a single capacitive loop. The high resistance and the low capacitance of the loop indicate it represents the natural protective oxide layer formed during the exposure to air acting as a protective layer on the surface of GA and not the corrosion process. The equivalent circuit for this system and the three other scans are given in Figure

47. The fitted data from the EIS results corresponding to the best fitting equivalent circuits are given in Table 12. The fitted data present very high values for the resistance, R_1, and very low values for the film capacitance, Q_1, representing the thick and dense LDH on the surface of MZ.
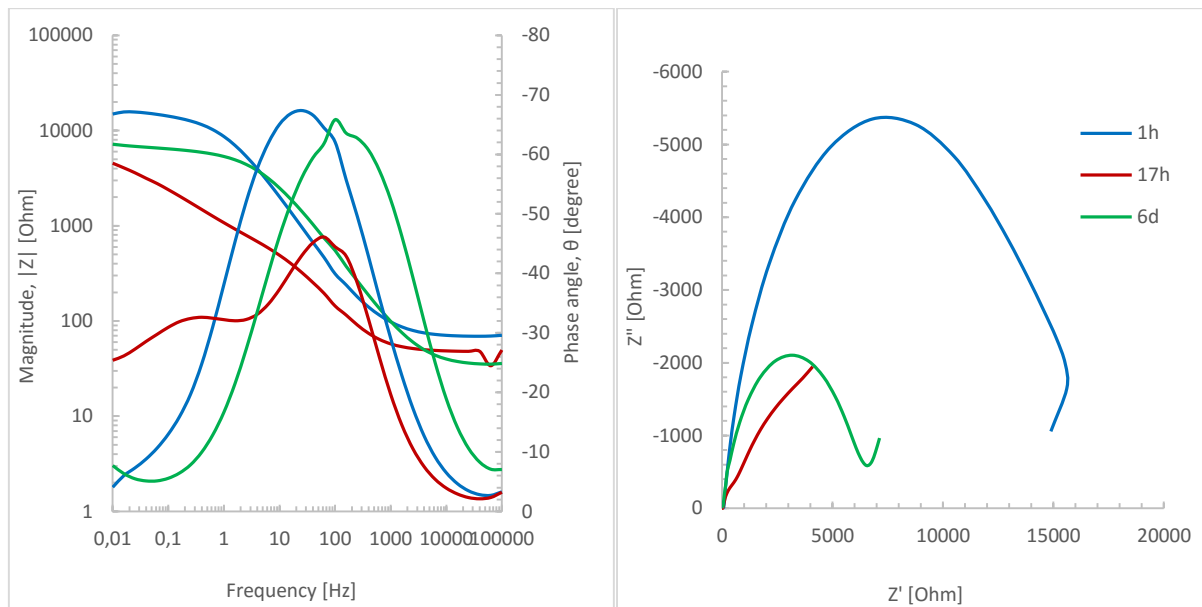
Figure 46: Bode (left) and Nyquist plot (right) of MZ immersed in a 0,1M NaCl reference solution.

The plot after seventeen hours of immersion is very different from the initial plots. The Nyquist plot now shows two capacitive loops, which correspond to the two peak and plateaus in the Bode plot. The high frequency capacitance corresponds to the electrode surface oxide layer resistors and capacitors and the low frequency capacitance corresponds to the charge-transfer reaction between the metallic interface and the solution. The very low resistance of the high-frequency capacitance loop indicates the oxide layer is porous and provides little protection from corrosion, which correlate to the increased capacitance which indicated film thickness reduction. The relatively large size of the low-frequency loop, which represent the charge transfer resistance (R_2), indicates corrosion products have formed on the surface.
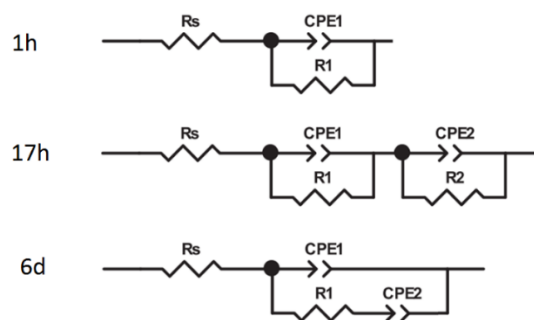
Figure 47: Equivalent circuits used to fit the EIS data at different immersion times.

After six days the Nyquist plot shows a very different system. The plot now consists of a capacitive loop with a diffusion element in the low-frequency range, which is represented by the equivalent circuit in Figure 47 (6d). The film resistance (R_1) has significantly increased (as can be seen in Table 12), indicating a protective layer covers the surface. The reduction of the capacitance to values below the initial capacitance value could suggest a thick layer has deposited over the surface. Given the relatively low resistance, compared to the initial resistance of the film, it is more likely the film is reinforced with

silicates. The addition of silicates with lower dielectric constant causes the decrease in the film capacitance. The Bode phase-angle plot shows a shift to higher frequencies, which indicates the morphology of the surface has changed. This supports the idea of silicates forming the protective layer as we saw during SEM observation.

Table 12: Fitted parameters of the EIS data of MZ in the BOF-slag solution after different immersion times.

Immersion time	R_s	Q_1	n_1	R_1	Q_2	n_2	R_2
(h)	(Ω cm^{-2})	(F cm^{-2} Hz^{1-n})		(Ω cm^{-2})	(F cm^{-2} Hz^{1-n})		(Ω cm^{-2})
1h	42	1,53E-05	0,79	15.571	-	-	-
17h	41	6,62E-03	0,84	411	5,15E-04	0,55	7.048
6d	34	1,13E-05	0.80	5.227	8,41E-04	0.21	-

In the low-frequency range the Nyquist plots shows a, what appears to be, Warburg diffusion element. This suggest the charge transfer reaction is under diffusion control. Something observed earlier in the formation of a plateau in the potentiodynamic polarization curves of MZ.

Similar results obtained for GA were obtained for MZ, using LF-slag in a later stage of the study instead of BOF-slag. In response, the surface of MZ passivates and showed almost complete capacitor behaviour due to the dense protective oxide film over the entire surface of the material. Since they have no contribution to the study of the inhibition mechanism, these plots are not covered in this work. Repetition of the experiment on both and GA and MZ with BOF-slag was not possible due time limitations and the unavailability of verified BOF-slag at the final stage of the study.

4.1.6 Inhibition mechanism

The combination of the different experiments in this study enables the formulation of the inhibition mechanism by which BOF-slag operates and is able to inhibit the corrosion of galvanized steel.

The initial chemical analysis of the solution showed the presence of mainly calcium and silicates in solution. A silicate solution consists of monomeric and polymeric species at which the concentrations of monomer and polymer partially depend on the silica content [69]. Low concentrations of silicates mainly consist of SiO_3^{2-} and $HSiO^-$, whereas solutions with higher concentrations are characterized by increasing polymer concentration and increasing size (up to 40 nm) [29, 70]. The polymer is in equilibrium with the soluble monomeric silicate ions via:

$$nSiO_3^{-2} + 3nH_2O = (H_2SiO_3)_n nH2O + 2nOH^-$$ (0.26)

Therefore, an equilibrium exists between the ionic silica and colloidal (polymerized) silica. It was observed in general that as pH and [OH^-] are decreased, silicate ions hydrolyse to form larger polymeric species, which causes the solution to remain highly alkaline. What can also be noted is that when the solution is very diluted, essentially all species get depolymerized and the solution just consists of monomeric silicate ions [29]. The polymers formed are uniform in size of which the interior consists of silicon linked by bridging oxygen and the exterior consists of neutral and charged silanol groups.

From the potentiodynamic polarization measurements we saw the oxygen reduction reaction was under diffusion control in the absence of inhibitor. Upon the addition this reduction reaction was partly controlled at the interface. The anodic dissolution reaction was reduced and a passivation or diffusion plateau is formed. These two observations indicate the strengthening of the passive layer or the

precipitation of a new layer on the surface. The shift to more noble potentials on GA suggest the layer forms on the anodic sites. The OCP of MZ has shifted to a slightly more negative potential suggesting a different modus operandi. The alkalinity of the solution was thought to have a large contribution to the suppressed anodic dissolution because of the passivation of zinc in alkaline conditions. Potentiodynamic polarization tests with an alkaline reference solution indicated a reduction of the anodic dissolution but the results did not match the obtained results from the slag solutions.

The theory of a deposited film over the surface was confirmed by SEM observation. Assessment of the surface of MZ and GI showed a gel-like porous film consisting of small spherical linked particles covering the surface. On GI the film appeared to mainly have deposited on the anodic sites (signs of dissolution of zinc underneath the film), covering pits that had formed on the surface.

On MZ the entire surface was covered with the porous film, with only small sections of the metallic surface visible. EDS analysis indicated the depletion of magnesium and aluminium from the surface. The active state of aluminium under alkaline conditions and the reactive nature of magnesium explains the depletion of both magnesium and aluminium from the metallic coating [62, 63, 70–72]. This observation correlates with the more active open circuit potential, indicating the active dissolution of aluminium and magnesium. The anodic dissolution of aluminium can cause breakdown of the passive film on MZ. Although magnesium is active under these conditions, it is stable on the surface in the layered double hydroxide LDH. Dissolution of aluminium causes the LDH to degrade and the magnesium erodes from the surface as a result.
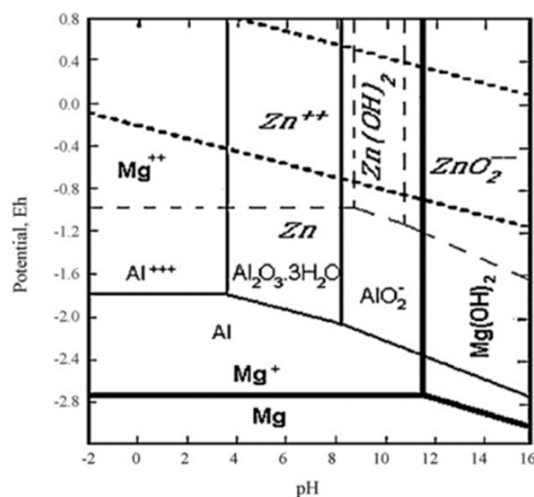
Figure 48: Potential pH diagram of Zn, Mg and Al [73].

XPS analysis confirmed this theory. By means of depth profiling it became evident magnesium had depleted from the direct vicinity of the surface together with aluminium. The content of metallic zinc also decreased significantly in the sample exposed to the slag solution. The zinc oxides content had considerably increased, indicating the formation and precipitation of corrosion products upon the anodic dissolution of after the breakdown of the LDH.

The high pH of the slag solution causes the dissolution of aluminium and facilitates the formation of $Zn(OH)_2$ upon the anodic dissolution of zinc, as can be seen in a E,pH diagram containing Zn, Mg and Al (see Figure 48). The recombination of zinc and hydroxide which retards the cathodic oxygen reaction, which correlates with the depressed cathodic current in the polarization scans. Lowering of the local pH by reacting with OH⁻ causes the silicates in the vicinity to polymerize locally and form colloids in suspension. The negative charge surrounding the colloids cause them to migrate to the positively charged anodic sites but are still repelled from one another by their own charge. The

presence of divalent Zn^{2+} is able to neutralize the charge of colloids and link the polysilicates. They deposit on the zinc-rich phases, blocking the further anodic dissolution of zinc, as is depicted in Figure 49. This suggest the formation of corrosion product is necessary to provide the conditions for colloidal silicates to precipitate and adhere to the surface. The bounded state between zinc and silicate was confirmed by XPS and the depth profile showed the increased amount of zinc oxides on the surface, covered by zinc silicates.
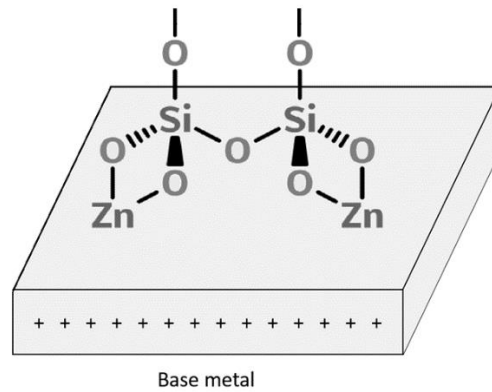
Figure 49: Schematic diagram of absorbed silicate over the corrosion products' surface [72].

EIS analysis of the immersed specimen confirm the necessity of corrosion prior to protection. In the initial stage the oxide layer gets broken, leading to active corrosion of the metallic coating indicated by a large reduction of the film resistance and the presence of a second capacitive loop. In the final stage the results indicate the protective film on the surface is restored. The relatively low resistance and the diffusion element suggest it is a porous layer covering the surface. The low capacity confirms the film consist of element with lower dielectric constant given the low thickness of the layer. This correlates with the lower dielectric constant of silicate.

To substantiate this theory, a precipitation experiment was performed. In this experiment, four solutions containing magnesium-, iron-, aluminium- and zinc chloride were added to a sample of slag-solution. It can be seen in Figure 50, that the addition of magnesium-, iron- and aluminium chloride did not result in a direct reaction/precipitation in the solution. The addition of the zinc chloride triggered the precipitation of a white gel and adherent type of substance from the solution which was sticking rather firmly to the bottle. This result supports the theory of silicates precipitating from the solution on the release of zinc ions in the solution. The addition of the zinc containing solution also lowers the pH of the solution to drop but this effect was assumed to be minor.
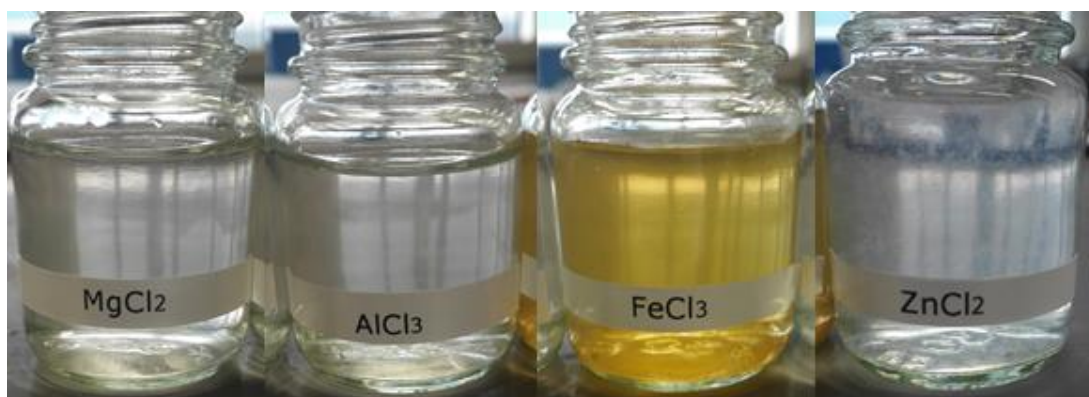
Figure 50: Precipitation test, in which magnesium-, iron-, aluminium- and zinc chloride were added to a sample of slag-solution.

Similar results were obtained in multiple studies on the corrosion inhibiting properties of sodium silicates on the corrosion of carbon steel after Lehrman et. Al discovered and studied the inhibiting properties in water piping [62, 70, 72]. Observation of the exposed surface by SEM showed a similar image of the surface, as can be seen in Figure 51.
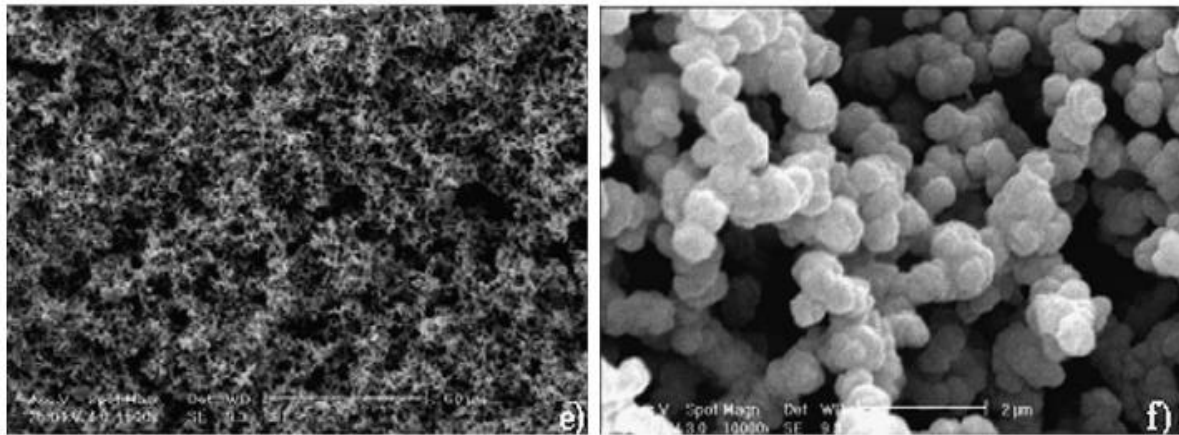
Figure 51: SEM micrographs obtained on the carbon steel surface after 15 days of immersion in the presence of 30 ppm silicate [72]*.*

Chemical analysis of the composition showed the layer consisted of silica gel adhered to the surface. They indicate the potential use of silicates in a number of situations to replace the use of chromates, due to the non-toxic character of silicates. Frankel et. Al investigated the inhibition effect of silicates on the corrosion of aluminium [69]. They confirm earlier statements that the silicates increase the alkalinity of the solution and promote dissolution of aluminium, as is the case for MZ. They found the aluminium formed soluble aluminate ions ($Al(OH)_4^-$), which were able to react with silicate anions in solution to form and precipitate as aluminosilicates. This observation could explains the lesser depletion of aluminium from the surface of MZ compared to the decrease of the magnesium content.

Recent studies have also shown that the addition of silicates can greatly enhance the corrosion resistance of organic coatings [74–76]. These obtained results indicate the potential effect of slag, once incorporated into an organic coating.

4.2   EFFECT OF BOF-SLAG IN A COATING SYSTEM

The aim of this second part of the study was to evaluate BOF-slag when it is incorporated in an organic coating. It has been demonstrated in the previous section that BOF-slag and XCA02 in solution significantly lower the current density of the galvanized coating and improve the appearance of the coating upon exposure to an aggressive environment. Whether these two compounds also have the ability to lower the corrosion current and/or improve the barrier properties when incorporated into an organic coating is researched in this section.

In an earlier collaboration between Tata Steel and Solvay Specialty Polymers, a water-based 50/50 polyamide-imide has been developed which showed to have good barrier properties and good chemical and thermal resistance. This coating (referred to as "PXM13159") was chosen to formulate three different coating; a reference coating with no added corrosion inhibitor, a coating with 1 wt% XCA02 and a coating with 1 wt% of the soluble part of slag. This slag 'pigment' was retrieved by evaporating the water from a filtered slag solution.

4.2.1 Scanning Electron Microscope

The coating was applied on GA and MZ samples with a dry coating thickness of 5~8 µm. After coating of the metallic samples, the coated specimens were examined visually and by SEM. Visual examination revealed an increase in the surface roughness and decrease in gloss of the coating. Both these deviations from the reference coating are due to tiny little bumps, where the coating seems to be covering pigment particles. Cross sections of the coated specimens were observed by SEM to evaluate the dry coating thickness and dispersion of the pigment particles. The average coating thickness of the reference coating was ~6.9 µm as is shown in Figure 53 for GA. The cracked surface of the GA coating is nicely depicted and it can be seen that the organic roughly follows the contours of the underlying surface, giving a homogeneous coating thickness.
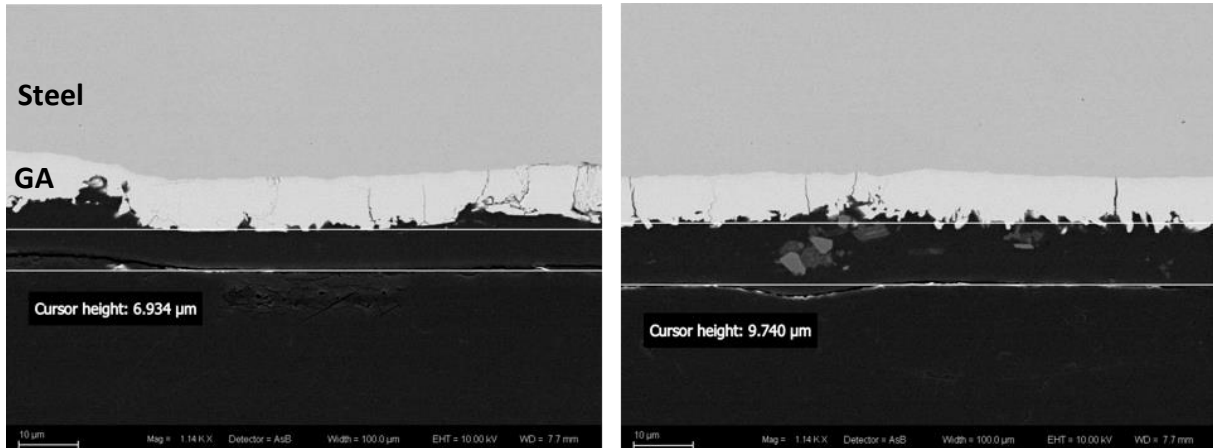
Figure 52: SEM image of GA coated with the reference coating (left) and slag coating (right). Average coating thickness is indicated by cursor height.

The coating containing 1 wt% of pigment has a fairly higher coating thickness, where the average thickness is measured to be ~9.7 µm (see Figure 53), which is above the desired ~5-8 µm range. As was thought earlier, the coating shows irregularities of a couple of microns on the surface where it covers pigment particles. The slag pigment particles are clustering and are concentrated near the metallic surface, despite their good solubility in the water-borne coating formulation. The poor distribution of the particles in the coating can cause trapping of water, high osmotic pressure and reduces the adhesion between the organic coating and the metal. The latter can have detrimental effects upon further handling of the specimens. Galvannealed coatings are harder and more brittle than hot-dip galvanized coatings, so during bending coating cracks and powdering are always present. This brittle behaviour makes it more difficult for coatings to adhere to the surface upon bending of the sample. The reduced adhesion due to clustered pigment particles between the metal and the organic coating can severely worsen this adhesive problem.

Similar images as on GA were obtained for the coated MZ. The reference sample showed a nice and even distribution of the coating, where the coating follows the contours of the wavy MZ surface (see Figure 53). The average dry coating thickness was ~5.7 µm, which is slightly thinner than on GA but still within the desired range.
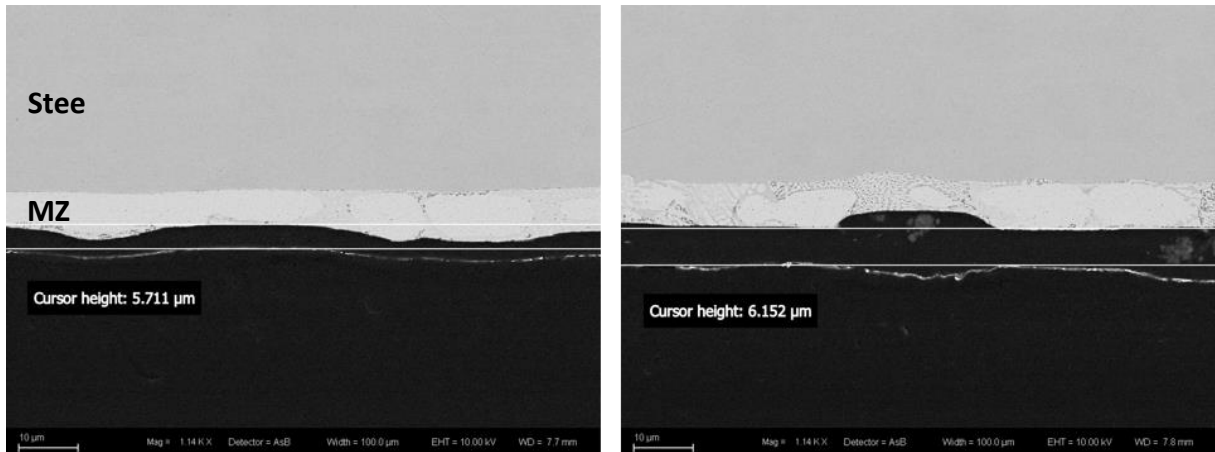
Figure 53: SEM image of the cross section of MZ with (left) the reference coating and (right) the slag coating. Where the average coating thickness is indicated by cursor height.

Like on GA, the SEM image of the slag coating on MZ reveals the slag pigment particles clustering together and concentrating near the metallic surface.

The general chemical composition of the incorporated particles was determined by EDS analysis. Two types of particles were distinguished by appearance and composition in the SEM images, a brighter compound with a straight/crystalline shape and a less bright porous compound, indicated by '1' and '2' respectively in Figure 54.
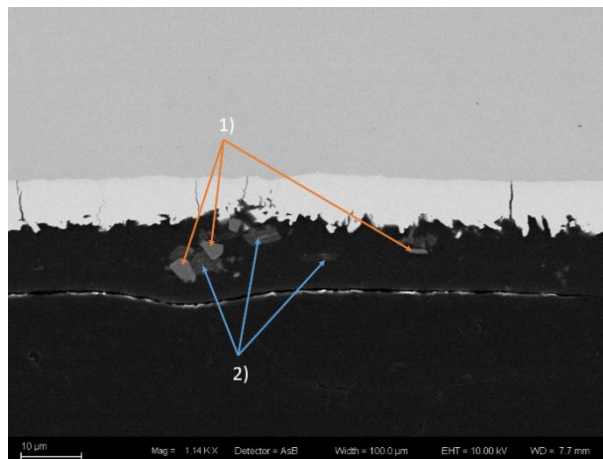
Figure 54: Atomic backscatter SEM image of GA coated with slag coating. Numbers '1' and '2' refer to spots measured by EDS with same composition.

The EDS spectrum of the two different compounds are given in Figure 55. The main elements in compound '1' are O, Ca and C. This indicated compounds consists of calcium carbonate which can be related back to the chemical composition of both BOF- and LF-slag. The traces of gold in the spectrum originate from the layer of gold lining applied to mark the organic coating, represented by the bright line in the SEM images. The main elements in compound '2' are Al and O with a trace of C. This indicated the particles consist of aluminium oxide, a compound that in these quantities can only originate from LF-slag and not from BOF-slag.
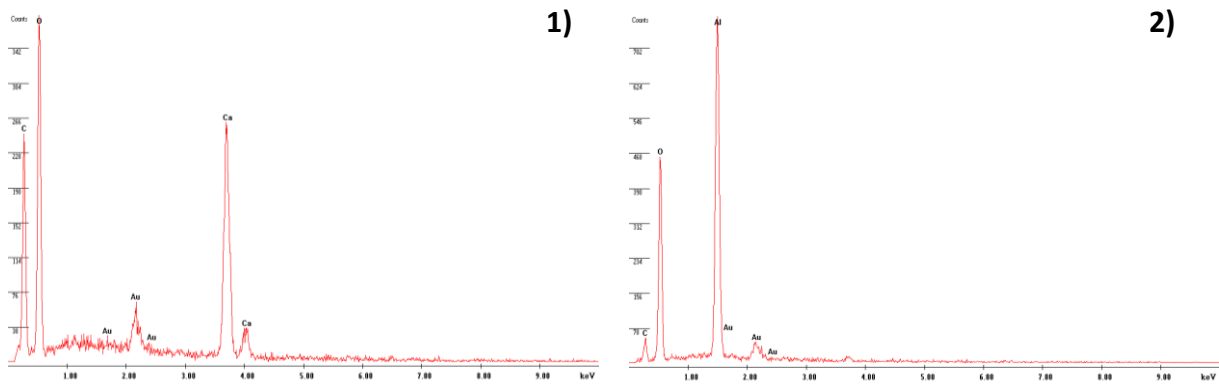
Figure 55: EDS spectra of spots denoted by 1) and 2) in Figure 54.

4.2.2 Salt-spray Test

After the metallic samples were coated, the specimens were bended lengthwise to induce artificial defects in the coating. The various coating systems were evaluated in a salt spray test (ASTM B117) under a 60° angle for 21 days. The samples were assessed after 10 days and upon the completion of the test, after 21 days. The most notable observations are discussed in this section. A complete overview of the results of the salt spray test are presented in *Appendix B*.

After 21 days of testing, the GA sample with the reference coating displays white rust over the entire length of the bend with some red rust showing along the bend and at the taped edges which is due to the high iron-content in the GA coating (see Figure 56) . At some points, both the organic and metallic coating are completely gone and corrosion of the steel substrate has initiated (marked in Figure 56). The MZ sample with the reference coating shows better performance with just white rust on the entire length of the bend and no failure of the coating on the taped edges. The occurrence of blisters is reduced in the case of MZ and they are smaller in size. On both GA and MZ, XCA02 enhances the corrosion resistance of the organic coating with much lower extent of corrosion on the bend. The addition of the inhibitor pigment to the coating does increase the presence of blisters on the lower tape-edges which is especially clear in the case of MZ. Although these blisters are smaller in size than the blisters in the reference coating.
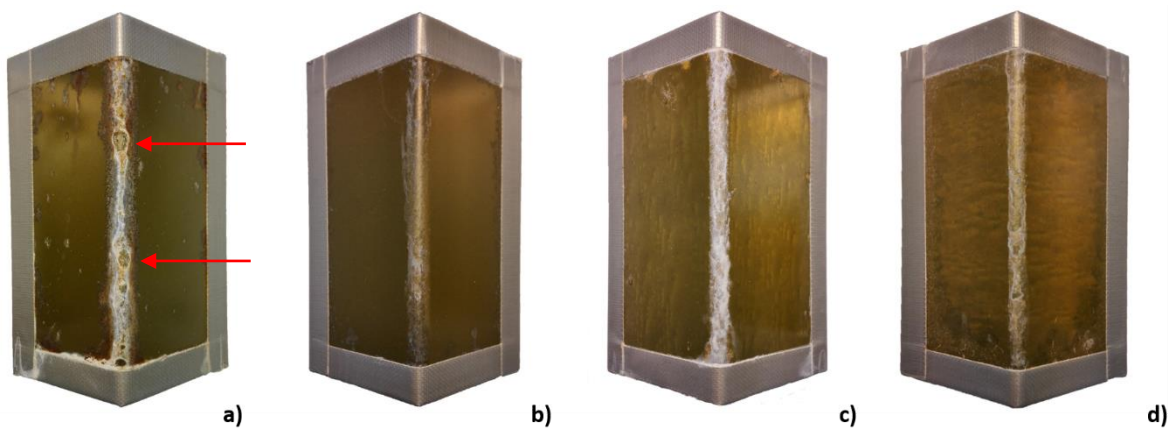
Figure 56: Results salt spray test after 21 days of GA with reference coating a) GA with 1wt% XCA02 coating b) MZ with reference coating c) and MZ with 1wt% XCA02 coating d).

The incorporation of slag pigment in the coating has proven worsen the corrosion resistance of the coating. The results of the slag coatings after the salt spray test are shown in Figure 57. In the case of GA, slag particles have significantly decreased the coating's barrier properties. The specimen shows

delamination over almost the entire length of the bend and the extent of corrosion is much more severe compared to the reference coating. On the flat parts of the panel, slag particles appear to have endorsed the occurrence of blisters (denoted by the darker parts). This has initiated corrosion severe corrosion on the flat panels, something barely present on the reference specimen.
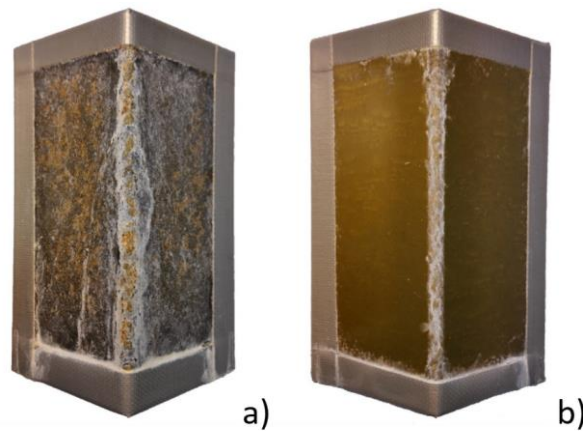
Figure 57: Results salt spray test after 21 days of a) GA coated with 1wt% slag coating and b) MZ with 1wt% slag coating.

On MZ, the addition of slag seems to have had little effect on the performance of the coating. Like the reference coating, white rust has formed over the entire length of the bend but the spread of corrosion product away of the bend appears to be limited. The slag-coating on MZ did improve the resistance against blistering, with reduced occurrence of blisters and a reduction of their size.

4.2.3   Electrochemical Impedance spectroscopy

EIS was used to examine the effect on the properties of the coating by adding the two inhibitors. The EIS measurements presented in the subsequent section were carried out with a 0.1 M NaCl aqueous solution, with the samples completely immersed.

In the plots in Figure 58, the Bode impedance plots of coated GA after one and eleven days are given. On the plot, it can be seen that on the first day of immersion, the sample with no inhibitors shows the highest impedance at low frequencies. It is interesting to look at the modulus of the impedance at low frequencies for this is often associated with the pore resistance of the coating. The modulus of the impedance at low frequencies is therefore often used to evaluate and compare coating performance [74]. The impedance is $\sim 10^5$ at 10 mHz and the plot of the reference coating shows an inflexion point around 100 Hz. The corresponding Nyquist diagram (not shown here) displays two semi-circles indicating that the coating is damaged and the metal substrate has contact with the solution. Looking at the Bode impedance plot after eleven days, we see a clear change in the shape of the plot. The impedance has severely dropped, mainly in the low-mid frequency region. This indicates the coating has a low resistance to degradation and corrosion as a result of the initial damage.
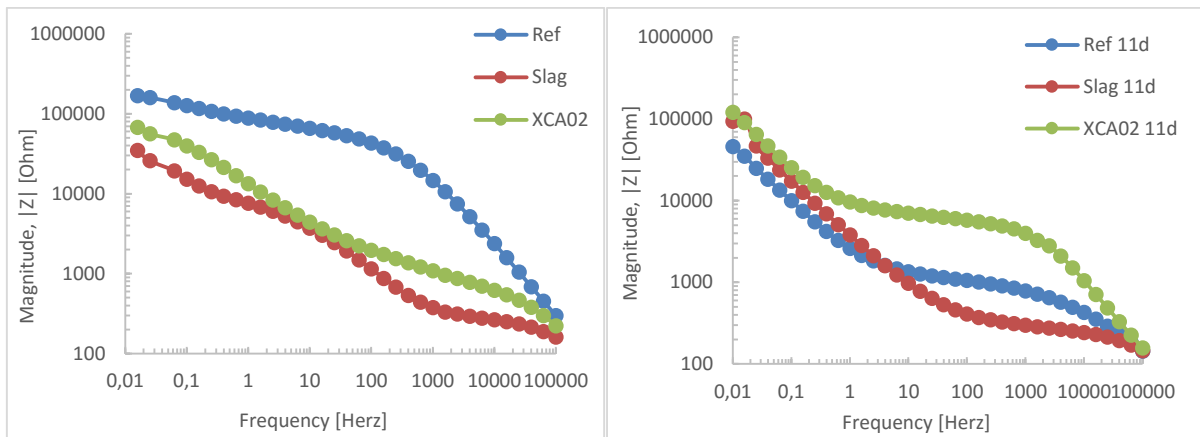
Figure 58: Bode impedance plot of coated GA EIS measurements after 1 day and 11 days.

The coating with slag pigment added shows the lowest impedance, which is over a decade lower than the impedance of the reference coating. The slag particles clearly negatively affect the barrier properties of the coating. This was predicted earlier based on the images of SEM observation. After eleven days, the state of the coating has worsened.

The plot of the coating containing 1 wt% XCA02 pigment is in between the reference and slag coating after one day. From the Bode impedance plot of XCA02 it also becomes clear the inhibitor particles have negatively affected the barrier properties of the coating. The plot of the XCA02 coating after eleven days shows a different trend than with the other two coating systems. The impedance of the coating has increased in the low-frequency region (~67 kΩ -> ~120 kΩ), but also in the mid-high frequency region where the other coatings had the largest depression. This indicates that the added pigment is able to enhance the resistance of the coating. From the Nyquist plot is this becomes more evident. In Figure 59 the Nyquist plot of the 1 wt% XCA02 coating is given over time. An intact coating with a developed pore resistance would be represented in the Nyquist plot by a semicircle.
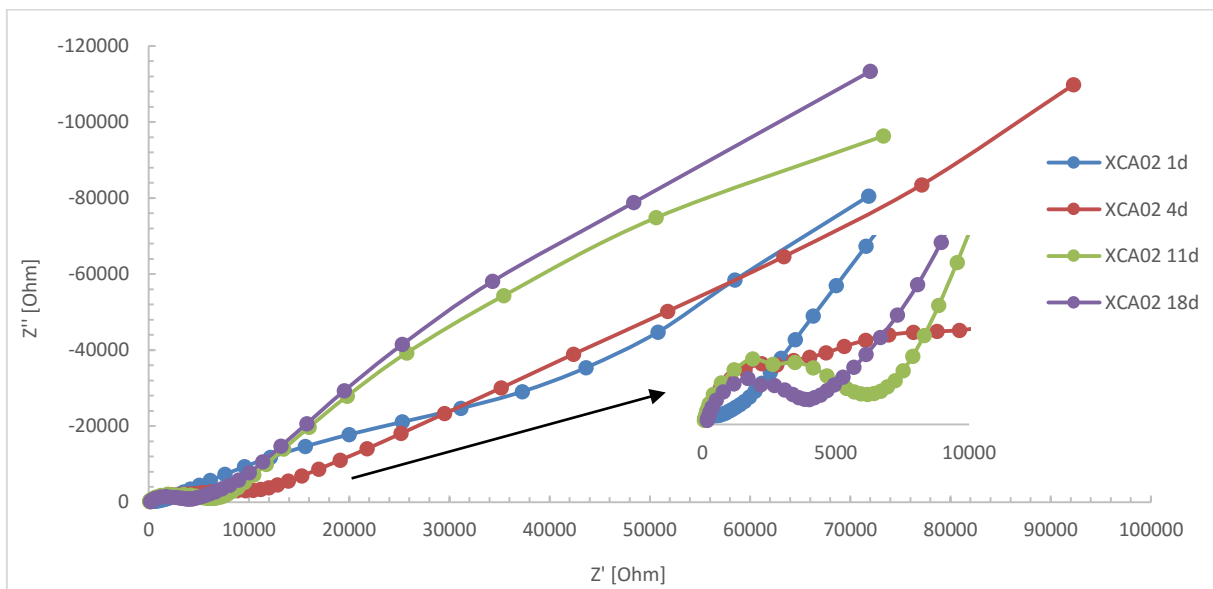
Figure 59: Nyquist plot of GA coated with XCA02 (1 wt%) coating over time.

The shape of the plot indicates the coating is more severely damaged. The small high-frequency capacitive loop represents the pore resistance, which is increased in the initial stage (1-4 days) and is then slowly decreasing over time. More interesting in the plot is the low-mid frequency region. A large

capacive loop arises and is growing in size over time. Indicating the formation of a new barrier in the coating, increasing the resistance to degradation of the coating and corrosion of the substrate. The observations in the EIS data correlate with the visual assessment of the coated samples, after being submitted to the salt spray test (SST).
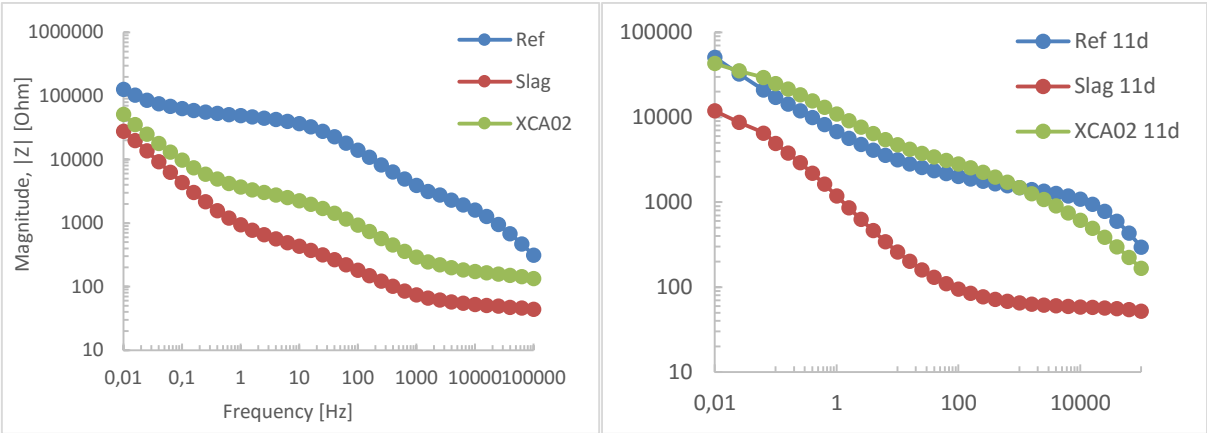
Figure 60: Bode impedance plot of coated MZ EIS measurements after 1 day and 11 days.

The plots of coated MZ (see Figure 60) show similar behaviour as we saw for coated GA. The reference coating has the highest impedance in the low frequency region. The shape of the plot indicates the coating is damaged more than the coating system on GA. The addition of slag to the coating also shows to decrease the barrier properties of the coating. The addition of XCA02 shows similar behaviour as on GA. It can be concluded that the addition of foreign particles in the coating has a negative effect on the barrier properties of the coating. Especially in the case of deformation (as is with our specimens), the particles function as stress concentrators and cause cracking of the coating.

After eleven days we see that both the reference and the slag coating have degraded the most. Although their impedance at low frequencies is stable, their resistance in the mid-high frequency region has significantly dropped. XCA02 again shows to decrease the degradation of the coating and the corrosion process. The modulus of the coating does indicate the pigment significantly improves the performance of the coating. This becomes even more clear if we plot the modulus of the impedance at 100 mHz versus time for the difference coatings (see Figure 61) .
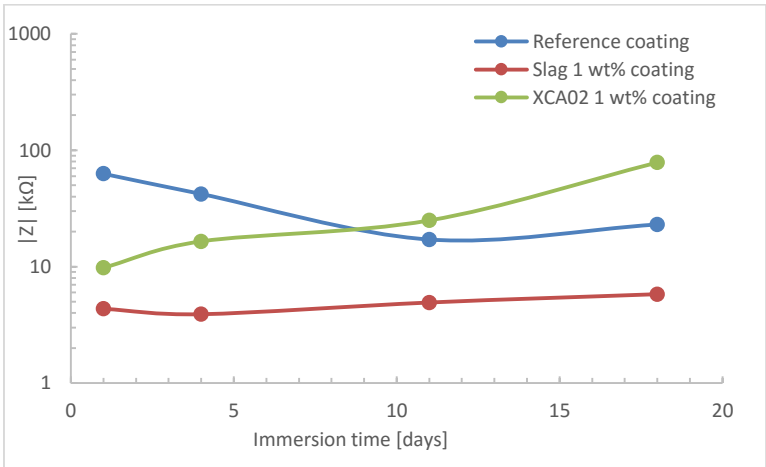
Figure 61: Evolution of the modulus of the impedance at 100 mHz of MZ coated with three different coatings (reference, slag and XCA02).

The plot gives a clear overview of the evolution of modulus of the impedance of the coating at low frequencies, indicating XCA02 is able to increase the total modulus of the coating over time. It hereby slows down the degradation of the coating. These results correlate with corrosion inhibiting properties in potentiodynamic polarization tests and the results of the coated MZ samples after being tested in the salt spray test.

5 CONCLUSIONS

In the first part of this study, the inhibition effect of BOF-slag on the corrosion of GA and MZ in solution was investigated. The results of the potentiodynamic polarization scans showed that, in solution, BOF-slag is able to suppress both the cathodic and anodic current. This causes the corrosion current density to be reduced by more than a decade for GA and almost two decades in the case of MZ. The plots indicated the formation of a protective film, which inhibits the anodic dissolution.

The variation of the OCP showed that the BOF-slag was able to shift the OCP of GA to much more noble values (-0.55 vs -0.95 V vs. SCE). This indicates the passivation of the surface and the suppression of the anodic reaction, which correlates to the results from the potentiodynamic polarization measurements. The potential of MZ was shifted to slightly more negative values, indicating the activation of the surface.

Surface analysis showed the deposition of a gel-like film over the surface of MZ, confirming the observations from the polarization curves. Similar images were obtained for GI (which was shortly used at the initial stage of the study) but due to the accidental usage of LF-slag no similar phenomena were observed on the surface of GA. Analysis with EDS indicated the film consisted mainly of zinc and silicates which correlates with the chemical analysis of the electrolyte and with literature.

XPS depth profiling of MZ confirmed the observations by SEM-EDS and indicated the formation of zinc (hydr-)oxides prior to the deposition of the film. Based on these findings it is suggested that the colloidal silicates require corrosion product formation and lowering of the local pH to adsorb on the surface as zinc silicates and inhibit the oxygen reduction and anodic dissolution by blocking the surface.

Pigment was retrieved from the soluble part of slag and was incorporated into a waterborne polyamide-imide coating. The addition of pigment caused roughening of the coated surface due to clustered particles in the coating as was observed by SEM. The relatively large particles caused significant damaging (cracking) of the coating upon deformation as was concluded from the results of EIS on immersed specimens. A commercial inhibitor, used as a reference, was able to improve the resistance of the coating over time despite the initial damaging of the coating due to cracking. The slag pigment was not able to restore the barrier properties of the coating. Analysis by EDS indicated the pigment consisted of alumina and calcium carbonate. Analysis of the slag showed LF-slag was used instead of BOF-slag, explaining the chemical composition and why the pigment did not show the expected corrosion inhibition in the coated system.

Recent studies have shown that the addition of silicates to organic coatings can improve the performance of coatings in with EIS and salt spray tests. Together with the fact that BOF-slag in solution was more efficient than the commercial inhibitors tested, confirms the potential has of being a suitable corrosion inhibitor for organic coatings.

6 REMARKS AND RECOMMENDATIONS

The main focus of this study was the investigation of the inhibition mechanism of BOF-slag on galvanized steel. It was mentioned in literature and in this work that the silicates in solution are in equilibrium between ionic and colloidal particles. The concentration plays a significant role in this equilibrium and could also play a similar role on the inhibiting properties of the slag solution. Future research could therefore focus on the effect of concentration on the inhibiting properties of slag. Once the optimal concentration has been discovered, this can also be correlated to different concentrations in the coating.

Different studies have looked at synergistic effects of inhibitors on the corrosion of galvanized steel. Aramaki et al. studied the synergistic effect of sodium-silicate and cerium(III)chloride, for example. This study could be repeated, using a solution of BOF-slag pigment, to study possible synergy [77].

For Tata Steel it can also be of great interest to look at the inhibition of the corrosion of cold-rolled steel (CRS). CRS is a product that is still used by many of Tata Steel's customers in the automotive industry and based on earlier results by Armstrong and Salasi, slag has great potential for being a good inhibitor for CRS [62, 72].

For this study a water-based polyamide-imide was used as a coating. Despite the good solubility of the pigment that was used, the final particle size was relatively large compared to the average coating thickness. This led to increased surface roughness and initiated damaging of the coating upon deformation. Many coated products of Tata Steel, for example Clearcoat©, are based on N-methylpyrrolidon (NMP), as a solvent. A study could be done on both the performance of slag in a NMP-based polymer coating and to investigate if the dispersion of particles is better in these coatings.

During this study LF-slag, instead of BOF-slag was accidentally used in the final stage. The pigment recovered from LF-slag showed to have very different chemical composition than the active components leached from BOF-slag. The great performance of BOF-slag as an inhibitor in solution could therefore not be correlated to the performance once incorporated into a coating system. The main aim of future work should therefore be to investigate the effect of BOF-slag pigment on the performance of corrosion resistant organic coatings.

REFERENCES

1.   Koch GH, Brongers MPH, Thompson NG (2002) Corrosion Costs and the Preventive Strategies in the united States. Houston (USA)

2.   Twite RL, Bierwagen GP (1998) Review of Alternatives to Chromate for Corrosion Protection of Aluminum Aerospace Alloys. Prog Org Coatings 33:91–100

3.   Mccafferty E (2010) Introduction to Corrosion Science, 1st ed. Springer Science+Business Media, Alexandria, USA

4.   Bardal E (2004) Corrosion and Protection, 1st ed. Springler-Verlag, London, UK

5.   De Windt L, Chaurand P, Rose J (2011) Kinetics of steel slag leaching: Batch tests and modeling. Waste Manag 31:225–235

6.   Reddy a. S, Pradhan RK, Chandra S (2006) Utilization of Basic Oxygen Furnace (BOF) slag in the production of a hydraulic cement binder. Int J Miner Process 79:98–105

7.   Jones DA (1996) Principles and prevention of corrosion, 2nd ed. Simon & Schuster, London, UK

8.   Dariva CG, Galio AF (2014) Corrosion Inhibitors - principles mechanisms and applications. In: Dev. Corros. Prot. InTech, p 16

9.   The World Bank (2015) Nominal GDP 1960-2015 the Netherlands. http://www.tradingeconomics.com/netherlands/gdp. Accessed 22 May 2015

10.   Atkins P, De Paula J (2006) Physical Chemistry. Oxford University Press

11.   Delahay P, Pourbaix M, Van Rysselberghe P (1951) Potential-pH Diagram of Zinc and its Applications to the Study of Zinc Corrosion. J Electrochem Soc 98:101

12.   Asgari H, Toroghinejad MR, Golozar MA (2007) On texture, corrosion resistance and morphology of hot-dip galvanized zinc coatings. Appl Surf Sci 253:6769–6777

13.   Queiroz FM, Costa I (2007) Electrochemical, chemical and morphological characterization of galvannealed steel coating. Surf Coatings Technol 201:7024–7035

14.   Ha HY, Park SJ, Kang JY, Kim HD, Moon MB (2011) Interpretation of the corrosion process of a galvannealed coating layer on dual-phase steel. Corros Sci 53:2430–2436

15.   Asgari H, Toroghinejad MR, Golozar MA (2007) On texture, corrosion resistance and morphology of hot-dip galvanized zinc coatings. Appl Surf Sci 253:6769–6777

16.   Silva PSG Da, Costa ANC, Mattos OR, Correia AN, Lima-Neto P De (2006) Evaluation of the corrosion behavior of galvannealed steel in chloride aqueous solution and in tropical marine environment. J Appl Electrochem 36:375–383

17.   Ha H-Y, Park S-J, Kang J-Y, Kim H-D, Moon M-B (2011) Interpretation of the corrosion process of a galvannealed coating layer on dual-phase steel. Corros Sci 53:2430–2436

18.   Almeida E, Morcillo M (2000) Lap-joint corrosion of automotive coated materials in chloride media. Part 1 - Electrogalvanized steel. Surf Coatings Technol 124:169–179

19.   Katiforis N, Papadimitriou G (1996) Influence of copper, cadmium and tin additions in the galvanizing bath on the structure, thickness and cracking behaviour of the galvanized coatings. Surf Coatings Technol 78:185–195

20.   Hosking NC, Ström MA, Shipway PH, Rudd CD (2007) Corrosion resistance of zinc–magnesium coated steel. Corros Sci 49:3669–3695

21.   Schuerz S, Fleischanderl M, Luckeneder GH, Preis K, Haunschmied T, Mori G, Kneissl a. C (2009) Corrosion behaviour of Zn-Al-Mg coated steel sheet in sodium chloride-containing environment. Corros Sci 51:2355–2363

22.   Diler E, Lescop B, Rioual S, Nguyen Vien G, Thierry D, Rouvellou B (2014) Initial formation of corrosion products on pure zinc and MgZn2 examined by XPS. Corros Sci 79:83–88

23.   Dutta M, Halder AK, Singh SB (2010) Morphology and properties of hot dip Zn-Mg and Zn-Mg-Al alloy coatings on steel sheet. Surf Coatings Technol 205:2578–2584

24.   Prosek T, Persson D, Stoulil J, Thierry D (2014) Composition of corrosion products formed on Zn-Mg, Zn-Al and Zn-Al-Mg coatings in model atmospheric conditions. Corros Sci 86:231–238

25.   Volovitch P, Vu TN, Allély C, Abdel Aal a., Ogle K (2011) Understanding corrosion via corrosion product characterization: II. Role of alloying elements in improving the corrosion resistance of Zn-Al-Mg coatings on steel. Corros Sci 53:2437–2445

26.   García SJ, Fischer HR, Van Der Zwaag S (2011) A critical appraisal of the potential of self healing polymeric coatings. Prog Org Coatings 72:211–221

27.   Choi H, Kim KY, Park JM (2013) Encapsulation of aliphatic amines into nanoparticles for self-healing corrosion protection of steel sheets. Prog Org Coatings 76:1316–1324

28.   Tan YJ, Bailey S, Kinsella B (1996) An investigation of the formation and destruction of corrosion inhibitor films using electrochemical impedance spectroscopy (EIS). Corros Sci 38:1545–1561

29.   Thompson JL, Scheetz BE, Schock MR, Lytle D a (1997) Sodium Silicate Corrosion Inhibitors : Issues of Effectiveness and Mechanism.

30.   Papavinasam S (2011) Corrosion Inhibitors. In: Uhlig's Corros. Handb. John Wiley & Sons, Inc., Hoboken, NJ, USA, pp 1021–1032

31.   Sinko J (2001) Challenges of chromate inhibitor pigments replacement in organic coatings. Prog Org Coatings 42:267–282

32.   Hannour F, Flores Ramirez JR, Oliveira UOB (2013) Method for manufacturing a steel product.

33. Mahieux PY, Aubert JE, Escadeillas G (2009) Utilization of weathered basic oxygen furnace slag in the production of hydraulic road binders. Constr Build Mater 23:742–747

34. Wang Q, Yan P (2010) Hydration properties of basic oxygen furnace steel slag. Constr Build Mater 24:1134–1140

35. Proctor DM, Fehling K a., Shay EC, et al (2000) Physical and chemical characteristics of blast furnace, basic oxygen furnace, and electric arc furnace steel industry slags. Environ Sci Technol 34:1576–1582

36. Kourounis S, Tsivilis S, Tsakiridis PE, Papadimitriou GD, Tsibouki Z (2007) Properties and hydration of blended cements with steelmaking slag. Cem Concr Res 37:815–822

37. Laan S van der (2015) Properties of ' steelslag ' as guidance for application in construction materials. IJmuiden, NL

38. Binici H, Aksogan O (2011) The use of ground blast furnace slag, chrome slag and corn stem ash mixture as a coating against corrosion. Constr Build Mater 25:4197–4201

39. Song HW, Saraswathy V (2006) Studies on the corrosion resistance of reinforced steel in concrete with ground granulated blast-furnace slag-An overview. J Hazard Mater 138:226–233

40. Lin D-F, Chou L-H, Wang Y-K, Luo H-L (2015) Performance evaluation of asphalt concrete test road partially paved with industrial waste – Basic oxygen furnace slag. Constr Build Mater 78:315–323

41. Slovaca AM (2009) Optimalization Slag Composition in Ladle Furnace Considering. 2:93–99

42. Garcia SJ, Markley T a., Mol JMC, Hughes a. E (2013) Unravelling the corrosion inhibition mechanisms of bi-functional inhibitors by EIS and SEM-EDS. Corros Sci 69:346–358

43. Mansfeld F, Xiao H, Wang Y (1995) Evaluation of Localized Corrosion Phenomena with Electrochemical Impedance Spectroscopy (EIS) and Electrochemical Noise Analysis (ENA). Mater Sci Forum 192-194:673–692

44. Lebrini M, Traisnel M, Gengembre L, Fontaine G, Lerasle O, Genet N (2011) Electrochemical impedance spectroscopy and X-ray photoelectron spectroscopy study of the corrosion behaviour of galvanized steel and electroplating steel. Appl Surf Sci 257:3383–3387

45. Loveday D, Peterson P, Rodgers B (2004) Evaluation of Organic Coatings with Electrochemical Impedance Spectroscopy Part 1 : Fundamentals of Electrochemical Impedance Spectroscopy. Jctr 88–93

46. Lillard RS, Kruger J, Tait WS, Moran PJ (1995) Using Local Electrochemical Impedance Spectroscopy to Examine Coating Failure. Corrosion 51:251–259

47. Chung SC, Cheng JR, Chiou SD, Shih HC (2000) EIS behavior of anodized zinc in chloride environments. Corros Sci 42:1249–1268

48. Rout TK (2007) Electrochemical impedance spectroscopy study on multi-layered coated steel sheets. Corros Sci 49:794–817

49. Huttunen-Saarivirta E, Yudin VE, Myagkova L a., Svetlichnyi VM (2011) Corrosion protection of galvanized steel by polyimide coatings: EIS and SEM investigations. Prog Org Coatings 72:269–278

50. Paliwoda-Porebska G, Stratmann M, Rohwerder M, Potje-Kamloth K, Lu Y, Pich a. Z, Adler HJ (2005) On the development of polypyrrole coatings with self-healing properties for iron corrosion protection. Corros Sci 47:3216–3233

51. Arenas M a., de Damborenea JJ (2004) Surface characterisation of cerium layers on galvanised steel. Surf Coatings Technol 187:320–325

52. Kwakernaak IC, Sloof IWG (2005) Introduction in the use and application of Scanning Electron Microscopy and Energy Dispersive X-ray Spectroscopy in materials It is compulsory that you study this text before attending the practical work .

53. Alford TL, Feldman LC (2007) Fundamentals of Nanoscale Film Analysis. Springer Science+Business Media, New York, USA

54. Kornienko E, Ossenbrink R, Michailov V (2013) Corrosion resistance of zinc-coated structured sheet metals. Corros Sci 69:270–280

55. Almeida E, Santos D, Uruchurtu J (1999) Corrosion performance of waterborne coatings for structural steel. Prog Org Coatings 37:131–140

56. Park J., Lee G., Ooshige H, Nishikata A, Tsuru T (2003) Monitoring of water uptake in organic coatings under cyclic wet–dry condition. Corros Sci 45:1881–1894

57. Loveday D, Peterson P, Rodgers B (2004) Evaluation of Organic Coatings with Electrochemical Impedance Spectroscopy, Part 2: Application of EIS to Coatings. JCT CoatingsTech Oktober:88–93

58. Wainer M (2013) Development of precoated metal sheet in collaboration with Toyota Motor : Focus on Corrosion inhibition.

59. Simões a. MP, Carbonari RO, Di Sarli a. R, del Amo B, Romagnoli R (2011) An environmentally acceptable primer for galvanized steel: Formulation and evaluation by SVET. Corros Sci 53:464–472

60. Lecercle A (2014) Report BOF slag as inhibitor in coatings. IJmuiden, NL

61. Laan S Van Der Properties of 'steelslag' as guidance for application in construction materials.

62. Armstrong RD, Zhou S (1988) The corrosion inhibition of iron by silicate related materials. Corros Sci 28:1177–1181

63. Mansfeld F (2005) Tafel slopes and corrosion rates obtained in the pre-Tafel region of polarization curves. Corros Sci 47:3178–3186

64. Pourbaix M (1973) Lectures on Electrochemical Corrosion, 1st ed. doi: 10.1007/978-1-4684-1806-4

65. Shams El Din a. M, Wang L (1996) Mechanism of corrosion inhibition by sodium molybdate. Desalination 107:29–43

66. Migahed M a., Abd-El-Raouf M, Al-Sabagh a. M, Abd-El-Bary HM (2005) Effectiveness of some non ionic surfactants as corrosion inhibitors for carbon steel pipelines in oil fields. Electrochim Acta 50:4683–4689

67. Seré PR, Culcasi JD, Elsner CI, Di Sarli a. R (1999) Relationship between texture and corrosion resistance in hot-dip galvanized steel sheets. Surf Coatings Technol 122:143–149

68. Fedrizzi L, Ciaghi L, Bonora PL, Fratesi R, Roventi G (1992) Corrosion behaviour of electrogalvanized steel in sodium chloride and ammonium sulphate solutions; a study by E.I.S. J Appl Electrochem 22:247–254

69. Lopez-Garrity O, Frankel GS (2014) Corrosion inhibition of aa2024-t3 by sodium silicate. Electrochim Acta 130:9–21

70. Lehrman L, Shuldener HL (1952) Action of Sodium Silicate as a Corrosion Inhibitor in Water Piping. Indrustrial Eng Chem 1765–1769

71. Nordström J, Nilsson E, Jarvol P, Nayeri M, Palmqvist A, Bergenholtz J, Matic A (2011) Concentration- and pH-dependence of highly alkaline sodium silicate solutions. J Colloid Interface Sci 356:37–45

72. Salasi M, Shahrabi T, Roayaei E, Aliofkhazraei M (2007) The electrochemical behaviour of environment-friendly inhibitors of silicate and phosphonate in corrosion control of carbon steel in soft water media. Mater Chem Phys 104:183–190

73. Badawy W a., Hilal NH, El-Rabiee M, Nady H (2010) Electrochemical behavior of Mg and some Mg alloys in aqueous solutions of different pH. Electrochim Acta 55:1880–1887

74. Fedel M, Deflorian F, Rossi S, Kamarchik P (2012) Study of the effect of mechanically treated CeO 2 and SiO 2 pigments on the corrosion protection of painted galvanized steel. Prog Org Coatings 74:36–42

75. Deflorian F, Fedel M, Rossi S, Kamarchik P (2011) Evaluation of mechanically treated cerium (IV) oxides as corrosion inhibitors for galvanized steel. Electrochim Acta 56:7833–7844

76. Aramaki K (2002) Preparation of chromate-free, self-healing polymer films containing sodium silicate on zinc pretreated in a cerium(III) nitrate solution for preventing zinc corrosion at scratches in 0.5 M NaCl. Corros Sci 44:1375–1389

77. Aramaki K (2002) Synergistic inhibition of zinc corrosion in 0.5 M NaCl by combination of cerium(III) chloride and sodium silicate. Corros Sci 44:871–886

ANNEXES

ANNEX A: LIST OF ABBREVIATIONS AND SYMBOLS

Abbreviations

AC	Alternating current
BF	Blast furnace
BOF	Basic oxygen furnace
BSE	Backscattering electrons
CE	Counter electrode
CRS	Cold rolled steel
DC	Direct current
EAF	Electric arc furnace
EC	Equivalent circuit
edl	Electric double layer
EDS	Energy dispersive X-rays Spectroscopy
EIS	Electrochemical impedance spectroscopy
emf	Electromotive force
FF	Full finish
GA	Galvannealed
GDP	Gross domestic Product
GI	Galvanized
GI	Hot-dip galvanized
HDG	Hot-dip galvanized
LDH	Layered double hydroxide
LF	Ladle furnace
MZ	MagiZinc©
NACE	National association of corrosion engineers
NMP	N-methylpyrrolidon
OCP	Open circuit potential
OHP	Outer helmholtz plane
PPM	Potentiodynamic polarization measurement
RE	Reference electrode
RE	Reference electrode
RMS	Root mean square
SCE	Standard calomel electrode
SE	Secondary electrons
SEM	Scanning electron microscope
SHE	Standard hydrogen electrode
SST	Salt spray test
SVET	Scanning vibrating electrode technique
WE	Working electrode
XPS	X-ray photoelectron spectroscopy

Symbols

A	Ampere/surface area
a	Atomic weight
C	Coulomb
E	Cell potential
$e_{a,c}$	anodic/cathodic half-cell potential
E_{corr}	Corrosion potential
F	Faraday constant
G	Gibbs energy
i	Current density
I	Current
i_0	Exchange current density
i_{corr}	Corrosion current density
m	Mass corroded material
n	Number equivalent
P	Pressure
Q	Reaction quotient
R	Gas constant
r	corrosion rate
Rp	Polarization resistance
T	Temperature
t	Time
V	Volts
$\alpha_{a,c}$	Charge transfer coefficiënt
β	Tafel constant

ANNEX B: LIST OF FIGURES

ANNEX C: LIST OF TABLES

APPENDICES

APPENDIX A

Detailed chemical composition of BOF-slag [37].

phase	PARC Wt%	Na2O	MgO	Al2O3	SiO2	P2O5	SO3	Cl	K2O	CaO	TiO2	V2O5	Cr2O3	MnO	Fe2O3
Lime (CaO)	5	0.0	0.9	0.2	0.2	0.1	0.1	0.0	0.0	76.1	0.2	0.1	0.1	7.7	14.0
Portlandite (Ca[OH]2)															
Calcite (CaCO3)															
Aragonite (CaCO3)															
Wuestite (FeO)	30	0.1	25.0	0.0	0.2	0.0	0.0	0.0	0.0	2.6	0.0	0.1	0.4	12.7	58.8
Mg-Wuestite ([Mg,Fe]O)															
Srebrodolskite (Ca2Fe2O5)	20	2.4	0.7	3.9	1.1	0.1	0.0	0.0	0.0	41.8	4.2	1.8	0.4	1.3	44.6
Larnite (Ca2SiO4)	31	0.1	0.1	0.7	27.8	3.6	0.3	0.0	0.0	61.4	0.9	1.4	0.4	0.2	3.1
a'-C2S (CaSiO4)															
Hatrurite (Ca3SiO5)	15	0.1	0.1	0.6	22.2	1.5	0.1	0.0	0.0	69.5	0.3	0.4	0.3	1.7	2.5
amorphous*															

Appendix B

Salt spray test results of all coatings systems, assessed after ten and twenty-one days.

Material	Inhibitor	Day 1	Day 10	Day 21
Galvannealed	Reference			
	Slag			
	Novinox -XCA02			
MagiZinc®	Reference			
	Slag			
	Novinox -XCA02			